Development of Mucin Analogues to Inhibit the Growth of Calcium Oxalate Kidney Stones

by

Daniel Lee French

Department of Mechanical Engineering and Materials Science
Duke University

Date:_____

Approved:

_____
Stefan Zauscher, Advisor

_____
Michael Lipkin

_____
Pei Zhong

_____
Stephen Craig

_____
Shyni Varghese

Dissertation submitted in partial fulfillment of
the requirements for the degree of Doctor
of Philosophy in the Department of
Mechanical Engineering and Materials Science in the Graduate School
of Duke University

2021

ABSTRACT

Development of Mucin Analogues to Inhibit the Growth of Calcium Oxalate Kidney Stones

by

Daniel Lee French

Department of Mechanical Engineering and Materials Science
Duke University

Date:_____

Approved:

_____
Stefan Zauscher, Advisor

_____
Michael Lipkin

_____
Pei Zhong

_____
Stephen Craig

_____
Shyni Varghese

An abstract of a dissertation submitted in partial
fulfillment of the requirements for the degree
of Doctor of Philosophy in the Department of
Mechanical Engineering and Materials Science in the Graduate School of
Duke University

2021

Abstract

Kidney stones disease (KSD) is infamous for the morbidity it renders to an afflicted individual by causing intense pain through abrasions the urinary tract during stone passage and/or by causing increased fluid pressure caused by outflow blockage. Symptomatic kidney stones are typically treated through lithotripsy, in which stones are broken into fragments which are small enough for active retrieval or spontaneous passage. However, many individuals experience incomplete passage, and some fragments remain in the kidney indefinitely. These residual stone fragments (RSF) serve as nuclei for further stone growth and cause KSD recurrence. RSFs can grow through two mechanisms: 1) calcium and other ionic stone precursors can directly crystalize on the surface of a fragment, and 2) small urinary crystallites become coated in an adhesive layer of urinary protein and adhere to the RSF. While dietary changes and a variety of medications have been shown to be effective at inhibiting this growth, and ultimately disease recurrence, a lack of patient compliance severely limits the efficacy of these approaches. In this work, we designed an analogue of mucins, biological surface coatings employed by the body as surface protectants and lubricants, to adsorb to the surface of RSFs and inhibit both mechanisms of stone growth. To do so, we performed phage display to identify peptides which bind to kidney stones. We designed genes for these peptides and expressed them as fusion peptides with elastin-like polypeptides to

facilitate expression. We also used a calcium depletion assay to probe their ability to inhibit growth of kidney stone. The peptides discovered by phage display were unable to inhibit growth of RSFs through calcium adsorption. Instead, we used oligoanionic binders to synthesize analogue mucins composed of elastin-like polypeptides and synthetic polymers. We characterized these mucin analogues at each step using a combination of NMR, IR, and GPC when appropriate. Stone-targeted mucin analogues successfully inhibited the growth of calcium oxalate monohydrate stone models. Finally, to monitor adsorption of these mucin analogues to model kidney stones, we functionalized sensors with calcium oxalate monohydrate using polyacrylate as an adhesive layer. In sum, this work explores the ability to synthesize mucin analogues to inhibit recurrent kidney stone disease and have potential to shift the paradigm of kidney stone treatment.

Dedication

This work is dedicated to my wife, Katherine, who is my solace and strength; to my children, Benjamin and Isabel, who are my greatest joy and frustration; and to my parents, Larry and Madonna, who taught me persistence and ethic.

Contents

List of Tables

List of Schemes

List of Figures

List of Abbreviations

AGET	Activators Generated by Electron Transfer
ARGET	Activators ReGenerated by Electron Transfer
ATRP	Atom Transfer Radical Polymerization
BIBOEDS	Bis[2-(2′-bromoisobutyryloxy)ethyl]disulfide
BSA	Bovine Serum Albumin
CKC	An ELP consisting of Collagen tag-ELPK100-Collagen tag
COM	Calcium Oxalate Monohydrate
Cy3	Cyanine 3
DMSO	Dimethyl Sulfoxide
EDTA	Ethylenediaminetetraacetic acid
ELP	Elastin-Like Polypeptide
GEB	Glycine Elution Buffer
GM	Growth Mechanism
IPTG	isopropylthio-β-galactoside
ISA	imidazole-1-sulfonyl azide, HCl salt
ISP	Ionic Stone Precursor
ITC	Inverse Transition Cycling
KSD	Kidney Stone Disease
LB(+T)	Lysogeny Broth (+ Tetracycline)

MA	Mucin Analogue
MALDI-TOF	Matrix Assisted Laser Desorption/Ionization-Time of Flight
MQ	MilliQ-grade water
OA	Osteoarthritis
OPN	Osteopontin
PAA	Poly(Acrylic Acid)
PAcH	Poly(2-aminoethyl methacrylate - co - 2-hydroxyethyl methacrylate)
PAMA	Poly(2-aminoethyl methacrylate)
PHEMA	Poly(2-hydroxyethyl methacrylate)
PMDETA	N,N,N′,N″,N″-Pentamethyldiethylenetriamine
POcF	Poly(oligo(ethylene glycol) methyl ether methacrylate – co – Fluorescein-o-methacrylate)
POEGMA	Poly(oligo(ethylene glycol) methyl ether methacrylate)
PtBA	Poly(tert-butyl acrylate)
(PtBAS)	Poly(tert-butyl acrylate) disulfide
QCM	Quartz Crystal Microbalance
RSF	Residual Stone Fragments
SAM	Self-Assembled Monolayer
SDS-PAGE	Sodium Dodecyl Sulfate Poly(acrylamide) gel electrophoresis

SMCC	Succinimidyl-*trans*-4-(maleimidylmethyl)cyclohexane-1-carboxylate
TBII	Terrific Broth II
TCEP	Tris(2-carboxyethyl)phosphine hydrochloride
THP	Tamm Horsfall Protein
THPTA	(tris-hydroxypropyltriazolylmethylamine)
x-gal	5-bromo-4-chloro-3-indolyl-β-D-galactopyranoside

Acknowledgements

This work would not be possible without the contributions of my mentors, colleagues, and friends who have helped me throughout my doctoral training. I express my heartfelt gratitude to the following:

To Stefan Zauscher, for excellent mentorship, training, and patience;

To the Zauscher Lab, especially Luis Navarro, for comradery, miscellaneous training, and helpful research discussions;

To Michael Lipkin and his colleagues at Duke University Medical Center for guidance in relation to the clinical aspects of my research;

To Farshid Guilak, for initial financial support;

To the Chilkoti Lab, for various training and materials support;

To the Craig Lab, especially Virginia Ritter, for training and assistance with GPC;

And to the Genzer Lab (NCSU), for running GPC in DMF.

1. Introduction

1.1 Overview

The prevalence of kidney stone disease (KSD) has doubled over the past two decades, with an estimated lifetime prevalence of 10.6% in men and 7.1% in women in the United States.[1] Large, symptomatic stones are commonly treated by shock wave lithotripsy and ureteroscopy with laser lithotripsy to fragment stones into pieces that are small enough for active retrieval or spontaneous passage.[2, 3] However, patients are rendered stone free in only 35% to 61% of cases, depending on the type of stone and procedure performed.[4-6] The residual stone fragments (RSF) can nucleate growth of new, symptomatic stones and are frequently the source of recurrent stone events.[7] While approaches to retard this growth, such as medication, increased fluid intake, or dietary restrictions, are generally effective when employed properly, lack of patient compliance and of appropriate patient evaluation severely limit the efficacy of these approaches.[8, 9] Furthermore, urinary stone disease is an economic burden on the healthcare industry, with annual estimated costs surpassing $10 billion as of 2006.[10, 11]

Residual stone fragments are thought to grow through two primary mechanisms.[12] *Growth Mechanism 1 (GM1):* The fragments serve as nuclei for further stone growth via adsorption of urinary ionic stone precursors (such as calcium) from solution. *Growth Mechanism 2 (GM2):* Urinary crystallites adsorb to the surface of the RSF via an adhesive protein coating.

1.2 Aims

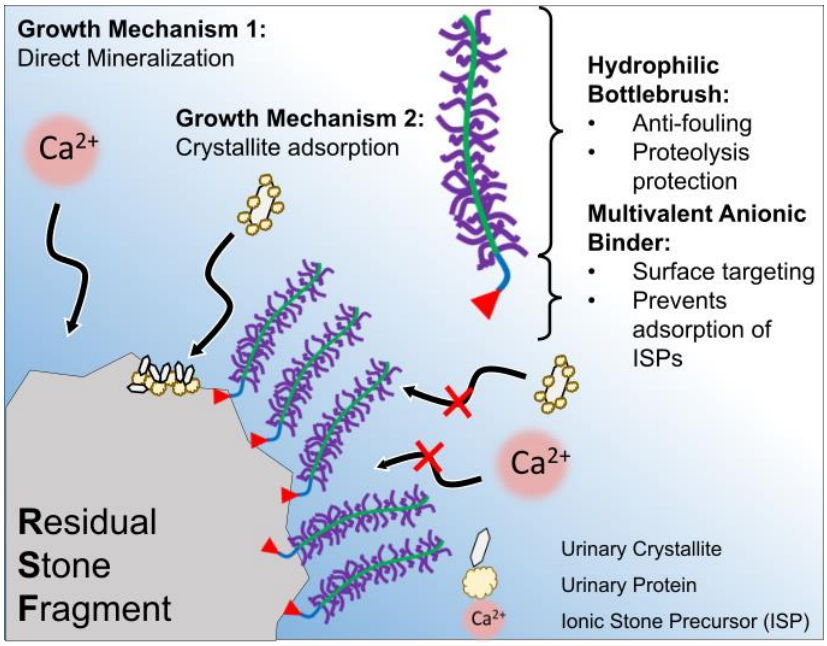

Figure 1: Schematic overview of the design of mucin analogues targeted to calcium oxalate stone fragments resulting from lithotripsy. Mucin analogues are comprised of (1) a multivalent anionic binder, which binds the stone and precents crystal growth and (2) an anti-fouling bottlebrush which prevents adsorption of protein-coated urinary crystallites.

Here, we propose the application of a long-lasting surface coating which addresses these two mechanisms of stone regrowth. Our solution is based on the structure of mucins: *i.e.,* bottlebrush glycoproteins which coat various biological surfaces and provide them with diverse surface-protective properties. We aim to harness the properties of these biological surface coatings and reengineer them to inhibit stone regrowth (Figure 1). The binding moiety of this mucin analogue (MA) is designed to adsorb to mineralized surfaces and to inhibit stone regrowth through direct mineralization (*GM1).* Grafted along the backbone of the MA are anti-fouling polymer

bristles, through which we aim to inhibit the adsorption of protein-coated urinary crystallites (*GM2*). We have broken this task into the following specific aims.

Aim 1: To identify peptide binders for calcium oxalate monohydrate kidney stones. There is a lack of concensus regarding what constitutes an optimal binder for kidney stones. Moreover, what constitutes an optimal binder does not necessarily correlate with strong growth inhibition. In this aim, we perform phage display to identify binders for patient-derived kidney stones which may elude conventional binder design.

Aim 2: To synthesize mucin analogues targeted to calcium oxalate monohydrate kidney stones. Our lab has designed a mucin analogue platform technology which is tunable to various applications. In this aim, we synthesize two sets of mucin analogues using peptide-based and synthetic polymer backbones.

Aim 3: To characterize the binding of stone-targeted mucin analogues and their ability to inhibit mineralization. In this aim, we characterize the ability of our mucin analogue to bind calcium oxalate monohydrate surfaces and to address the two mechanisms of stone regrowth.

The **impact** of this research will be the development of a modular platform technology to inhibit stone regrowth, engendering several unique features: (i) dual mechanism of action (ii) reduced necessity of patient compliance, and (iii) tunability. This will relieve individual patients, who will suffer fewer stone events, and the over-

burdened healthcare industry by reducing the number of patients coming to the emergency department for treatment.

1.3 Significance

For 30 years, the paradigm to combat KSD recurrence has centered around two goals: to more efficiently fragment the stone and to develop novel ways to increase the stone-free rate. To our knowledge, our technology is the first to our knowledge that could provide a long-lasting coating to inhibit kidney stone growth long-term and thus circumvent the reliance on the patient which currently limits the efficacy of traditional techniques to inhibit stone growth such as increased water intake, daily medication, or modified diet.[8, 9] We envision this coating to be delivered through a urinary catheter during lithotripsy or in a clinical setting. This method of delivery is very familiar and accepted by urologists. In the operating room, the injection of materials (typically iodinated contrast agents) into the renal collecting system is a standard part of lithotripsy procedures.[13] Furthermore, urologists frequently perform cystoscopy in the clinic, in which they place a small catheter into the ureter to inject material.[14] This familiarity with the overarching delivery technique should facilitate the adoption of the proposed device in the operating room post-procedure and in the clinic for incidentally identified stones and/or re-administration.

Our ability to control the architecture and chemistry of mucin analogues provides flexibility to optimize their performance for a broad range of applications. The

modularity afforded by our MA platform enables us to independently pair desired backbone function (here, an antifouling bottlebrush) with binding to surfaces of interest, including different stone types, other tissues, or foreign surfaces. In turn, this modularity enables two features of our technology: 1) it allows us to synthesize a homologous series of bottlebrushes for rapid, parallel optimization of the construct, and 2) it allows us to tune our platform technology to applications beyond kidney stone disease including vascular calcification, calcification of renal epithelium, nephrocalcinosis, osteoarthritis, or to prevent fouling of biomedical devices.[15, 16]

1.4 Organization

In this dissertation I describe the work I have done in developing mucin analogues as inhibitors of kidney stone disease. In Chapters 2 and 3, I provide background which will be helpful in understanding the general field of my research as well as some of the considerations that impacted our design and approaches. In Chapters 4-6, I describe the experimental work I have performed to synthesize and characterize mucin analogue coatings. In these chapters, a statement of effort, rationale, results and discussion, detailed methods and conclusion are self-contained. In Chapter 7, I draw global conclusions about my research as a whole and propose future directions for the research. Finally, in Appendix A, I describe the application of similar mucin analogues to addressing the down-regulation of lubricin in osteoarthritis.

2. Kidney Stone Disease

2.1 Prevalence of Kidney Stone Disease

Kidney stone disease (KSD), more properly known as urinary stone disease because stones can exist anywhere throughout the urinary tract, is a well-known morbidity which plagues millions of people worldwide. The prevalence of KSD has doubled over the past two decades, with an estimated lifetime prevalence of 10.6% in men and 7.1% in women in the United States.[17, 18] KSD is frequently associated with significant morbidity, most commonly recurrent bouts of pain associated with stone passage. Additionally, ureteral occlusion by large stones can lead to further complications such as renal failure, infection, sepsis and ureter stricture due to accumulated damage from calculus passage.[19] Beyond a burden for patients, these factors cause urinary stone disease to be an economic burden on the healthcare industry, with annual estimated costs surpassing $10 billion in 2006.[10, 11]

2.2 Onset of Disease and Diagnosis

The presence of stones is typically diagnosed by one of two methods. The primary method of diagnosing the presence of a stone is by the presentation of symptoms, typically including nausea, back pain, and hematuria. Though presentation of symptoms remains the dominant method of stone discovery, recently discovery of asymptomatic stones by computed tomography (CT) has provided a way to monitor stone growth to predict future stone events.[20] Additionally, with the increasing use of

CT to examine the kidney, the incidence of asymptomatic stones is increasing. The natural history of asymptomatic renal stones is such that over 50% will grow and 26% will require surgery.[21]

2.3 Current Primary Treatments of Kidney Stones

Symptomatic stones that are too large for spontaneous passage (typically those above 5 mm) require surgical intervention for their removal. Several surgical techniques exist for stone removal, but most share a common goal: to fragment the stone into pieces which are small enough to pass. In extracorporeal shock wave lithotripsy, which has traditionally been the preferred method of stone fragmentation, a focused acoustic wave is used to create a surface acoustic wave on the stone, providing energy for fragmentation. Recently, however, the use of ureteroscopy with laser lithotripsy has gained popularity, perhaps because of the decreased potential for secondary procedures.[22] Percutaneous removal (removal of the stone through an incision through the back) is a third, albeit less popular, technique.

2.4 Disease Recurrence

Despite numerous procedural and technological advances in the above treatments since their inception, there is often residual stone material which is unable to be cleared from the kidney following a lithotripsy procedure. These residual stone fragments (RSF) can serve as nuclei for stone growth and are frequently the source of recurrent stone events.[7, 23] The stone free rates reported using computed tomography

(CT) after these procedures ranges from only 35% to 61%.[4-6] In a recent study evaluating the natural history of stone fragments following URS, 44% of patients had a complication or secondary procedure within 12 months of the index procedure as a result of the RSFs.[7] The lifetime rate of recurrence is even more alarming – up to 69% of individuals with initial stones will experience multiple instances of KSD.[3] Additionally, a large portion of patients with residual stones post-surgery will experience growth of their fragments and develop symptoms or require additional surgery.[7, 23]

2.4.1 Mechanisms of Stone Regrowth

Residual stone fragments are thought to grow through two primary mechanisms. *Growth Mechanism 1 (GM1):* The fragments serve as nuclei for further stone growth via adsorption of urinary ionic stone precursors (such as calcium) from solution. *Growth Mechanism 2 (GM2):* Urinary crystallites adsorb to the surface of the RSF via an adhesive protein coating.

2.4.2 Natural Inhibitors of Stone Growth

In response to abnormal crystallization in the kidney, several proteins – most notably osteopontin (OPN)[15, 24, 25] and Tamm-Horsfall protein (THP)[26] – are upregulated and secreted into the lumen of the kidney.[16, 25] These proteins bind stone through sequences rich in glutamate and aspartate and the binding of these sequences competes with the addition of stone-forming ions, thereby reducing growth. Others have demonstrated that osteopontin protects against nephrocalcinosis, calcification of renal

epithelium, and even vascular calcification, *in vivo*.[15] THP, ordinarily the most abundant of urinary protein, is a natural inhibitor of both crystal growth and aggregation.[12]

One will note certain similarities between these two proteins which may point toward these special abilities (Figure 2). Both proteins contain numerous oligo-anionic domains for binding stones. Additionally, both proteins are glycosylated, which may serve as anti-fouling moieties to inhibit the adsorption of urinary crystallites.

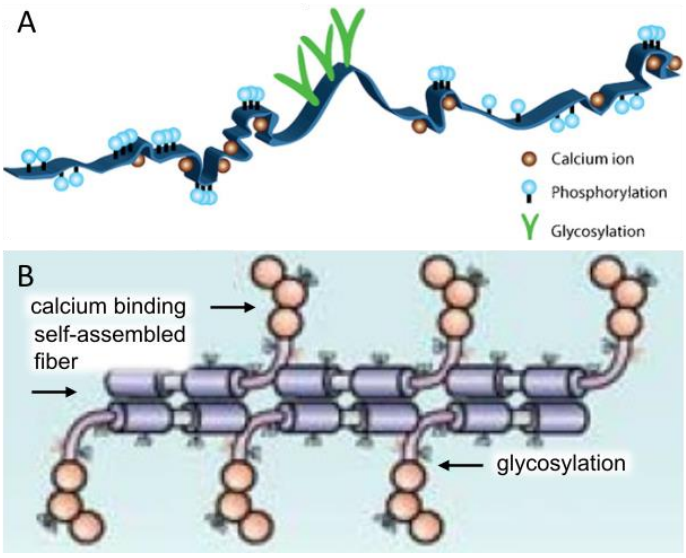

Figure 2: Osteopontin and Tamm-Horsfall Protein: two natural inhibitors of calcium oxalate crystallization. Osteopontin (A) and Tamm-Horsfall Protein (B) have common features which likely contribute to common function, including an extended conformation, calcium binding motifs and glycosylation. Figures reproduced with permission from Klaning[27] and Rampoldi[28], respectively.

2.5 Mitigation of Recurrence

2.5.1 Fragment Removal to Eliminate Nuclei for Stone Growth

Regardless of which primary procedure is used, a surgeon may elect to either allow resulting stone fragments to pass spontaneously or to actively remove them from the kidney. Numerous mechanical devices for the removal of kidney stone fragments are in clinical use. Typically, such devices are baskets (for scooping out fragments) or graspers (for plucking out fragments). However, other methods exist. In one technique, blood is harvested from the patient and injected into the kidney.[29] Upon coagulation, the entire clot-stone complex is removed by a basket or grasper. More recently, others have employed synthetic polymers which emulate this principle, but without the need to harvest blood from the patient.[2] Even more recently, a novel technology has been developed in which magnetic particles decorated with a stone-binding peptide have been used to magnetically pull the stone fragments out of the kidney.[3, 30] In yet another method to facilitate passage, an injectable polymer is crosslinked up-stream of the stone.[31] Fluid then pushes this polymer plug, which is somewhat flexible and forms a tighter seal with the ureter, and the stone along with it out of the urinary system.[31]

These techniques are not without their limitations. Mechanical constraints limit the efficacy of fragment removal, as small fragments can be difficult to grasp with removal tools. Recent evidence utilizing computed tomography (CT) imaging demonstrates that even when active stone fragment retrieval is diligently performed,

patients are rendered stone free in only 35% to 61% of cases.[4-6] A large portion of patients with residual stones post-surgery will experience growth of their fragments and develop symptoms or require a second surgery.[7, 23] Others have demonstrated the possibility of binding iron-oxide particles to stone fragments for magnetic removal,[3, 30] but this technique does not consider particles that may elude capture, as with mechanical removal tools.

2.5.2 Dietary Methods to Inhibit Stone Growth

Due to the ability of residual stone fragments to grow into symptomatic stones, a variety of methods of slowing calculus growth have been developed. Dietary measures to reduce urinary concentrations of stone-forming constituents combat three common risk factors for growth including abnormal urine pH, hyperuria, hypercalciuria.[12, 32] This is done primarily by avoiding certain foods containing these constituents and increasing fluid intake to dilute the urine.[33, 34]

2.5.3 Pharmacological Methods to Inhibit Stone Growth

Because of the threat of USD recurrence, physicians frequently attempt to promote passage of RSFs or the initial stone to curtail the need for surgery. Many approaches involve reducing smooth muscle contraction of the ureter – ideally a more compliant ureter will be easier to pass stones through. Calcium channel blockers have been employed in this regard, as well as to reduce hypercalciuria which may be the original cause of the stone.[35] Alpha-adrenergic blockers have also been used as muscle

relaxants as well with some success, with 80-85% passage for those on muscle relaxers compared to 62-65% on placebo controls.[35] A beta-adrenoreceptor agonist isoproterenol was also shown to facilitate stone passage by reducing smooth muscle contraction of the ureter as well.[36] Furthermore, NSAIDS have been used to reduce ureteral inflammation, and therefore a decrease in ureteral compliance, resulting from stone passage.[35] Thiazide diuretics are prescribed to increase urine volume.[8]

Citrate is commonly prescribed as a daily oral medication. Similar to OPN and THP (and the resulting model peptides), citrate has been shown to inhibit growth by occupying sites on the stone surface which would otherwise be bound by additional stone constituents.[12, 37] However, it has also been shown that citrate may promote crystallite aggregation, making it an imperfect treatment modality for KSD recurrence.[37]

The efficacy of current preventative measures is further limited by lack of appropriate evaluation and poor patient compliance. Very few patients with recurring stones or risk factors for recurrence undergo an appropriate evaluation to determine the cause of their stones; guidelines recommend evaluation with 24 hour urine collections prior to initiating preventative therapy, however only 7% of patients at high risk for stone growth or recurrence perform 24 hour urine collection.[38] Many of the agents prescribed are daily oral medications and, as with many daily regimens, poor patient compliance further contributes to recurrence.[9]

2.5.4 Inhibition of Stone Growth Through Adsorption

To understand how these proteins modulate crystal growth, researchers have focused on the polyanionic binding motifs found in these proteins and discovered that even short anionic peptides[39, 40] and synthetic polymers[41-43] are able to bind stone and inhibit mineralization *in vitro* over short time spans.

In attempting to understand how these proteins modulate crystal growth, researchers have primarily focused on those regions of natural proteins which bind stone, namely regions rich in acidic residues.[39, 40] More recently, cationic peptides have been demonstrated to bind calculi.[44-46] Some of such peptides were capable of inhibiting stone growth, much like their acidic counterparts. However, others actually facilitated stone growth and no concrete link was established between the sequence of these basic peptides and whether they inhibited or facilitated growth. To date there have been only limited studies that elucidate the similarities and differences in how these acidic and basic peptides bind and retard stone growth. For example, Sheng *et al.* have used adhesion-force AFM to determine that guanidino group of arginine and carboxylic acids have highest affinity for the stone, but did not probe whether binding was correlated with stone inhibition.[47] In another study, it was determined that slight differences in sequence can have pronounced effects on crystal growth.[40] These contradictions demonstrate the lack of understanding necessary for a rational design of peptides or peptide-polymer conjugates that bind stone and inhibit stone growth and aggregation.

In addition to peptides, synthetic polymers have been shown to bind stone and inhibit growth. Poly(acrylic acid) (PAA), because of its chemical similarity to the acidic binding motifs of OPN, was one of the initial polymers shown to bind COM and prohibit crystal growth.[41] Since then, vinylsulfonic acid and other poly anionic polymers have been shown to bind and inhibit growth.[42] Some have even studied the effects of PEG-block-PAA adsorption to stones, asserting that the addition of the PEG decreases the ability of the PAA to bind.[43]

3. Mucins and Mucin Analogues

3.1 Statement of Effort

This chapter is adapted from a review published in *Current Opinion in Colloid and Interface Science* with equal contribution from Luis Navarro and with aid from Stefan Zauscher.[48]

3.2 Native Mucins

Mucins are a class of natural surface coatings deployed by the body for a diverse range of functions, including the lubrication of articular joints and within the eye,[49, 50] removal of pathogens from the airway,[49, 51] and facilitation of digestion by creating an appropriate environment for the culture of commensal bacteria.[49, 52] Specifically, we will focus on lubricin,[53-55] which is involved in the protection of articular contacts. As such, this glycoprotein has been the inspiration for many mucin mimics. Secreted by synoviocytes and chondrocytes, lubricin adsorbs onto cartilage surfaces where it offers boundary lubrication, wear protection, and prevents synovial cell overgrowth.[56]

3.2.1 Structure-Function Relationships in Mucins

Despite the functional diversity they exhibit, mucins generally have two preserved structural features which give rise to its function: a central bottlebrush and terminal association domains (Figure 3).[57, 58] A mucin's bulky bottle-brush structure is its defining feature. The core of this structure is a long polypeptide that is rich in proline, threonine, and serine (the "PTS" domain).[49, 59] Threonine and serine provide grafting

points for *O*-linked glycosylation in the Golgi apparatus to create a hydrated bottlebrush structure.[57, 60] These bristles are typically 5-15 units long and frequently capped with negatively-charged sialic acid moieties. Up to 90% of the mucin's large molecular weight (0.25-20 MDa[58]) stems from these oligosaccharides.[61] Thus, the dense packing of these short, yet frequently charged, decorations force the glycoprotein to adopt an extended, rod-like conformation with contour lengths ranging from 100 to 5000 nm.[62] The hydrophilic nature of these bristles contributes to osmotic swelling, which confers many of the functions attributed to mucins. The specific roles of individual mucins may depend on the particular glycosylation pattern of that mucin. This is especially important for mucins which selectively associate with microorganisms. While the physical properties of the bottlebrush are less sensitive to these glycosylation patterns, they contribute strongly to mucin function. For example, the hydration shells provided by oligosaccharide bristles prevent overgrowth of native tissues, microbial adsorption, and biofilm formation.[63] Additionally, swollen mucin networks may act as a depot for enzymes and immunological factors.[64]

The central bottlebrush is flanked by non- or lightly-glycosylated, terminal domains for associating with other macromolecules in solution or on tissue surfaces. For example, oral mucin populations are differentiated as binding hydroxyapatite or soft-tissue surfaces in the enamel pellicle or mucosal pellicle, respectively.[65] Additionally, the non-glycosylated blocks are generally hydrophobic, which facilitates non-specific

gelation and adsorption to hydrophobic surfaces. The frequent presence of cysteine residues in these domains enables chemical crosslinks with other mucins.[57, 58, 66]

In some regards, this general structure is much like our modular platform: different modules can be inserted to each position for a specified biological purpose. For example, Round *et al*.[50] have shown that two mucins in the eye have different surface conformations which arise from a difference in charge density in the carbohydrate brush of each mucin. These mucins are expressed from the same gene (binding and scaffold modules) but are differently modified in the Golgi (bristle modules) to produce two functionally distinct mucins necessary for the eye's function. Similarly, differences in mucin binding modules can lead them to self-assemble into different macrostructures, which can lead to altered function.[51] In another example, mucins in the gut have been shown to form mucin-specific layers on gastric epithelium. The layer in immediate contact with the epithelium is designed to prohibit bacterial attachment while the layer facing the gut lumen is designed to harbor commensal microflora.[49, 52] Some oral mucins have even been shown to bind hydroxyapatite. Various salivary mucins associate with the teeth to assist in lubrication. They also concentrate anti-microbial molecules like lysozyme and cystatin at the mucosal surface for modulation of oral microflora.[64]

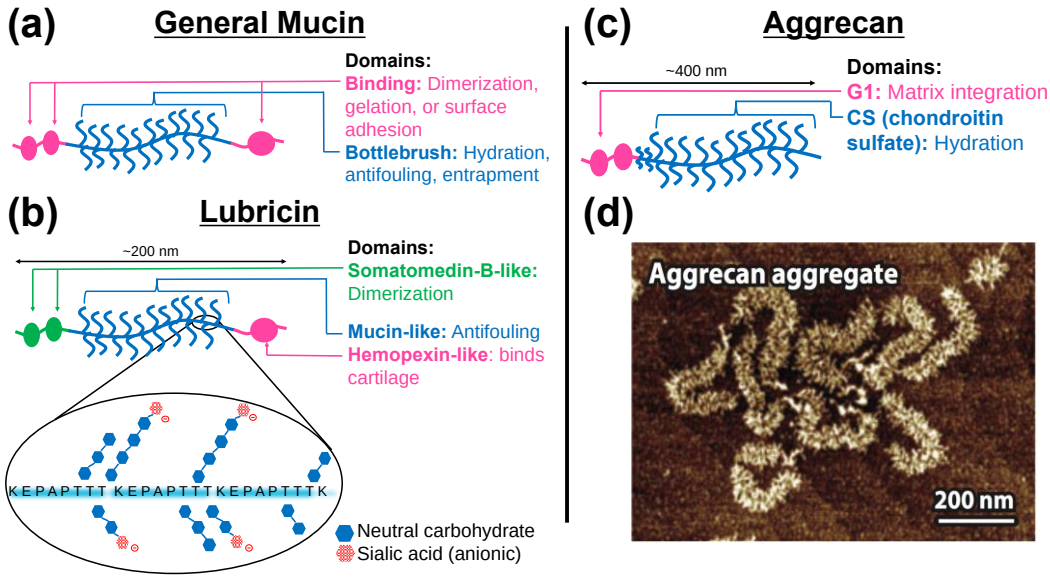

Figure 3: Structures of mucins and mucin-like compounds. (a) A general structure of mucins showing a hydrophilic central brush flanked by relatively hydrophobic domains. (b) Structure of lubricin (proteoglycan-4 or superficial zone protein). (c) Structure of aggrecan. (d) AFM image illustrating the brush-like structure of aggrecan aggregates.[67, 68] Reproduced with permission from Kopesky, copyright Elsevier.

3.2.2 Lubricin

The initial inspiration for our modular construct was lubricin[53-55] — a mucinous glycoprotein secreted by chondrocytes and synoviocytes in the joint,[69] but also found in tendon, and optical aqueous humor—coats biological surfaces, imparting them with lubricious and non-fouling properties. Lubricin shares many of the same architectural features of other mucins, *i.e.*, terminal association domains and a central glycosylated bottlebrush. Its C-terminal hemopexin-like domain binds articular cartilage,[70] and hemopexin itself is known to bind type I collagen[71] and hyaluronan.[72] N-terminal somatomedin B-like domains allow lubricin to form homodimers,[66] but play no role in

cartilage adhesion.[70] The central domain is a heavily glycosylated and negatively charged bottlebrush that is responsible for lubricin's lubricating and anti-fouling properties.[73] Furthermore, lubricin protects cartilage surfaces from wear.[74, 75] This central bottlebrush uses a peptide scaffold containing a repeat sequence of KEPAPTTT, in which the threonine residues are functionalized by o-glycosylation.[60] Carbohydrate bristles bound to lubricin are typically 3 to 7 units long and about 70% are capped with negatively-charged sialic acid.[60] In addition to providing lubrication and wear protection, lubricin has also been shown to prevent fouling by synoviocytes[56] in the joint and bacteria in *in vitro* systems.[76]

Joint injury and disease commonly lead to lubricin deficiency, and the corresponding loss of this protective bottlebrush contributes to further damage in a cascading effect. This is especially true in anterior cruciate ligament injury, after which the concentration of lubricin decreases.[77, 78] This decreased concentration of lubricin is associated with increased damage to the surface of articular cartilage.[74] Thus, there has been substantial interest in using lubricin as a therapeutic to treat osteoarthritis, a chronic joint disease characterized by the deterioration of articular cartilage.[74, 79, 80] Intra-articular injections of native lubricin,[81] recombinant lubricin,[75, 82, 83] and lubricin mimics[80] have been shown to effectively mitigate cartilage degradation, where current treatments fail.[84, 85]

3.2.3 Issues with Using Native Mucins Therapeutically

Several obstacles hinder the study of native mucins and our ability to harness their properties for biomedical or engineering applications, thus motivating the synthesis of mucin analogues. For one, it is challenging to harvest or recombinantly express many mucins. For example, lubricin is typically harvested from the joints of calves in limited yield.[54] This challenge can be addressed by recombinant techniques. However, recombinant glycoproteins require a large degree of post-translational glycosylation, normally achieved through non-trivial and expensive expression in mammalian cells.[82, 86] Furthermore, native mucins suffer from variable glycosylation in both extent and composition,[50, 87, 88] leading to high batch variability. Finally, mucins deteriorate upon isolation and storage, as can be seen in commercial mucins harvested from animals, which often fail to adequately replicate the rheological properties of native mucus.[89] This is further supported by findings of Zappone *et al.*, who observed decreased mucin lubrication after long-term storage and repeated freeze-thaw cycles.[90] Taken as a whole, these issues severely limit the use of native mucins for biomedical applications and limit the systematic study of their structure-property relationships.

3.3 Mucin Analogues

3.3.1 Advantages of Mucin Analogues

The controlled synthesis of mucin mimics can overcome the issues with sample heterogeneity and low yield that plague native mucins. Thus, mimics offer a route to

systematically study mucin structure-property relationships and enable their use for biomedical applications. For example, Schuman *et al.* studied the conformations of MUC1 by using nuclear Overhauser effect spectroscopy of a synthetic peptide with the properly glycosylated MUC1 PDTR (Pro-Asp-Thr-Arg) sequence.[91] They found that glycosylation shifted the peptide from a type I β turn to an extended, nonimmunogenic state. Corzana *et al.* took a similar approach by comparing α-GalNAc-Ser to α-GalNAc-Thr to study *O*-linked glycosylation at serine versus threonine residues.[92] They found the two compounds structured nearby water differently, explaining how antifreeze glycoprotein loses activity when Thr is replaced by Ser. These studies on glycopeptide conformation demonstrate how mucin mimics can be used to elucidate the conformations of native mucins.

While these groups focused on studying mucin conformations, other groups attempt to replicate mucin functions. For instance, Sterner *et al.* studied a polymer that functions as an adhesion layer to elucidate the role of oral mucins in lubricating hydrophobic surfaces.[93] This study demonstrated that preventing friction induced by hydrophobic-hydrophobic contacts is likely a key facet of mucin lubrication. Banquy *et al.* made a purely synthetic analogue of lubricin that mimics its ABA triblock structure.[94] This polymer was able to outperform native lubricin in lubrication, showing that replicating a mucin's architecture, as opposed to its specific chemical structure, can be sufficient to capture mucin physical properties.

Our ability to replicate mucin functions also empowers the design of novel, mucin-like therapeutics. To illustrate this, Lawrence *et al.* made an analogue of lubricin that mimics its ability to link hyaluronan and cartilage, ultimately reducing friction on cartilage.[80] Sharma *et al.* incorporated a similarly structured hyaluronan-binding mimic of aggrecan, and found that it protected synthetic cartilage from proteolytic degradation.[95] Prudnikova *et al.* made PAA-*g*-chondroitin sulfate as an aggrecan analogue that showed a much larger water uptake than aggrecan itself.[96] These examples illustrate the ability of mucin mimics to outperform the mucins that inspired their designs and enable their use as therapeutic agents.

3.3.2 Mucin Analogue Motifs

Several groups have attempted to create synthetic mucins for therapeutic or research purposes. Numerous backbone chemistries (including peptides,[97] carboxyanhydrides,[98] polyacrylate,[93] and vinylpyrrolidone[93]), bristle chemistries (including poly(2-methacryloyloxyethyl phosphorylcholine)[94] and sugars[97, 98]), and anchoring techniques (including peptide recognition,[80] tetrazine-norbornene chemistry,[98] ionic association,[94] and hydrophobic interactions[93, 99]) have been employed. However, regardless of the chemistry used, all were capable of lubrication to some extent, indicating – as we also think – that it is the general structure of lubricin and mucins that is crucial for their function.

We observed that researchers who synthesize mucin analogues focus on mimicking one of four aspects of mucin structure or function, which we categorize as motifs in **Table 1**.[48] *Motif I, Chemical Structure:* Several groups synthesize bottlebrush structures that precisely reflect the characteristic glycosylation patterns in mucins. These studies typically focus on the chemistry involved to make these complicated structures. *Motif II, Monolayer Coatings*: In many approaches, it is preferable to replicate the overall mucin structure rather than the specific chemical glycosylation. To this end, several groups make hydrophilic bottlebrushes with functional terminal domains. These mimics are best suited to study the adsorption behavior, surface conformation, and activity of native mucins that form surface coatings. *Motif III, Gel Formation*: Other mucin mimics employ bristles capable of binding various biomacromolecules, allowing them to mimic the ability of mucins to form gels. *Motif IV, Adhesion Promoter*: In mucin mimics that promote adhesion, two types of side chains are used—one to attach to a surface of interest and the other to recruit a polyelectrolyte from solution. These adhesive mucin mimics are well-suited for studying the interactions of mucins with other native macromolecules or recruiting them to serve specific functions.

Table 1: Mucin Analogue Motifs that are Commonly Employed by the Field

Motif	Role	Application	Mimic Function	Ref.
I	Chemistry	n/a	These mimics focus on recapitulating glycosylation in mucins with high fidelity.	96, 97, 100
II	Monolayer Coatings	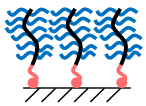	(Terminal) binding domain(s) tether a bottlebrush to a surface from the end(s). These most closely mimic mucin monolayers.	98, 101-111
		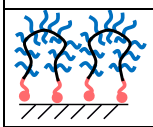		94
		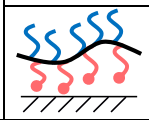		111-114
III	Gel Former	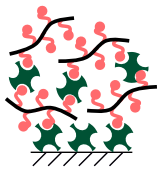	The mimic acts as an adhesive material to make a gel with other biomacromolecules.	115
				95, 116
IV	Adhesion Promoter		The mimic acts purely as an adhesion promoter to recruit polyelectrolytes (*i.e.* hyaluronan or polyvinylpyrrolidone) to a surface.	80, 93

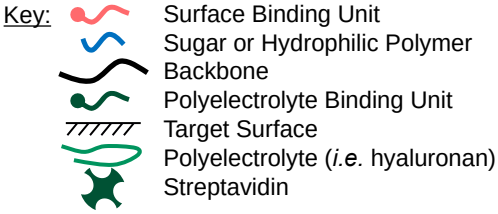

3.3.3 Highlighted Mucin Analogues

3.3.3.1 Biopolymeric Mimics

Since mucins are themselves biomacromolecules, biopolymers are a reasonable starting point for our discussion on mucin-mimics. These mimics are typically sugar-protein conjugates designed to faithfully reproduce mucin composition. Strategies used in their synthesis employ a variety of chemical modifications and coupling reactions to assemble sugars and proteins into a desired structure.

One method, developed by the Panitch lab, is to decorate a chondroitin sulfate backbone with short peptides that have affinity for specific biomacromolecules.[80, 95, 116] Briefly, chondroitin sulfate is oxidized by sodium periodate to reveal reactive aldehyde groups followed by reaction with the heterobifunctional crosslinker BMPH to couple peptides of interest. The goal with these compounds is to mimic the binding capabilities of mucins. In one example, a chondroitin-sulfate backbone is modified with collagen-binding and hyaluronan-binding peptides.[80] When applied to guinea pig cartilage, the collagen-binding peptides anchor the compound to the cartilage surface, while the hyaluronan-binding peptides recruit hyaluronan to the surface. In this context, the mimic acts as an adhesion promoter (*Motif IV)*, thus emulating lubricin's proposed ability to recruit hyaluronan to the surface of cartilage.

Using a similar approach, the Panitch group synthesized an aggrecan mimic that functions in conjunction with hyaluronan and collagen as one of the key constituents of synthetic cartilage.[95, 116] Specifically, the addition of the aggrecan mimic (chondroitin

sulfate-*g*-(hyaluronan binding peptide)) improved bulk mechanical properties,[116] increased proteolytic resistance, and altered chondrocyte gene expression (*Motif III*).[95]

Other biological mimics focus on glycosylating proteins through chemical means. For example, Tachibana *et al.* made glycopolypetides by polymerizing Ala-Thr-Ala trimers with *O*-linked di- or trisaccharides.[97] This approach hinges on the heavy use of acetate and *O*-benzyl protecting groups on the sugar precursor's alcohols to synthesize tripeptide-disaccharides which are subsequently polymerized. The synthetic glycoproteins inhibited the growth of ice crystals depending on the identity of the sugar side chains, just like the antifreeze glycoprotein these compounds were designed to mimic (*Motif I*). While this technique produces high fidelity mimics, it is quite complex and inefficient. Despite the use of high yielding reactions, Tachibana's glycoproteins required 11 to 14 steps to produce, with 10% and 30% total yield, respectively.

In a similar vein, Kramer *et al.* made poly(α-GalNAc-Ser) by polymerization of *O*-glycosylated serines.[98] These polymers were coupled to norbornene-modified proteins embedded in membranes of live mammalian cells using tetrazine head groups (*Motif II*). These compounds have potential application in studies of membrane-tethered mucins. Also using *O*-glycosylated amino acids, Artigas *et al.* synthesized short glycosylated peptides representing one repeat within the mucin scaffold.[100] These glycosylated peptides were used in a custom microarray to assay concentration-dependent associations with various galectins (*Motif I*).

Purely biological mimics have the distinct advantage of staying in the realm of biomolecules, giving them the potential to retain the biocompatibility and biological activity of their parent compounds. Despite this, biological mimics suffer from several key drawbacks. First, biomacromolecules are susceptible to enzymatic degradation, which can dramatically reduce their lifetimes *in vivo*. For instance, Lawrence *et al.*'s lubricin mimic showed an *in vivo* lifetime between 6 hours and one week in guinea pigs.[80] While it is unclear whether this is due to degradation or displacement by other biomacromolecules, this timeframe is too short for treating chronic diseases. Second, although the compounds used are derived solely from biological sources, there is no guarantee that the mimic will avoid immunogenicity when deployed as a biomaterial. This is most evident with collagen-based biomaterials, which frequently suffer from host rejection and contamination with cytotoxic reagents used in their preparation.[117] Lastly, while a plethora of synthetic strategies for controlled coupling of proteins, nucleic acids, and lipids are widely available, the same cannot be said for sugars, as it is difficult to create a bond at a specific position amidst the many alcohols. The typical workarounds are to only use monosaccharides or disaccharides,[98] to heavily use protecting groups,[97] to choose from the limited pool of polysaccharides with reactive head groups,[96] or to use polysaccharides for the backbone instead of the bristles.[116]

3.3.3.2 Synthetic Mimics

Biomacromolecular approaches to mimic mucins are ultimately limited by the range of compatible chemistry available for producing compounds of interest. The next rational step is to use synthetic polymers to imitate key functions or chemical groups of mucins. To date, work with synthetic mucin mimics is predominantly focused on fundamental studies about the mechanisms and architectures that give mucins their properties. In particular, many synthetic mimics focus on boundary lubrication, as polymer brushes are well-known for their lubricating properties. As the precise mechanisms of mucin lubrication are still debated, we direct the reader to other reviews with a more thorough discussion of this nuanced topic.[61, 118, 119]

In one case, Sterner *et al.* prepared polyallylamine modified with perfluorophenylazide side chains as a mucin mimic to study mucin lubrication on glass and Poly(dimethyl siloxane) substrates.[93] This polymer's unreacted amines allowed it to adsorb to the substrates. The polymer was then used as an adhesion promoter to recruit hyaluronan or polyvinylpyrrolidone to the surface (*Motif IV*). This system greatly reduced friction between opposing surfaces and exhibited friction coefficients more than an order of magnitude lower than for bovine submaxillary mucin.

The Seo group recapitulated the function of oral mucins with zwitterionic copolymers containing methacryloyloxyethyl phosphate (MOEP).[101, 102] The phosphate groups in the MOEP comonomers provide adhesion to hydroxyapatite model surfaces,

while zwitterionic comonomers impart antifouling properties to the coating (*Motif II*). These polyzwitterionic coatings reduced *Streptococcus mutans* biofilm formation on hydroxyapatite by over 60%.[101, 102]

Banquy *et al.* made an entirely synthetic mimic of lubricin as an ABA triblock copolymer.[94] Lubricin's heavily glycosylated brush-like domain was modeled using a polyzwitterionic PMPC-based bottlebrush in the B block. To recapitulate the function of adhesive terminal domains of lubricin dimers, Banquy designed a mimic with PDMAEMA side A blocks for electrostatically driven adsorption to mica surfaces (*Motif II*). The triblock copolymer adsorbed to opposing mica surfaces and yielded friction coefficients of $\mu = 0.01$, compared to $\mu = 0.04$ for lubricin. Liu *et al.* made a functionally similar diblock copolymer with a polycationic block to bind negatively charged silica (*Motif II*).[109, 110] A hydrophilic, PEG-based brush block turned the coatings into potent boundary lubricants, exhibiting friction coefficients of $\mu = 0.03$ in water and $\mu = 0.06$ in saline solution. These studies show how mucin architectures can be reduced to simple structural components to reproduce and improve on the function of the original mucin.

Similarly, Samaroo *et al.* made a mimic of lubricin as a thiol-terminated poly(acrylic acid-*g*-PEG) brush polymer and adhered it to bovine cartilage by disulfide bridges (*Motif II*).[103, 104] By exploiting the chemistry used to make these mimics, the researchers probed the effect that brush structural parameters have on adsorption and lubrication. They found that increasing backbone length, bristle length, and bristle

density all impeded adsorption. Surprisingly, these parameters had little correlation with lubrication. This study uniquely highlights the potential of synthetic chemistry to systematically probe relationships between structural parameters and mucin functions.

Current work with synthetic mucin mimics focuses on reducing a mucin to a few key structural components or functional groups. Synthetic polymers offer materials where components can be assigned simple properties like hydrophilicity, charge, and binding affinity without the complexities inherent to the more nuanced structures of proteins and sugars. This makes synthetic mucin mimics ideal for fundamental studies. However, to date, these mimics have limited therapeutic potential. Biocompatibility issues aside, it is difficult to incorporate the specificity required for targeted therapies into purely synthetic polymers.

3.3.3.3 Hybrid Mimics

As seen above, biomacromolecules make it possible to create mucin mimics that can interact with biological systems with a high degree of specificity. Synthetic polymer chemistry offers improved access to controlled architectures and a variety of functional groups. Therefore, hybrid mucin mimics with both biological and synthetic components benefit from the advantages of both with minimal fundamental drawbacks. The architectures of these hybrids can be tailored through the synthetic polymer components, which typically act as either bristles in a mucin-like bottlebrush[107] or as a scaffold for biomolecules.[96, 106] Furthermore, biological components worked into these

hybrids offer a high degree of specificity. These components can include short peptides with affinity to another biomacromolecule,[107] or sugars recognized by certain receptors.[105]

In one case, Prudnikova *et al.* made synthetic aggrecans by grafting chondroitin sulfate to poly(acryloyl chloride) via the polysaccharide's terminal amines (*Motif I*).[96] They were able to achieve up to 80% grafting efficiency after four days, and could control grafting density by the bristle to backbone feed ratio. These polymers showed hydration exceeding that of natural aggrecan, chondroitin sulfate, and hyaluronan while displaying limited cytotoxicity. This study demonstrates how synthetic chemistry provides structure control while biomacromolecules retain their native function.

Poly(methyl vinyl ketone) (PMVK) has attracted attention for making glycoprotein-mimicking hybrids, as it can be directly modified with amine-containing sugars. For example, Chen *et al.* synthetically glycosylated PMVK with α-GalNAc.[105] They also incorporated a lipid head group that allowed the mimic to associate with hydrophobic carbon nanotubes, simulating the integration of cell-surface mucins with cell membranes (*Motif II*). To demonstrate the ability of PMVK to properly display sugars, they further showed that an α-GalNAc receptor specifically recognized nanotubes decorated with PMVK-*g*-α-GalNAc but not with PMVK-*g*-β-GalNAc, despite the subtle difference between α- and β-linked sugars. Similar to Chen, Parthasarathy *et al.* created lipid-terminated P(MVK-*g*-α-GalNAc) mucin mimics.[106] They showed that

their constructs were able to integrate into lipid bilayers and had affinity for an α-GalNAc receptor. They furthermore showed that their mucins were lying flat on the membrane, contrary to native mucins which adopt an extended conformation. Furthermore, by controlling the extent of glycosylation, they were able to tune the polymer's Kuhn length.

Authimoolam *et al.* recreated the network-forming ability of mucins in the oral mucosal pellicle by exploiting streptavidin-biotin coupling.[115] Differing from prior work, they used filomicelles rather than isolated macromolecules as mucin analogs. In this work, a PLA-*b*-PEG block copolymer assembled into filomicelles with a PLA core a PEG corona with 9% of the polymers containing a biotin head group. This enabled layer-by-layer deposition of the filomicelles onto streptavidin-coated polystyrene to create surface-bound, mucus-like networks (*Motif III*). These multilayer coatings promoted adhesion of *Staphylococcus aureus*, while spherical micelles of the same composition inhibited the adhesion.

Each of these studies took advantage of architecture control provided by synthetic polymer chemistry while using biomacromolecules to achieve biological functionality. In doing so, the groups were able to probe the effects of different morphologies, backbone lengths, and bristle densities on the performance of the hybrid mimics. Moreover, by using biological components, these groups were able to incorporate properties absent in fully synthetic approaches, namely molecular

recognition to facilitate supramolecular assembly, surface targeting, and interaction with saccharide-specific receptors.

3.3.3.4 Modular Mimics

As the field evolves, modular synthetic strategies are becoming increasingly important to broaden the applicability of mucin mimics. In the context of hybrid mucin synthesis, modularity is the ability to easily mix and match a wide variety of functional components using a defined set of chemical reactions. Modular approaches enable the synthesis of mucin mimics that can be readily repurposed for different applications by incorporating different structural features or (bio)chemical functionalities. Additionally, modular platforms uniquely enable the systematic study of structure-function relationships in mucins. For these reasons, we see the synthesis of modular hybrids as the natural progression in the synthesis of mucin mimics.

While modularity is an extremely valuable trait, it comes with several requirements. First, modular techniques must use chemistry which is high yielding, tolerant of a wide variety of functional groups, and, for biomedical applications, physiologically compatible. The general class of click reactions are the preferred option for a modular approach.[120] Second, it is critical to consider side reactions introduced with new materials when adapting a modular technique for a specific application. For instance, although copper-catalyzed azide-alkyne cycloaddition is heralded for its specificity and lack of side reactions, even this technique can damage arginine[121] or

histidine[122] side chains in polypeptides. Lastly, it is critical that each component functions independently from the others. This is best illustrated with *Motif II* mimics, which are typically composed of a functional brush and a binding domain that guides adsorption to a surface of interest. For the two structural elements to function independently, the binding domain must dramatically outcompete the brush's interaction with the surface. This can be a challenge with small binding domains, as the slightest brush-surface interaction will be dramatically amplified by the brush's large molecular weight. This is best seen in work by Parthasarathy *et al.* with P(MVK-*g*-(α-GalNAc)), in which the authors found that the macromolecules successfully integrated into a cationic lipid bilayer through a terminal lipid.[106] However, the macromolecule still lied flat on the surface despite the rigidity and hydrophilicity provided by the glycosylation of the backbone, likely due to a weak sugar-bilayer interaction amplified by the large number of pendant sugars.

To illustrate how this modular synthesis strategy can be applied in practice, our lab recently made conjugates of elastin-like polypeptide (ELP) connected to synthetic bottlebrushes (*Motif II*).[107, 123] This technique relies heavily on Huisgen cycloaddition for macromolecular coupling of proteins and synthetic polymers. The key point in this work was to use water-compatible diazotransfer reagents to convert amines in a poly(2-aminoethylmethacrylate) (PAMA) to azides. This allows click reactions to be used both to couple an azide-modified protein to alkyne-terminated PAMA, and to subsequently

graft alkyne-terminated POEGMA bristles to the protein-P(azido-AMA) conjugate backbone. This innovative "double click" approach enabled the efficient conjugation of an azide-containing biomacromolecule to backbone and dense grafting of bristles (~70%). Furthermore, the grafting reaction is highly efficient because the triazole-containing polymer acts as a chelating ligand for the copper, leading to autocatalytic behavior.[124] This modular approach facilitates the synthesis of a variety of mucin mimics by incorporating different protein-based binding domains and bristle polymers.

Taken together, we observe several features which are shared among mucins which we believe will translate to a successful calcium oxalate coating. Mucins have two major domains, one which tethers the molecule to the surface of interest and one which provides anti-fouling character to the surface. These will directly translate to our approach to inhibiting two mechanisms of kidney stone growth, as will be detailed in subsequent chapters. Additionally, there is a rapidly growing field of making mucin-mimicking compounds as replacement therapies, especially for osteoarthritis and joint injury. We aim to learn from these approaches to apply mucin analogues to a surface for which there is not a natural stone coating, calcium oxalate monohydrate kidney stones.

4. Phage Display to Determine Peptide Sequences That Bind Calcium Oxalate Monohydrate Kidney Stones

4.1 Statement of Effort

Work in this section was a joint effort among two undergraduate Pratt Fellows, Andrew Wang and Neil Gupta, and myself. Andrew performed much of the phage display with training, direction, and planning from myself. Andrew and I both analyzed the data. I performed the genetic engineering, protein expression, and calcium assays. Neil synthesized calcium oxalate monohydrate microcrystals.

4.2 Rationale

Oligoanions, especially oligoaspartate, have historically been used as a stone-binding moiety due to the presence of anion-rich sequences in proteins which are commonly found in the proteinaceaous matrix of urinary stones. However, other moieties, especially oligocations, have also been implicated in stone binding.[44-46] Despite these observations, there has been little systematic work to optimize stone binding beyond a small number of influential studies.[39] The lack of such optimization led us to question whether more complex sequences may bind calcium oxalate better than the oligoanions which are commonly used. To determine this, we performed phage display to determine peptide sequences which bind patient-derived kidney stones.

4.3 Results and Discussion

4.3.1 Phage Display

We used phage display[125-127] to identify potential COM binding candidates from a library of over 10^9 potential sequences. To this end, patient-derived stones were collected during the normal course of treatment, and those comprised of at least 90% calcium oxalate monohydrate were reserved for further study under IRB# Pro00064585. These stones were ground and incubated in a library of M13 phage expressing a 7-mer amino acid tag. Following three rounds of phage panning, DNA was harvested from the surviving phage and analyzed to reveal peptides which bind calcium oxalate monohydrate kidney stones.

Table 2: COM-Binding Sequences Discovered by Phage Display

ID	*Sequence*	*Charge (+/-)*	*Kyte-Dolittle*
P1	SKYRADA	(2/1)	-1.5
P2	LPNKETQ	(1/1)	-1.8
P3	AMTAAPN	(0/0)	0.21

While no unique consensus was reached, three peptides were enriched in the population of the final phage titer: SKYRADA (P1), LPNKETQ (P2), and AMTAAPN (P3) (Table 2). The phage display was repeated from the original library, and SKYRADA was again identified as a possible binder, though LPNKETQ and AMTAAPN were not. SKYRADA and LPNKETQ are both zwitterionic species, with (+2/-1) charge on P1 and (+1/-1) on P2. Each of these peptides has only a single acidic residue which contradicts

the currently held paradigm of stone growth modulation research which typically focuses on poly-anionic species.[40] However, previous studies also found that, in some cases, cationic residues were able to bind and inhibit growth, which would agree with the observation of the prevalence of basic residues in our peptides.[44, 45, 128] The presence of asparagine and glutamine in P2 also suggests strength of binding, as these specific amino acids have also been implicated in stone binding.[129] Furthermore, these two sequences are relatively hydrophilic, with Kyte-Doolittle[130] scores of -1.5 and -1.8, respectively, where a more negative score indicates a more hydrophilic peptide. The scale ranges from -4.5 to 4.5 and scores assigned for peptides are reported as the averages of their constituent amino acids. Based on these findings, we are confident that peptides P1 and P2 are promising candidates for stone binding. We are somewhat less confident in P3, an uncharged, hydropathic peptide (Kyte-Doolittle score = 0.21). The divergent nature of these peptide sequences thus provides an interesting platform from which to explore and elucidate similarities and patterns which may be less conspicuous than total charge or hydrophilicity.

To our knowledge, only one other group has performed phage display on COM crystals, and their results serve as a source for comparison and validation of our own findings.[131] As with our experiment, there was a lack of consensus: out of 44 sequences from the latter three rounds of a 6 round experiment, only one sequence was over-represented: LRKHADLPGSLSGRVLARPV. Similar to our peptides, the 20-mer is

highly charged (+4/-1). However, the sequence is only slightly hydrophilic with a Kyte-Doolittle score of -0.125. Among all the 20-mer sequences, the average charge is (+2.54/-1.58), which suggests that net positively charged peptide sequences may be more potent binders of COM than negatively charged sequences. Furthermore, these results suggest that the overall hydropathy of the peptide may be less important for binding, which decreases some concern about P3.

Phage display on other calcium minerals, such as hydroxyapatite, do not appear to correlate well with calcium oxalate monohydrate. Hydroxyapatite-binding peptides in the literature tend to have repeating proline residues,[132, 133] which are similar to the canonical sequence of collagen I, found in bone matrix. However, in some examples (SVSVGMKPSPRP), we still do see repeating charged residues and alcohols interspaced with aliphatic residues.[133] Additionally, the addition of glutamate-rich sequences to such peptides has been shown to increase binding strength of such peptides.[134, 135]

4.3.2 Expression of COM-targeted Peptide Binders as ELP-fusion Peptides

We synthesized binder-ELP hybrid polypeptides to facilitate ease of synthesis and to model a situation in which a large non-binding polypeptide might interfere with the binding of our peptide to the surface of COM stones, as might be the case when incorporated into bottlebrush moieties. Using traditional genetic engineering and peptide synthesis techniques outlined in section 5.5, we synthesized binder-ELP hybrids for further analysis. Molecular weight and sample purity were confirmed using

MALDI-TOF (Table 3) and SDS-PAGE (**Error! Reference source not found.**Figure 4), respectively. Surprisingly, gel migration did not correspond to the relative molecular weights of the peptides. Specifically, the control ELP4-30 appears higher molecular weight than any of the test peptides and A-tag appears higher molecular weight than either S-tag or L-tag. This may be because those two peptides are uncharged and may thus migrate at a slightly different rate than the two charged peptides. However, the MW obtained by MALDI was generally in accordance with the calculated molecular weight of each peptide.

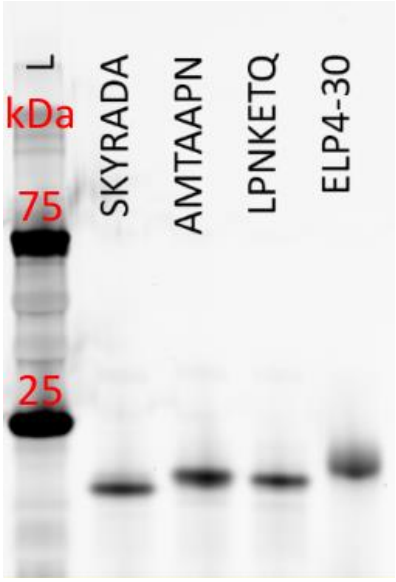

Figure 4: SDS-PAGE of ELP-binder hybrids.

Table 3: Peptide Sequence and Molecular Weights of ELP-Binder Hybrids

Abbreviation	*Sequence*	*Theoretical MW*	*MALDI MW*
S-tag	$(GVGVP)_{30}(GGGS)_2$**SKYRADA**GGY	14031	14087
L-tag	$(GVGVP)_{30}(GGGS)_2$**LPNKETQ**GGY	14092	14103
A-tag	$(GVGVP)_{30}(GGGS)_2$**AMTAAPN**GGY	13938	13946
E4-30	$(GVGVP)_{30}$GY	12508	12512

The transition temperatures of the peptides (S-tag: 51.3°C; A-tag: 52.3°C; L-tag: 56.7°C; ELP4-30: 44.3 °C) were measured in solution conditions which mirrored those used in crystallization assays (Section 4.3.4). While the dramatic increase was unexpected for the relatively small addition to the peptide, none of the transition temperatures are low enough to complicate characterization at body temperature.

4.3.3 Fabrication of Calcium Oxalate Monohydrate Seed Crystals

To provide a surface to nucleate growth in a calcium depletion assay, we synthesized calcium oxalate monohydrate seed crystals according to established protocols.[136] Seed particles ranged from 5-7 um in the long direction and were the characteristic shape of COM (**Error! Reference source not found.**). Because of the irregular shape of COM crystals, more traditional methods of microparticle size determination, such as light scattering or tunable resistive pulse sensing,[137] would be

inaccurate. The crystals were additionally confirmed as COM using infrared spectroscopy (**Error! Reference source not found.**).

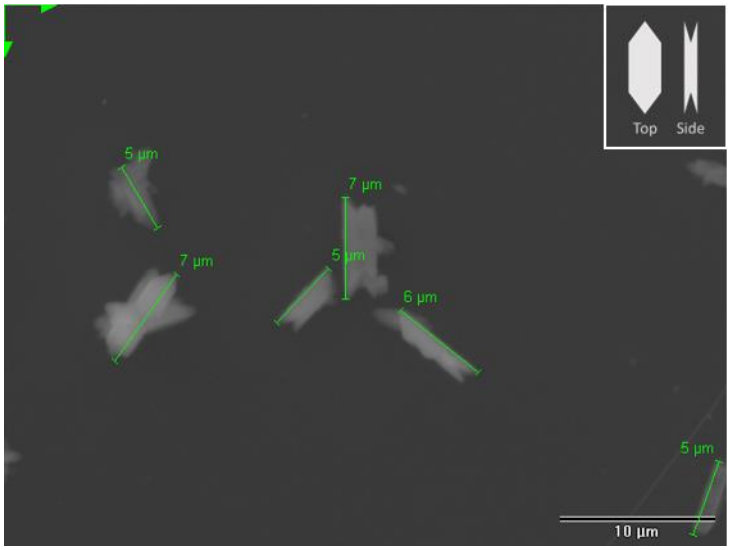

Figure 5: SEM micrograph of COM seed crystals. Crystallites are identified by shape characteristic of crystalline COM, as depicted in the insert.

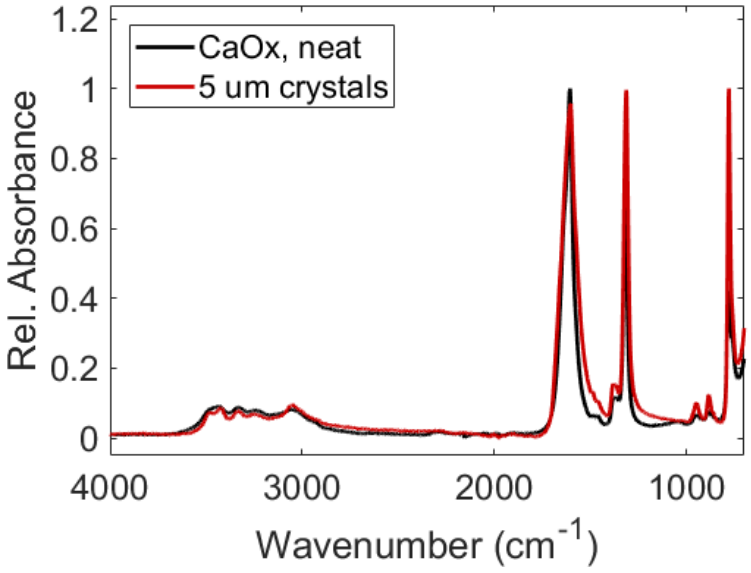

Figure 6: Infrared spectrum of COM seed crystals.

4.3.4 Inhibitory Effect of Binder-ELP Hybrids

We next examined the ability of our test peptides to modulate stone growth. In total, seven potential inhibitors (our four peptide tags, citrate, oligoaspartate (D10), and poly(acrylic acid)(PAA)) were tested in quadruplicate at three different concentrations. A set of four samples with no inhibitor (only water to maintain equal concentrations) was used as a baseline for crystallization. Finally, samples with no oxalate or calcium precursor served as positive and negative controls, respectively. Measurements were taken over 12 hours.

Across all concentrations, the two most potent inhibitors of crystallization were D10 and pAA (**Error! Reference source not found.**). Though they did not inhibit crystallization as much as D10 or poly-acrylate, the COM-binding tags did inhibit COM crystallization compared to the control with no inhibitor, especially in lower concentrations. However, we note that all peptides performed similarly to ELP4-30 with no COM binder. Therefore, one might postulate that the fusion of our peptide tags with ELP (and ultimately our MA) may inhibit their ability to bind COM stone. An alternate explanation for this behavior is the way we normalized analyte concentrations. Citrate and pAA, as polyelectrolytes, were normalized to the ionic strength of D10. Conversely, our peptide tags varied greatly in charge. To more directly address which tag would serve as a better binding module, they were normalized to the molar concentration of D10. Because of this difference in normalization procedure, the total ionic strength of

our charged peptides is quite low compared to our controls. If ionic strength is, in fact, the most important factor for stone binding, these peptides would therefore be at a lower effective concentration than the controls.

It was observed in this work that none of the phage-displayed peptides inhibited crystal growth compared to the ELP tail alone. Though we adjusted the concentration to keep the total ionic concentration comparable to the citrate control, it may be that the peptides were too short or neutrally charged to overcome the steric hindrance provided by the ELP tail. This may be rectified by including multiple tags in series or repeating phage display with a library containing longer peptides. It may also be that the peptides did, in fact, successfully bind the COM seed crystals but did not inhibit growth. This has been demonstrated for additional peptides which were derived from proteins discovered in the proteinaceous matrix of patient-derived stones.[45] To determine which of these is the case, we will reexamine the binding and stone inhibition of the ELP-free peptides using isothermal titration calorimetry and the calcium assay, respectively. To determine whether a longer peptide is needed, one could produce peptides with several iterations of the desired sequences in series, with or without peptide spacers. If it is determined that the peptides do bind, but do not inhibit crystal growth, they still may be useful to help anchor the MA to the surface and may be used in combination with PAA if necessary by coupling peptides at differing ratios to the PAA via carboimide crosslinking chemistry.

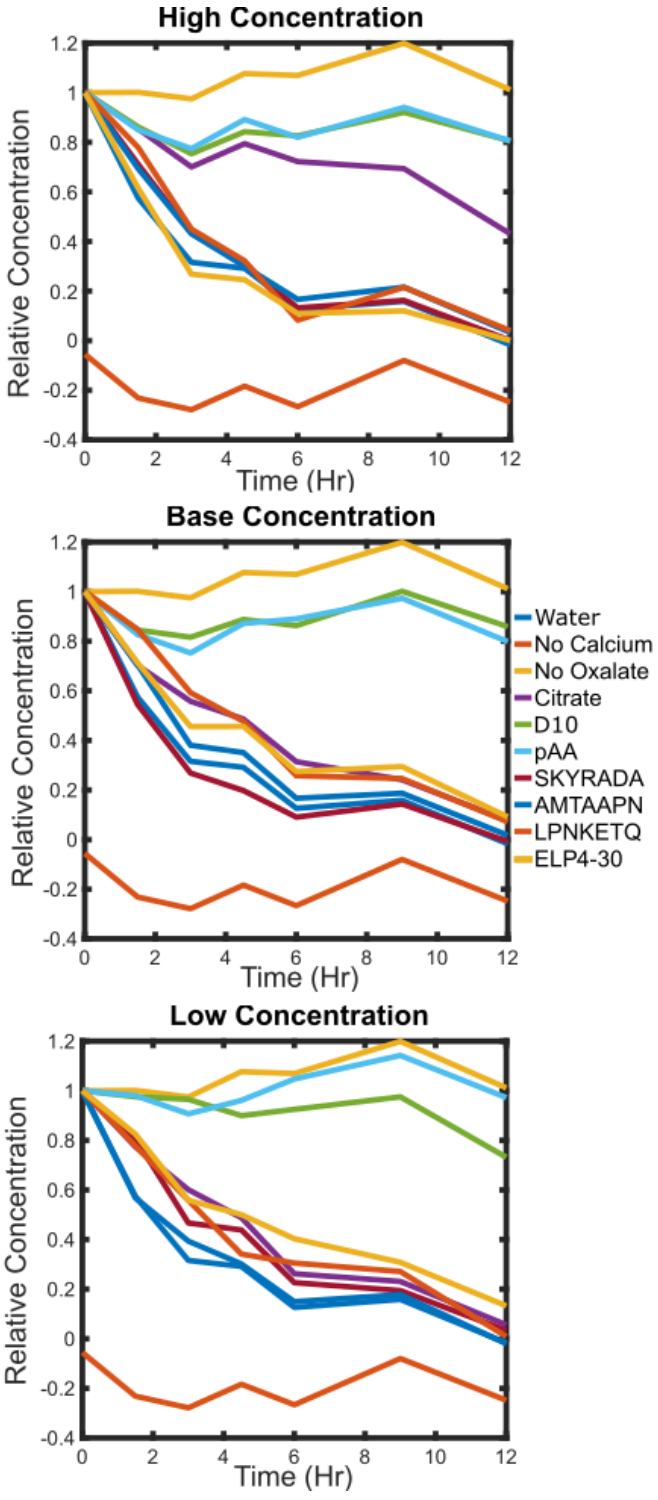

Figure 7: Mineral inhibition of ELP-binder hybrids.

4.4 Materials and Methods

4.4.1 Materials

All materials not specifically listed here are listed in sections which describe the specific methods which use those materials. This is specifically true for genetic engineering, protein expression, and the calcium assay. Detailed methods for these activities are organized thematically into different chapters and sections. Here, I direct the reader to those sections when appropriate.

Forward and reverse oligonucleotides encoding for SKYRADA, LPNKETQ, and AMTAAPN flanked by GGGS spacers were purchased from Integrated DNA Technologies (IDT) and used as received. A JMD2 plasmid containing a gene for $(VPGVG)_{30}$ (hereafter, "ELP4-30") was obtained from Ali Ghoorchian, a post-doctoral researcher with the Research Triangle Materials Research Education and Science Center (RT-MRSEC).

5-bromo-4-chloro-3-indolyl-β-D-galactopyranoside (x-gal, GoldBiotechnology), Bacto™ agar (Becton Dickinson), bovine serum albumin (BSA, BioReagent, Sigma-Aldrich), glycerol (99.5%, EM Science), glycine ("UltraPure™, Invitrogen), LB medium (MOBio), PhD7 phage display kit (New England Biolabs; contains Phage Display 7-mer peptide library, -96 gIII sequencing primer, -28 gIII sequencing primer, E. coli ER2738, and streptavidin), poly(ethylene glycol) (8000 Da, BioUltra, Sigma-Aldrich), sodium azide (99.5%, Sigma-Aldrich), sodium iodide (99.5%, Sigma-Aldrich), tetracycline HCl

(molecular biology grade, GoldBiotechnology), tris-buffered saline (10x concentrate, Sigma-Aldrich), tris-HCl (molecular biology grade, Promega), tween-20 (BioXtra, Sigma-Aldrich) were used as received.

4.4.2 Phage Display

4.4.2.1 Phage Panning

Phage display was performed per instructions accompanying the PhD7 phage display kit. 10 mL LB medium supplemented with tetracycline (20 mg/L, LB+T) was inoculated with a frozen stock of ER2738 cells and shaken at 37°C for 5-10 hours. Meanwhile, patient-derived kidney stones (verified minimum 90% calcium oxalate monohydrate by infrared spectroscopy prior to our taking possession) were collected from the operating room and ground into a fine powder using an agate mortar and pestle. A small amount of the powder (approximately 50 mg) was added to a microcentrifuge tube and resuspended in tris-buffered saline with 0.1% Tween-20 (0.1% TBST) by flicking. The resuspension was centrifuged for 30 seconds using a low-speed benchtop centrifuge. The supernatant was removed by pipette. The COM pellet was resuspended in 1 mL blocking buffer (5 mg/mL BSA, 0.02% NaN_3, $NaHCO_3$, pH 8.6) and incubated at 4°C for one hour. The ground stone was pelleted and washed in 0.1% TBST 5 times by iterative pelleting and resuspension. After washing, the pellet was resuspended in a 100-fold overrepresentation of the provided phage library in 100 μL TBS. The pellet was gently mixed and incubated for 15 minutes at room temperature,

mixing occasionally. The ground stone was pelleted and washed 10 times with 0.1% TBST. Bound phage was eluted by suspending the stone in 1 mL glycine elution buffer (GEB, 0.2 M glycine HCl, 1 mg/mL BSA, pH 2.2) and incubating 10 minutes at room temperature. The ground stone was pelleted; the supernatant was transferred to a new microcentrifuge tube and neutralized with 150 μL 1M Tris-HCl, pH 9.1. The phage solution was stored overnight at 4°C. 5 mL LB+T was inoculated with the culture from earlier in the day and grown overnight.

4.4.2.2 Phage Amplification

200 μL cell culture and the phage eluate were diluted in 20 mL LB+T and was shaken at 37°C for 4.5 hours. The culture was transferred to a centrifuge tube and spun at 12,000 RCF at 4°C. The top 80% of supernatant was transferred to a fresh centrifuge tube, to which was added 3.5 mL 20% PEG8000/2 M NaCl and allowed to incubate at 4°C overnight to precipitate the phage.

4.4.2.3 Phage Purification

5 mL LB+T was inoculated with ER2738 from a plate streaked the previous night and shaken for 4.5 hours at 37°C. The phage precipitate was collected by centrifugation and the supernatant discarded. The pellet was resuspended in 1 mL TBS, transferred to a fresh microcentrifuge tube and re-centrifuged to remove any non-dissolving solids. The supernatant was transferred to a fresh tube and reprecipitated with 167 μL PEG/NaCl solution. The solution was incubated on ice for one hour. Meanwhile, a 7

mg/mL solution of bactoagar in LB was melted using a microwave and maintained at 45°C. The precipitated phage was collected by centrifugation and resuspended in 200 μL TBS. The solution was recentrifuged and the supernatant transferred to a new tube. This amplified phage was stored in 1:1 glycerol solution at -20°C. The phage titer was calculated by making serial dilutions of the phage from 10x to 1000x. 10 μL of each dilution was added to 200 μL of the incubated ER2738, vortexed quickly and incubated for 3 minutes. The infected cells were transferred to the bactoagar solution, vortexed briefly and poured over pre-warmed LB/IPTG/X-gal plates. After tilting the plates to evenly spread the agar, they were left to solidify for 5 to 10 minutes, then incubated overnight at 37°C. Titer was calculated by counting plaques on each plate and multiplying by the dilution factor. Two subsequent rounds of phage display were performed using 0.5% TBST.

4.4.2.4 Phage Sequencing

200 μL overnight ER2738 culture were incubated in 20 mL LB, then dispersed into 1 mL fractions. A blue plaque from a final titer plate was stabbed and used to inoculate each of the fractions. Cultures were shaken for 4.5 hours at 37°C, then pelleted by centrifugation. The supernatant was added to a fresh tube and re-spun. 500 μL from the top of the centrifugation was added to 200 μL PEG/NaCl to precipitate the phage, mixed, and then incubated 15 minutes at room temperature. The solution was centrifuged, and the supernatant discarded. The pelleted phage were lysed in 100 μL

freshly-prepared iodide buffer (10 mM Tris-HCl, 1 mM EDTA, 4 M NaI, pH 8.0). 250 μL ethanol was added and incubated for 15 minutes at room temperature to precipitate the phage DNA. The precipitated DNA was collected by centrifugation. The supernatant was discarded, and the pellet was dried briefly under vacuum. The DNA pellet was resuspended in 30 μL milli-q grade water. DNA concentration was calculated by nanodrop and submitted for sequencing using custom-made primers.

4.4.3 Genetic Engineering and Peptide Expression

See section 5.3.3 for general methods of genetic engineering and peptide expression. Using PReRDL[138], these genes were coupled to give the final sequences described. Protein was expressed in LB medium without supplementation with n-acetylcysteine. Transition temperature was measured using a Cary Series 300 UV-VIS Spectrophotometer (Agilent Technologies) in accordance with the conditions relevant to the calcium assay (0.13 mM protein, 150 mM NaCl, 10 mM sodium cacodylate, 1 mM Na_2Ox). Data were collected using Cary WinUV (Agilent) and spectra were analyzed using MATLAB student edition.

4.4.4 Calcium Oxalate Monohydrate Crystallite Formation

Crystals were synthesized using procedures adapted from Sun et al.[136] 20 mM calcium chloride and sodium oxalate precursor precursors in pure water were heated to 60°C in a water bath. After reaching temperature, the calcium precursor was added to the oxalate precursor while stirring at 1250 rpm. The mixture was stirred for 10 minutes,

then stored until use. Immediately prior to use, the particles were centrifuged and resuspended 3 times to remove NaCl from solution. Crystals were characterized via scanning electron microscopy using an FEI XL30 ESEM with Bruker XFlash 4010 EDS and infrared spectroscopy.

4.4.5 Calcium Assay

See Section 6.5 for general methods used for calcium assays.

4.5 Conclusions

There remains a lack of consensus concerning the fundamental relationship governing peptide adhesion to mineral. Though there is general agreement that anionic residues adhere well to mineral surfaces, especially calcium-based minerals, peptides containing positively charged amino acids have been shown to both promote and inhibit mineralization. Furthermore, what is known for individual amino acids has not informed peptide design sufficiently to enable *de novo* binder design. This is particularly true concerning peptides with a mix of positive, negative, and neutral residues. The contribution of the order of these charge states in a peptide to the strength of adhesion and effects on mineralization remain poorly understood. This work seems to suggest that an alternation of charge, including spacing with neutral residues, is favored for adhesion strength.

However, strength of adhesion does not necessarily correlate with anti-mineralization properties.[45] Though I observed reproducible enrichment of certain

peptides against calcium oxalate monohydrate kidney stones, none of the peptides inhibited mineralization more than that of a non-binding ELP control. In light of these results, I opted to use oligoanions, such as oligoaspartate (D_{10}, hereafter "D10") and poly(acrylic acid), for the remainder of this work.

5. Synthesis of Mucin Analogues Targeting Calcium Oxalate Monohydrate Kidney Stones

5.1 Statement of Effort

The work detailed in this chapter is my own with the exception of the following reagents I used in my synthesis, which were synthesized by Luis Navarro: 1-sulfonyl azide hydrochloride (ISA), tris-hydroxypropyltriazolylmethylamine (THPTA), 2-aminoethyl methacrylate (AMA), alkyne-initiated poly(oligoethyleneglycol methylether methacrylate) (alkyne-POEGMA), and 3-(Triisopropylsilyl)-2-propynyl-2-bromo-2-methylpropanoate (hereafter, "alkyne initiator").[107]

5.2 Rationale

Though the general architecture of mucins is fairly conserved, diversity in the individual "modules" of natural mucins – binding, scaffold, and glycosylation – have been tuned to diverse functions within the body. By altering binding modules, for instance, mucins are able to bind different tissue surfaces, crosslink, or bind solution proteins.[49, 139] By altering glycosylation patterns, mucins in the gut have been shown to form two distinct layers.[59] One, adjacent to the endothelium, forms a barrier against microbial infection. Sitting on top of this base layer is a layer of mucin which facilitates a suitable environment for colonialization of commensal microflora.[52]

Drawing inspiration from the modularity exhibited by natural mucins, we hypothesized that an equally modular analogue mucin platform should be tunable to

the application of choice. Moreover, a grafting-to approach for bottle brush synthesis allows for stocks of bristle to be mix-and-matched with different backbones, amplifying the number of different constructs to explore. We created a generalized mucin analogue synthesis strategy for creating mucins which would adsorb to biotinylated model surfaces.[48, 107] Our modular platform engenders three general structural features preserved among mucins[57] which we, and others, have identified as key to their function: 1) a polypeptide backbone containing at least one "association" block for binding surfaces or other proteins and 2) a highly repetitive grafting domain which is decorated with 3) hydrophilic bristles.

Here, we propose to adapt our MA platform to create a long-lasting coating which retards urinary stone growth. In this modular design, multivalent anionic oligomeric binders are coupled to the cysteine residues of a long diblock elastin-like polypeptide backbone (ELP[$(K)_{5n}(VC)_{8m}$]) via hetero-bifunctional maleimide-NHS crosslinkers. Initially, we will use oligo-aspartate (oAsp, D10) —a much-studied inhibitor of crystal growth due to its homology with OPN and THP— as our binder.

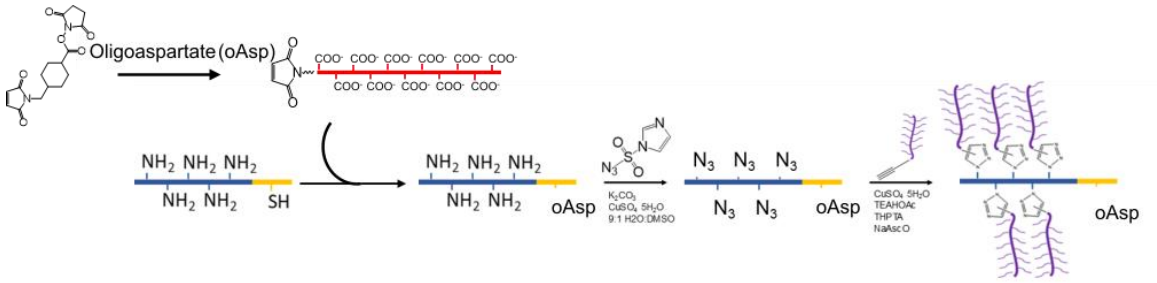

Scheme 1: General Strategy for ELP-based Mucin Analogues. We use orthogonal bioconjugation techniques to couple (1) anionic binders and (2) antifouling bristles using SMCC and diazotransfer/Huisgen cycloaddition, respectively.

My initial strategy for synthesizing mucin analogues was to use elastin-like polypeptides as the main component of the MA backbone (Scheme 1). By using a peptide scaffold, we avail ourselves to diverse chemical functionality with which we can incorporate binding, crosslinking, and scaffolding functionalities into a single backbone molecule. Using this strategy, we can use conventional genetic engineering techniques to easily modify the order and identity of modules in the backbone, and therefore tune it to the intended application with exact sequence control. In Section 5.3 we show a lysine-rich elastin-like polypeptide which provides evenly-spaced grafting points through the pendant primary amines of the lysine residue. Our MA platform is, to our knowledge, the first to adapt the modularity of the mucin architecture into a bio-synthetic platform engineering techniques to easily adjust the arrangement of our backbone, and therefore tune it to the intended application with exact sequence control. Second, this arrangement is stored as genetic information, guaranteeing batch-to-batch consistency.

However, a side reaction ultimately limited the practicality of this approach and prompted us to adopt the fully-synthetic construct described in Section 5.4 (Scheme 2).

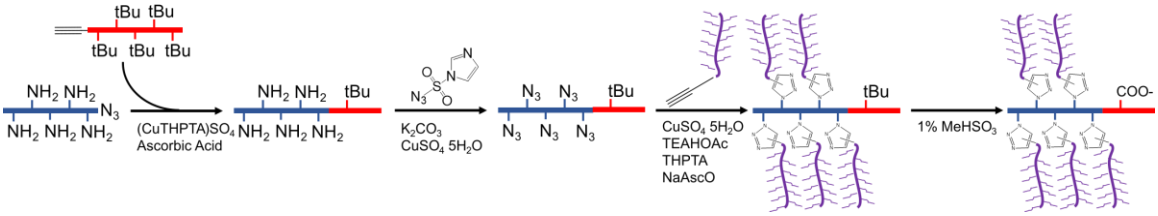

Scheme 2: General Scheme for Mucin Analogues using Synthetic Backbones. We synthesize mucin analogues using sequential click reactions to incorporate PtBA and POEGMA antifouling bristles. PtBA is then hydrolyzed to give an oligoanionic binder.

5.3 Synthesis of Mucin Analogues using Elastin-like Polypeptide Backbones

5.3.1 Genetic Design and Synthesis of $(VPGKG)_{50}(VPGVGVPGCG)_8$ (ELPK50x8)

We used recursive directional ligation by plasmid reconstruction (PReRDL)[138] to construct the gene for the backbone $(VPGKG)_{50}(VPGVGVPGCG)_8$ (hereafter, "ELPK50x8"). A gene containing 5 inserts of the VPGKG repeat was designed to have overhangs compatible with PReRDL and to avoid cut sites for enzymes used in PReRDL. Special care was also taken to maximize the melting temperature of the desired dimer while lowering the transition temperature of any hairpins or "mis-matched" dimers.

The forward and reverse oligonucleotides were annealed and inserted into an opened JMD2 plasmid. In this process, a random number of inserts can concatenate to form genes with different number of inserts because of the symmetrical overhangs. We

were fortunate to have had five inserts (25 repeats total) in our first round. This length was doubled to ELPK50, and finally we added a gene for a cysteine-rich ELP to the n-terminus of the peptide, which was donated by the Chilkoti Laboratory.

5.3.2 Expression of ELPK50x8

ELPK50x8 was expressed in 2x YT medium supplemented with n-acetyl cysteine. In previous work with lysine-based ELPs, we observed very low yield of around 7 mg/ml under normal conditions used at the time for ELP expression (data not shown). We believe that this is due to the high charge density of the peptide. To enhance the expression of lysine based ELP backbones, we include a short leader sequence of GGGS to the peptide. This flexible linker is commonly used to enhance the folding and stability of fusion proteins,[140] and was initially included as part of the binding sequences for the collagen-I targeting moieties described in appendix A. We additionally modify our growth media, switching from TBII to 2x YT and supplementing media with n-acetyl cysteine. Using these modifications, we were able to increase expression yield by over an order of magnitude to 125 mg/L.

Lysine-based elastin-like polypeptides additionally have a very high transition temperature because of their charge and overall hydrophilicity. We therefore neutralize the primary amine of the lysine residues by transitioning the ELP under basic conditions and with sodium sulfate. Sodium sulfate is a highly chaotropic salt, meaning it is more effective at disrupting the hydration shell of the ELP and lowering the transition

temperature.[141] Finally, we perform a "bake-out" immediately prior to the hot spin in inverse transition cycling by incubating the transitioned peptide for 30 minutes at 37°C.

These solutions for increasing final ELP yield in cysteine-free ELPs significantly hindered the final yields obtained for ELPK50x8. We observed irreversible crosslinking at multiple steps of expression and subsequent functionalization reactions. Upon initial lysing of the bacterial pellet, we observed a lysate which was much more viscous than previous ELPK constructs. Additionally, pellets after transitioning were very difficult to redissolve because of crosslinking. Disulfide bridges are favored under basic conditions which are naturally present through the numerous lysines and further enhanced to lower the transition temperature of the ELP. To break up the aggregates, we attempted to reduce the disulfides using TCEP with mixed results. However, we were able to express ELPK50x8, albeit at limited yield.

We did observe a consistent pattern of bands at lower molecular weights with relatively even spacing in all of our lysine-based elastin-like polypeptides (Figure 8). We have hypothesized that this "banding pattern" is the result of endotoxin contamination resulting from expression in *E. coli*. However, the pattern persists even after treating the peptide with an endotoxin-removal resin (data not shown). If not an artifact, this pattern would indicate that the tail-end of the ELP is not expressed, which would create ELPs which lack the appropriate functionality to incorporate surface binding motifs. This, in turn, would artificially inflate the concentration of the full mucin analogue

which is capable of surface adsorption and skewing any adsorption equilibria which may be measured.

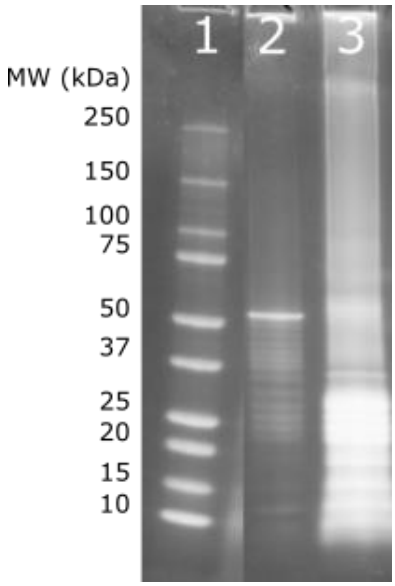

Figure 8: SDS-PAGE of CKC and K50x8. Lane 1: Ladder, Lane 2: CKC, Lane 3: ELPK50x8. The most intense top band corresponds to the theoretical molecular weight of the peptide. However, we also observe a consistent banding pattern at lower molecular weights.

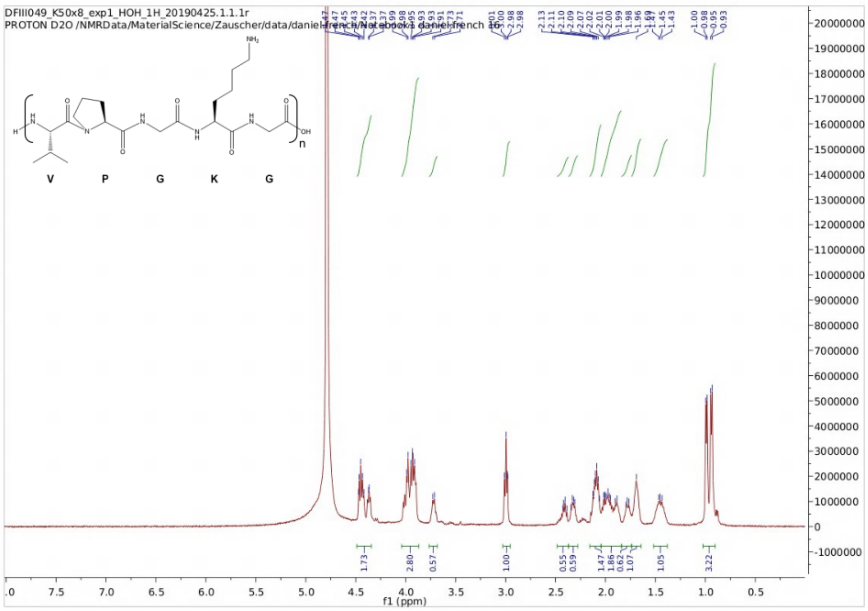

Figure 9: ^{1}H NMR of ELP50x8. Key peaks for further analysis include the triplet at 3.0, corresponding to the final CH_2 of lysine and the doublet-of-doublets at 1.0, corresponding to the valine CH_3.

5.3.3 Oligo-aspartate Binder Attachment via a Hetero-bifunctional Crosslinker

We functionalized K50x8 with oligoaspartate binders, which are known to adsorb to COM stones and to inhibit growth of COM crystallites. To do so, we first functionalized D10 with (succinimidyl 4-[N-maleimidomethyl]cyclohexane-1-carboxylate) (SMCC, a heterobifunctional crosslinker). Briefly, D10 and SMCC were stirred in DMSO for two hours at room temperature, purified by dialysis and lyophilized.

The efficiency of the coupling of SMCC to D10 was middling. The combination of the amide peaks from the D10 peptide around 1600 cm^{-1} and the peak from SMCC at around 1700 cm^{-1} demonstrates the coupling (Figure 45, Appendix C). Moreover, the

NMR peak integration (Figure 10) between the peaks at 0.85 and 0.97 ppm, corresponding to a proprietary initiator present in the D10 peptide and one set of two carbons in the cyclohexyl group of the SMCC indicates reaction efficiency of 43%. We attribute this low reaction completion to solvent incompatibility between DMSO and the D10 peptide, as a slight haziness was observed during the reaction. In this purified product, an excess of unmodified D10 is present which can cause gelation when introduced to the positive charge of ELPK50x8.

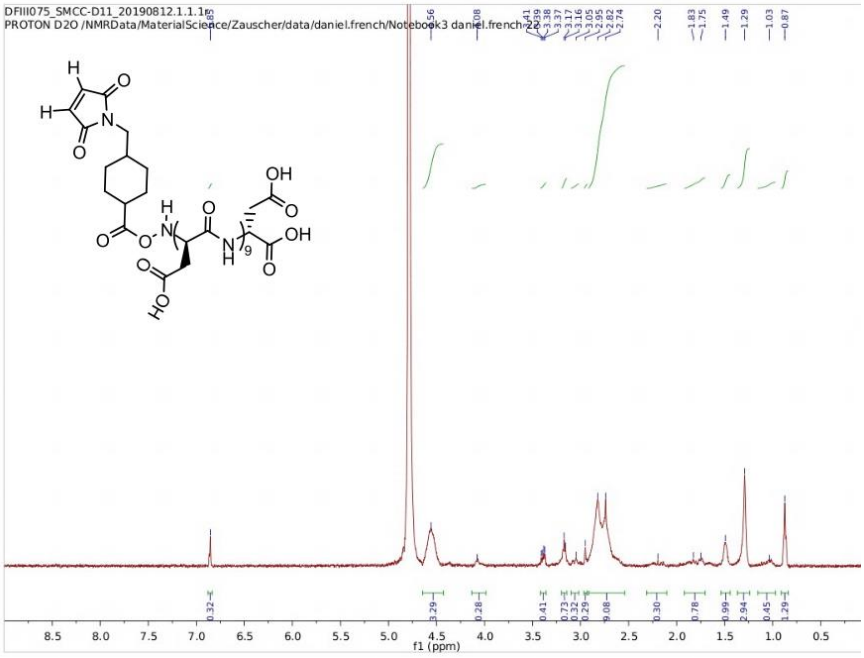

Figure 10: ^{1}H NMR of SMCC-D10. Reaction efficiency is calculated at 43% by the ratio of peak integrals at 1.03 (CH_3 cyclohexyl ring adjacent to ester) and 0.87 (proprietary initiator for D10 synthesis).

We then coupled SMCC-D10 to the ELPK50x8 backbone by mixing the two in PBS for overnight at room temperature. As with expression and purification of ELP50x8, we observed aggregation which limited reaction yield. We hypothesized that

the strong and opposite charge on the D10 and ELPK50x8 caused a physical gel to form when mixed. However, additional salinity did not prevent aggregation, nor did it help dissolve the aggregate once formed. We next added TCEP to reduce any potential disulfide formation, as this helped to increase yield during protein expression. While the modification did help, aggregation was not altogether prevented. None the less, we observed by IR and NMR spectroscopy that the coupling succeeded. Specifically, the lack of a peak in the ^{1}H NMR at 6.75 ppm indicates that the alkene of the maleimide has been reacted with the cysteine of ELPK50x8 (Figure 11).

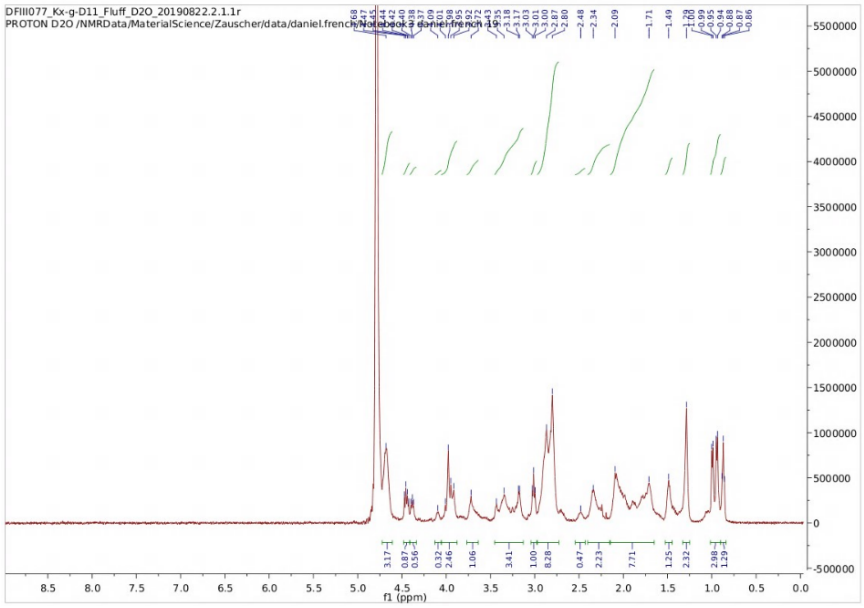

Figure 11: ^{1}H NMR of ELPK50x8-g-D10. Reaction efficiency is calculated by the ratio of peak integrals at 0.95 (valine CH_3) and 0.86 (proprietary initiator for D10 synthesis).

5.3.4 Diazotransfer and Attachment of Non-fouling Bristles via Huisgen Cycloaddition

We were able to couple POEGMA bristles to ELPK50x8 and synthesize the full mucin analogue. Diazotransfer of the primary amines of the lysine residues of the ELP backbone was performed as previously reported,[107] with the exception of a substitution of DMSO for methanol as the co-solvent. Successful diazotransfer is particularly indicated by the characteristic peak at 2100 cm^{-1} (Figure 12). We then decorated the diazotransfered backbone using 6000 kDa alkyne-POEGMA bristles. Successful coupling is indicated by the disappearance of the azide peak at 2100 cm^{-1} in the IR spectrum. A single peak in the scattering data following GPC confirms the absence of non-reacted bristle. Mn was calculated at 59.8 kDa. However, we do note that this is very low grafting density. The theoretical molecular weight of the backbone itself is 28.9 kDa, indicating only 12-16% final grafting efficiency compared to 60-75% reported in literature[107] and in other indications (Appendix A). We primarily attribute this to the low efficiency of the diazotransfer reaction, which is indicated by the low intensity of the azide peak compared to that for other cysteine-free, lysine-based ELPs (Figure 12). Likely, this is in turn the result of the gelation which additionally caused low yield.

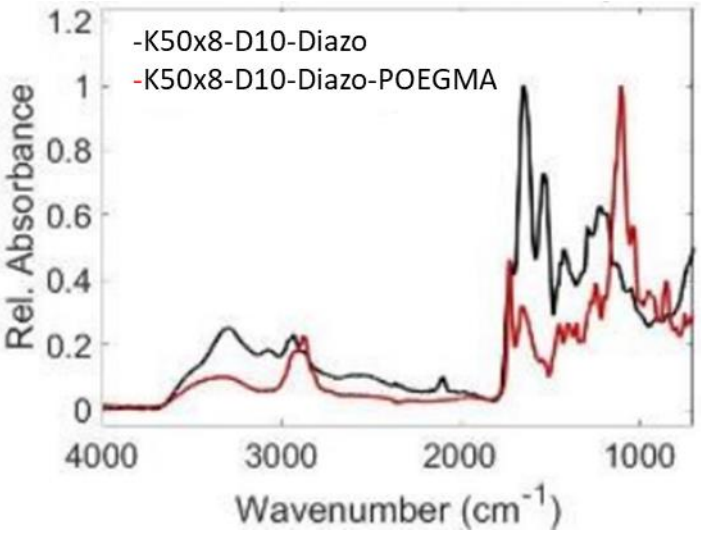

Figure 12: Infrared spectrum of the diazotransfer and bristle attachment of ELPK50x8-D10. Coupling is suggested by the disappearance of the azide peak at 2100 cm^{-1}.

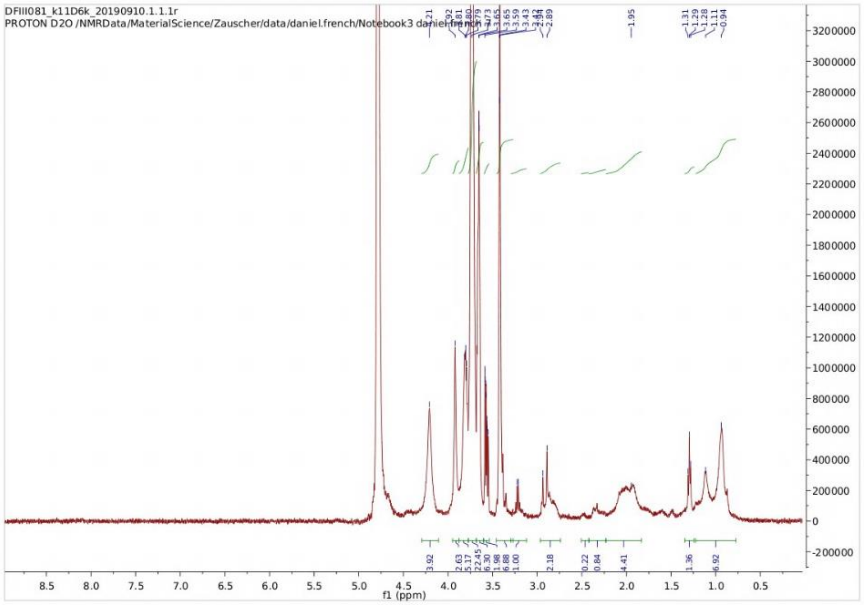

Figure 13: ^{1}H NMR of ELPK50x8-g-D10-g-POEGMA. Coupling efficiency is calculated by ratio of integrals at 3.43 (terminal OMe of POEGMA bristles) and 0.94 (valine CH_3).

5.4 Synthesis of Mucin Analogues Using Synthetic Backbones

5.4.1 Synthesis of Azido-poly(aminoethyl methacrylate – co – hydroxyethyl methacrylate)(azide-PAcH)

Azido-poly(2-aminoethyl methacrylate – co – 2-hydroxyethyl methacrylate) was polymerized via AGET ATRP. Much as with the ELP backbone described in Section 5.3, we sought to roughly mimic the average bristle spacing of lubricin and peptide-based MAs as much as possible. Therefore, we polymerized PAcH with a 4:1 HEMA:AMA feed ratio, which was roughly conserved in the final polymer with a 3.8:1 incorporation ratio and indicates that the polymers are likely random co-polymers. To test the reactivity of the azido head group, we performed a diagnostic click reaction (Figure 15). Specifically, lane 7 depicts the polymer having undergone diagnostic click with alkyne-Cy3. Comparison with lane 6, which was not labeled, shows that the headgroup is active. Lane 8 depicts the polymer having been diazotransfered before click with alkyne-Cy3.

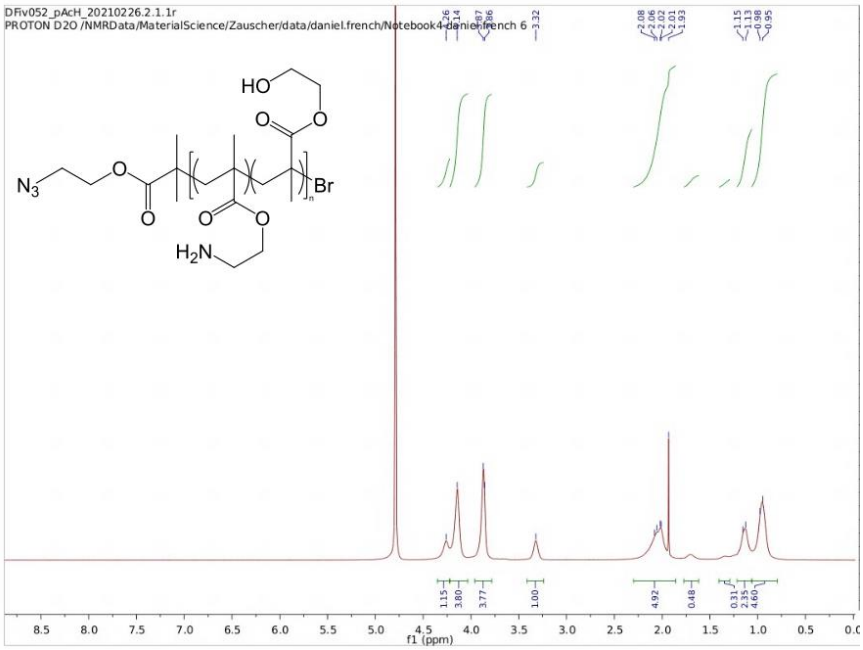

Figure 14: ^{1}H NMR of azide-initiated PAcH. Incorporation ratio between HEMA and AMA monomers is calculated by ratio of peak integrals at 4.14/3.86 and 4.26/3.32, respectively. Absence of peaks from 5-7 ppm indicates absence of monomer.

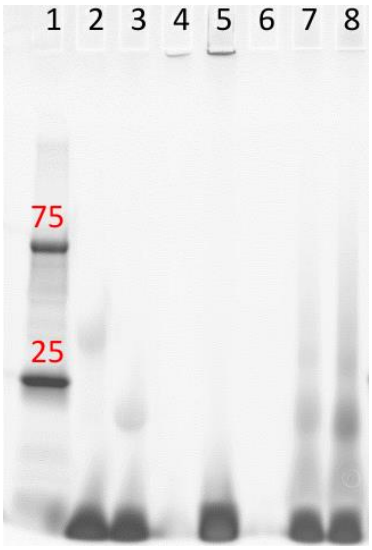

Figure 15: SDS-PAGE of MA backbone components. Lanes: (1) ladder, (2) Cy3-alkyne control click with PEG-azide, (3) Cy3-azide control click with PEG-alkyne, (4) alkyne-PtBA, (5) Cy3-azide + alkyne-PtBA, (6) azido-PAcH, (7) Cy3-alkyne + azido-PAcH, (8) Cy3-alkyne + azido-PAcH (backbone amines diazotransfered)

5.4.2 Synthesis of Propargyl-poly(tert-butyl acrylate)(alkyne-PtBA)

Alkyne-functionalized PtBA binder was synthesized using ARGET ATRP. Polymers of different molecular weights were selected, ranging from 5200 Da to 30 kDa. It was determined empirically that the smaller molecular weight binders were easier to solubilize for downstream reactions (data not shown) and were selected for further study. Here is depicted the ^{1}H NMR for the smallest polymer (Mn = 5.223 kDa, Mn/Mw = 1.05), which was used in the synthesis depicted here (Figure 16). Additionally, we previously determined that even very small oligoanions coupled to large synthetic polymers were able to inhibit stone growth (see section 6.5). Therefore, we are not too concerned that the small molecular weight will inhibit the ability of the MA to inhibit stone growth. As with azido-PAcH, we confirmed head-group activity by reacting the polymer with azido-Cy3 dye (Figure 15). Specifically, lanes 4 and 5 depict unlabeled alkyne-PtBA and Cy3-labeled PtBA, respectively. Because PtBA is quite hydrophobic, it precipitates in aqueous running buffer and sits in the well without entering the gel. Increased intensity in lane 5 indicates that the polymer has been labeled.

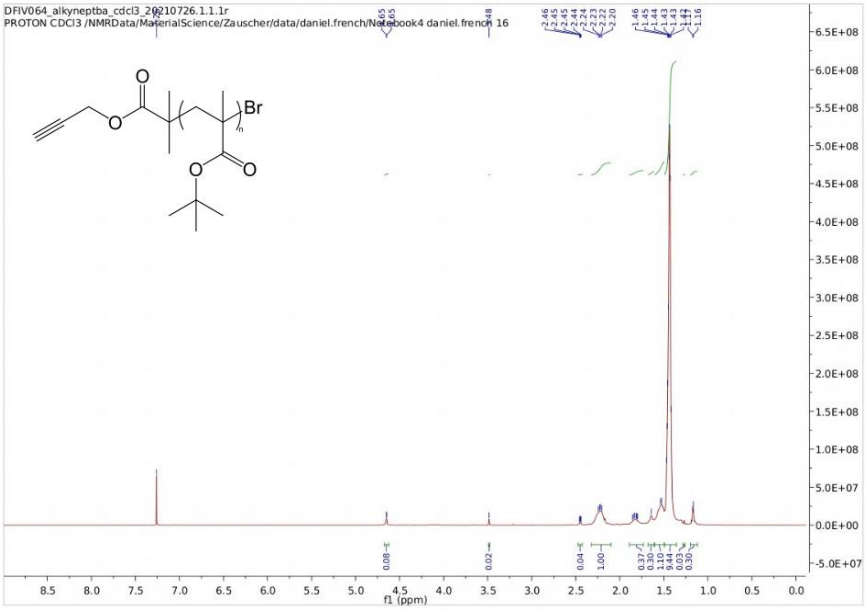

Figure 16: ^{1}H NMR of alkyne-initiated PtBA.

5.4.3 Synthesis of Poly((aminoethyl methacrylate-co-hydroxyethyl methacrylate)-b-tertbutyl acrylate) (PtBA-b-PAcH)

Azido-PAcH and alkyne-PtBA were coupled into a block co-polymer using Huisgen cycloaddition. Briefly, Azido-PAcH was stirred in a 5x excess of alkyne-PtBA in the presence of $CuBr_2$ and THPTA ligand in DMF. We elected to use an excess of alkyne-PtBA because of its relative abundance and hydrophobicity, which helped to purify the polymer through addition of water. By ^{1}H NMR, we determined that the reaction only proceeded to 42.2% completion (comparison of AMA CH_2 peak at 4.80 and tert-butyl group at 1.39) (Figure 17). This is considerably lower than expected for click chemistry. One possible reason for this is the differing hydrophilicity of the polymers: PAcH is generally soluble in polar solvents. PtBA, on the other hand, prefers non-polar solvents due to contributions from the tert-butyl protecting group.

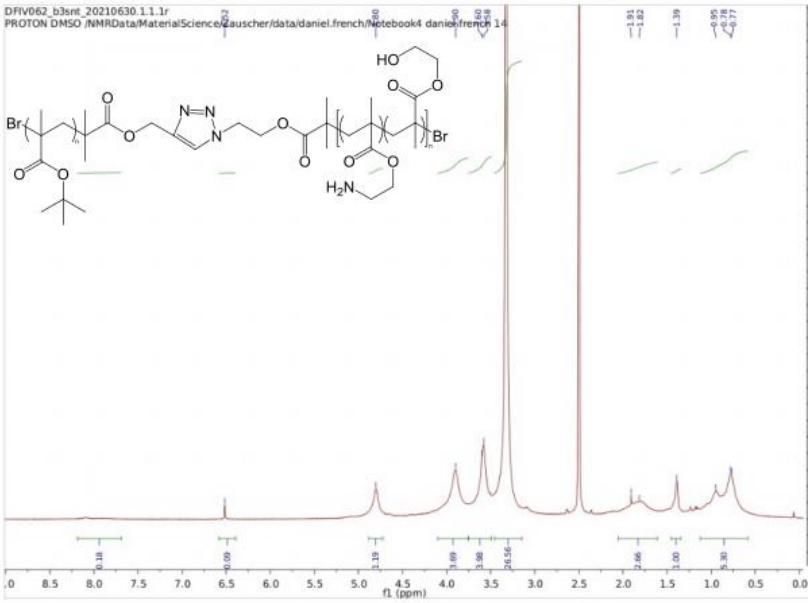

Figure 17: ^{1}H NMR of coupled PAcH-b-PtBA. Coupling efficiency is calculated by the ratio of peak integrals at 4.8 (AMA CH_2) and 1.39 (PtBA tert-butyl Me). A small peak is observable at 8.1 corresponding to the presence of the triazole formed during the coupling reaction.

Lack of complete reaction is confirmed by SDS-PAGE diagnostic (Figure 18). The sample mixture was diazotransfered and clicked with alkyne-Cy3. Presence of Cy3 band remaining in the well indicates that the coupling proceeded and that the PtBA is preventing the coupled PAcH from entering the gel. However, there is still a band corresponding to unreacted PAcH present. This is preferable to excess PtBA, which would adsorb to the stone surface in the final application without the anti-fouling bottlebrush. Excess PAcH bottlebrush, on the other hand, would play a "bystander" role by remaining in solution and keeping the surface free for adsorption of full mucin. This does, however, artificially inflate the working concentration of mucin analogue in solution.

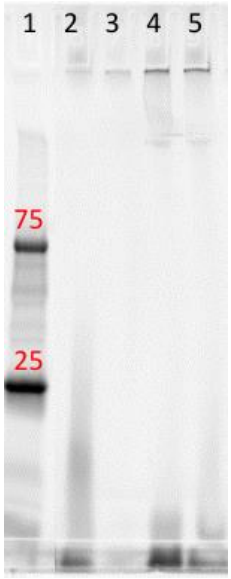

Figure 18: SDS-PAGE of PtBA-b-PAcH. Lanes: (1) ladder, (2) Cy3-alkyne + azido-PAcH (backbone amines diazotransfered), (3) PtBA-b-PAcH, (4) Cy3-alkyne + PtBA-b-PAcH, (5) Cy3-azide + PtBA-b-PAcH.

5.4.4 Synthesis of Propargyl-poly((oligoethylene glycol methyl ether methacrylate)-co-(fluoresceine-o-methacrylate)) (alkyne-POcF) bristles

Fluorescent anti-fouling bristles were synthesized by ARGET ATRP using an alkyne-initiator to facilitate coupling to the backbone. Navarro *et al.* examined the effect that backbone and bristle molecular weights impacted adsorption kinetics, anti-fouling, and anti-adhesion.[123] Anti-adhesion is distinguished from anti-fouling by the size of the challenge. Anti-fouling examines the repulsion of species of a like size with the brush (*i. e.* proteins) whereas anti-adhesion examines the repulsion of micron-sized particles from the surface. He determined that longer bristles, specifically 10 kDa bristles, exhibited enhanced anti-adhesion properties compared to short bristles of 1.7 kDa. We therefore targeted 10 kDa bristles for our MA design. We successfully synthesized bristles of

adequate size (9.082 kDa, Mw/Mn = 1.226). Fluoresceine-o-methacrylate was co-polymerized with the POEGMA to provide the option of fluorescence to measure adsorption and can be identified by ^{1}H NMR (Figure 19) and observation under UV irradiation.

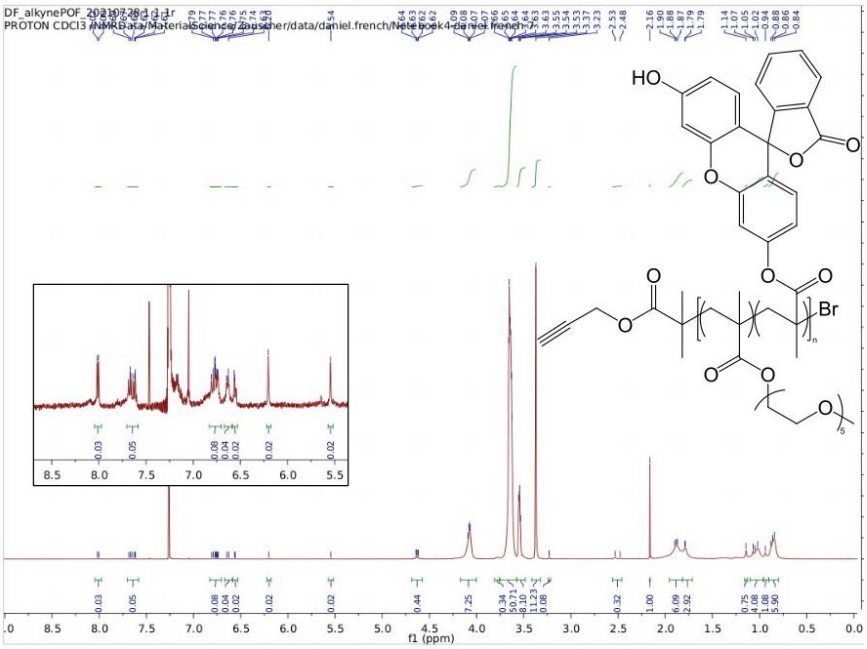

Figure 19: ^{1}H NMR of alkyne-initiated POcF. Incorporation of FOM indicated by presence of small peaks from 5.5 to 8.0 ppm.

5.4.5 Synthesis of Poly(tertbutyl acrylate) – b – (poly(aminoethyl methacrylate – co – hydroxyethyl methacrylate) – g – poly((oligoethylene glycol methyl ether methacrylate) – co – fluoresceine-o-methacrylate))

Fluorescent bristles were coupled to PtBA-b-PAcH by copper-based click chemistry. Unlike with the ELP-based backbones of Section 5.3 and Appendix A, we observed no diazotransfer reaction under standard conditions. However, we did observe successful incorporation of fluorescent Cy3 dye by gel. We therefore adopted

the conditions for serial diazotransfer and bristle attachment without purification and By comparison of the integrated area of the AMA CH_2 peak at 4.82 with that of the POcF CH_2, we calculate the overall grafting efficiency at 17%. Just as with the backbone coupling, this is much lower than typical for Huisgen cycloaddition, which is known to be highly efficient. The common factor that distinguishes these reactions from other reactions is the presence of the PtBA. We therefore postulate that the solvent conditions may be optimized to increase reaction efficiency.

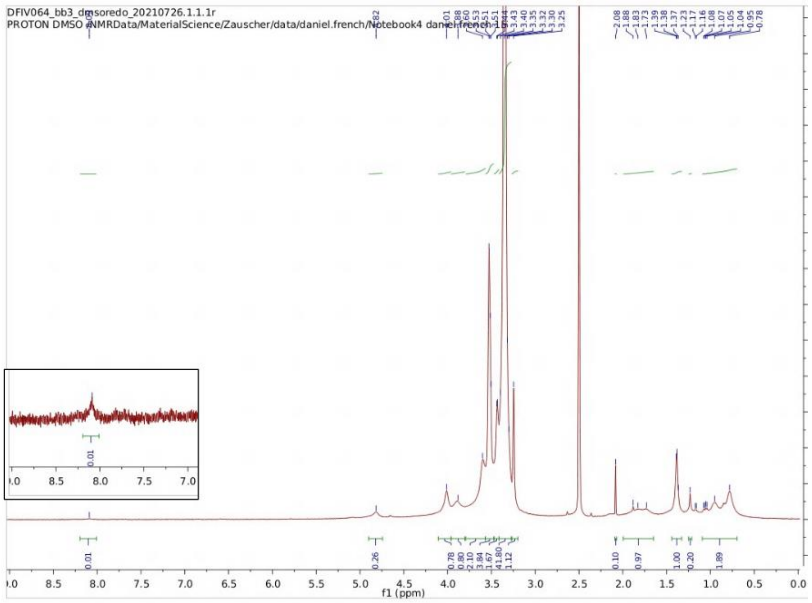

Figure 20: ^{1}H NMR of PtBA-b-PAcH-g-POcF. Coupling efficiency is calculated by the ratio of peak integrals at 3.32 (POEGMA terminal OMe) and 4.82 (AMA CH_2). Presence of triazole peak at 8.1 further supports coupling.

5.4.7 Hydrolysis of Tert-butyl Moieties

The tert-butyl protectant for the mucin analogue was hydrolyzed in a 1% solution of methylsulfonic acid in dichloromethane (Figure 21). Importantly, the strong

tert-butyl peak at 1.4 is absent while the OEGMA peaks at 4.21, 3.42, etc. and the HEMA peak at 3.8 are present. Because of the similar chemistries of the backbone and bristle, it is impossible to distinguish these peaks between PAcH and POEGMA.

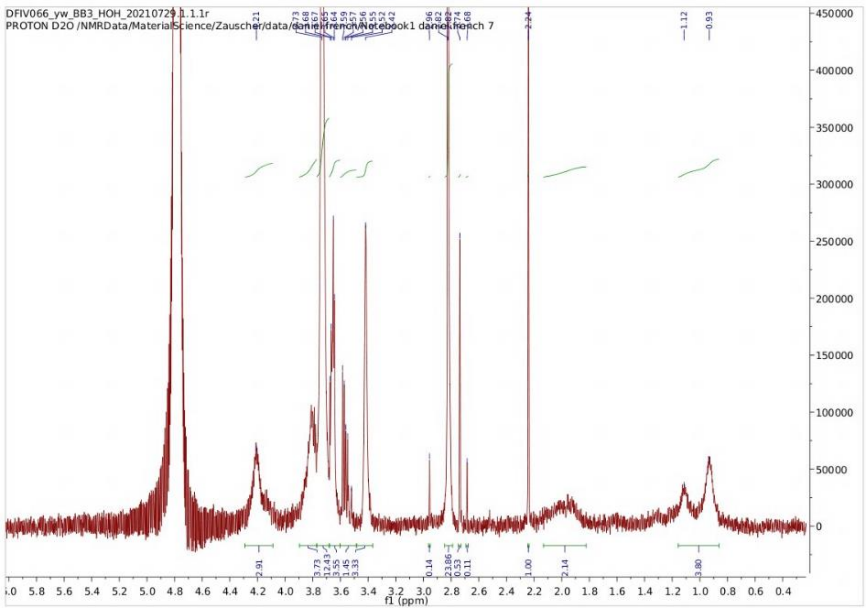

Figure 21: ^{1}H NMR of deprotection of PtBA-b-PAcH-g-POcF. Lack of peak at 1.4 ppm indicates the tBu group has been hydrolyzed from the MA.

5.5 Detailed Methods

5.5.1 Materials

AcuI (New England Biolabs), agarose (molecular biology grade, Bio-Rad), aldolase MW standard (Sigma-Aldrich), ammonium sulfate (99%, Sigma-Aldrich), BglI (New England Biolabs), BL21 competent *E. coli* (New England Biolabs), BseR1 (New England Biolabs), calf intestinal phosphatase (CIP, New England Biolabs), cutsmart buffer (2x, New England Biolabs), isopropyl β-D-1-thiogalactopyranoside (IPTG, 99%, Gold Biotechnology), kanamycin sulfate (KAN, USP grade, Gold Biotechnology), Laemli

buffer (2x, BioRad), N-acetyl-L-cysteine (NAC, 99%, Sigma-Aldrich), NEB10β competent *E. coli* (New England Biolabs, Ipswich, MA), polyethyleneimine (PEI, 50% aqueous solution, 50-100 kDa, MP Biomedicals), QIAprep spin miniprep kit (Qiagen), QIAquick gel extraction kit (Qiagen), Quick Ligase (New England Biolabs), Quick Ligase Buffer (2x, New England Biolabs), SybrSafe (Invitrogen), Terrific Broth II (TBII, MO Bio), tert-butyl alcohol (tBuOH, 99%, Alfa Aesar), and XbaI (New England Biolabs) were used as received.

Forward and reverse oligonucleotides encoding for 1) a lysine-containing elastin-like polypeptide (VPGKG), and a flexible linker $(GGGGS)_3$ were dissolved to a concentration of 100 μM in MQ (4 nmol "ultramer", Integrated DNA Technologies). Intact plasmid JMD2 and a gene insert for a cysteine-rich ELP $(VPGVGVPGCG)_8$ were donated from the Chilkoti Laboratory (Duke University, Durham, NC). JMD2 has been adapted from pET-24 to work with Recursive Directional Ligation by Plasmid Reconstruction (PReRDL), as has been described elsewhere.[138]

2-aminoethyl methacrylate, Imidazole-1-sulfonyl azide hydrochloride, THPTA, and azido-POEGMA were synthesized by Luis Navarro, Ph.D.[107]

5.5.2 Oligonucleotide Design and Annealing

Forward and reverse oligonucleotides (4 nmol "ultramer") encoding for an elastin-like polypeptide containing lysine as the guest residue (VPGKG) was annealed into double-stranded DNA inserts. A solution comprised of 1 μL of each

complementary oligonucleotide (100 μM), 25 μL of 2x Quick Ligase buffer (1x: 66 mM Tris-HCL, 10 mM MgCl2, 1 mM Dithiothreitol, 1 mM ATP, 7.5% PEG6000, pH 7.6), and 23 μL of water was heated to 92°C in a dry bath to melt the DNA. After holding the solution at this temperature for two minutes, the dry bath was unplugged and allowed to cool to ambient temperature, annealing the oligos.

To linearize the plasmid in preparation for accepting an insert, 15 μL plasmid DNA, 1 μL BseRI, 9 μL NEB Cutsmart Buffer (1X: 10 mM MgOAc, 50 mM KOAc, 20 mM Tris-OAc, 100 μg/ml BSA, pH 7.9), and 65 μL water incubated at 37°C for three hours. 1 μL calf intestinal phosphatase was added and the solution was incubated an additional 30 minutes. Linearized plasmid DNA was purified with a QIAquick gel extraction kit. To concatenate the oligoes into the prepared plasmid, 10 μL vector preparation, 1 μL binding insert, 12 μL 2x Quick Ligase buffer, and 1 μL Quick Ligase were incubated at room temperature for 10 minutes.

JMD2 plasmids containing concatenated inserts were transformed into NEB10β cloning *E. coli* by heat shock transformation. Competent cells were thawed on ice for 10 minutes. 3 μL plasmid DNA was added to 25 μL competent cells and mixed by gently bubbling air through the liquid using a pipette. After incubating on ice for 30 minutes, the transformations were heated to 42°C in a dry bath for exactly 30 seconds, then returned to ice for an additional five minutes. To this culture was added 50 μL Terrific Broth II (TBII). The cells were recovered by shaking at 37°C for one hour and plated

onto pre-warmed TBII-agar plates supplemented with 45 μg/mL kanamycin. Plates were incubated at 37°C overnight. Individual colonies were cultured in 5 mL TBII-KAN medium with shaking at 37°C for 18 hours. Plasmid DNA was isolated with a QIAprep Spin Miniprep Kit and submitted for sequencing at Eton Bioscience (Durham, NC branch). Plasmids containing no mutations were selected to continue.

5.5.3 Recursive Directional Ligation by Plasmid Reconstruction (PReRDL)

Briefly, "A-" and "B-cuts" were performed on two plasmids containing genes to be ligated, respectfully. A-cut: 40 μL plasmid DNA, 2 μL AcuI, 4 μL BglI, 9 μL Cutsmart Buffer, and 35 μL water were added to a 1.5 mL microcentrifuge tube and incubated 3 hr at 37°C. B-cut: identical to A-cut with a substitution of BseRI for AcuI. Cuts were purified by gel electrophoresis. Pertinent bands were cut from the gel and DNA was extracted with a QIAquick gel extraction kit.

To ligate the two cuts, 3 μL "A-cut", 3 μL "B-cut", 10 μL 2x Quick Ligase Buffer 1 μL Quick Ligase, and 1 μL water were incubated at room temperature for 10 minutes. The resulting plasmid was transformed into NEB10β cloning competent *E. coli* by heat shock and plated, as described above. Individual colonies were cultured, processed, and sequenced as before. Plasmid inserts were verified by a combination of DNA sequencing and gel electrophoresis with a diagnostic digestion by *Bam*HI and *Xba*I.

5.5.4 Peptide Expression

The ELPK50x8 plasmid was transformed into BL21 (DE3) expression *E. coli* using heat shock transformation. Colonies were used to inoculate 5 mL cultures of 2x YT-KAN (Per Liter: 16g Tryptone, 10g Yeast Extract, 5g NaCl, 45mg Kanamycin Sulfate, sterilized via autoclave prior to addition of KAN), which were cultured for 18 hr at 37°C. Of the 5 mL cultures, 650 μL was used to seed a 65 mL starter culture (2x YT-KAN) and the remainder was isolated and sequenced to ensure against potential mutations. The 65 mL cultures were incubated with shaking an additional 16-18 hours at 37°C. 1 L cultures of 2x YT-KAN were inoculated with 10 mL of the starter culture and 1.6 g N-acetyl cysteine (80 mg/mL, sterile filtered). 12 L were prepared in total. Cultures were incubated with shaking at 37°C for 6 hours, at which point IPTG (1M, sterile filtered) was added to a final concentration of 1 mM. Cultures were then incubated with shaking an additional 16-18 hours at 37°C.

5.5.5 Peptide Purification

The cultures were collected in 1 L bottles and centrifuged at 4000 RCF, 4°C for 20 minutes. Pellets were resuspended in 7.5 mL PBS, collected in a polypropylene centrifuge tube, and lysed by probe sonication. Insoluble cell debris was removed from the protein by addition of 2 mL 10% poly(ethylene imine) (PEI, to sequester chromosomal DNA) per liter culture and centrifugation at 15,000 RPM at 4°C for 30 minutes, leaving an amber cell lysate. Protein was purified from cell lysate using

inverse transition cycling (ITC), as described previously.[142] In ITC, the inverse phase transition of the ELP moiety to selectively isolate the peptide in either the liquid phase (cold cycles) or solid phase (hot cycles), to the exclusion of non-ELP contaminants. ELP in cell lysate was transitioned to the solid state by addition of ammonium sulfate, adding just enough for the ELP to become insoluble, as denoted by increasing turbidity of the solution. Once transitioned, a hot cycle was completed by centrifuging the samples at 15000 RPM, 35-40°C for 20 minutes. The supernatant of the "hot spin" was kept for further analysis and the pellet (containing the sample) was resuspended in 25 mL milli-q grade water (MQ). Samples were kept on ice during resuspension, after which they were centrifuged at 15000 RPM, 4°C for 20 minutes. Following the "cold spin", the supernatant (now containing the construct, which became soluble again in cold, unsalted water) was transferred to a fresh centrifuge tube and the pellet (containing cell debris) was discarded. The process was repeated for a total of three rounds of ITC (each round consisting of one hot spin and one cold spin). Following the final cold-spin, the peptide was dialyzed against Milli-Q grade water for two days with three exchanges. A final exchange into 0.1% acetic acid was performed to control the counterion of the peptide. The final peptide was analyzed by SDS-PAGE and MALDI-MS.

5.5.6 Oligo-aspartate Binder Attachment via a Hetero-bifunctional Crosslinker

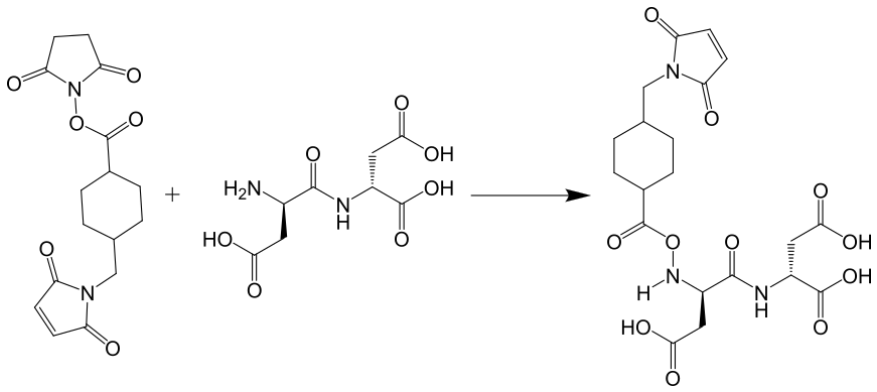

Scheme 3: Synthesis of maleimide-D10.

Sulfosuccinimidyl 4-[N-maleimidomethyl]cyclohexane-1-carboxylate (SMCC, 36.5 mg, 100 μmol, 5 Eq) and D10 (30.2 mg, 20 μmol, 1 Eq) were stirred in 5 mL PBS for one hour at room temperature. In a separate vessel, ELPK50x8 (15.8 mg, 4 μmol cysteine, 1 Eq) was stirred with TCEP (6.35 mg, 20 μmol, 5 Eq) in 5 mM EDTA in PBS for one hour. Both reactions were purified by dialysis against 0.1 mM HOAc for two days with three buffer exchanges and dried.

Reduced ELPK50x8 (8.56 mg, 2.4 μmol cysteine, 1 Eq) was stirred with SMCC-D10 (20.6 mg, 12 μmol, 5 Eq) overnight, purified by dialysis for two days with three buffer exchanges against 0.1 mM HOAc, and dried.

5.5.7 Polymerization of Azido-poly(2-aminoethyl methacrylate – co – 2-hydroxyethyl methacrylate)

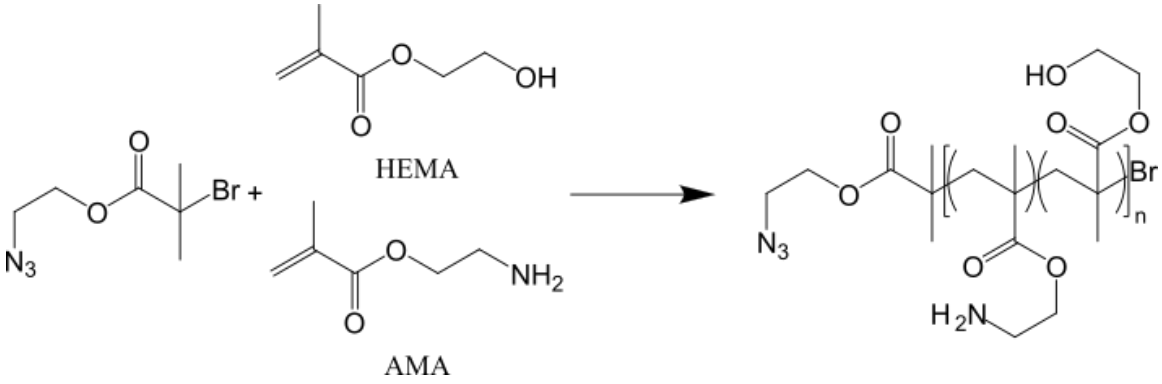

Scheme 4: Synthesis of poly(2-aminoethyl methacrylate - co - 2-hydroxyethyl methacrylate).

Excess hydroxyethyl methacrylate was passed through a plug of basic alumina to remove inhibitor. To a three-neck 10 mL round bottom flask was added 534 μL of excess MeOH, copper II bromide (17.8 mg, 0.08 mmol, 5 Eq), and Tris(2-pyridylmethyl) amine (TPMA, 27.9 mg, 0.096 mmol, 6 Eq). After stirring for 30 minutes, HEMA (333.2 mg, 2.56 mmol, 160 Eq) and AMA (106.9 mg, 0.64 mmol, 40 Eq) were added to the flask and sealed. To a separate two-neck 25 mL round bottom flask was added 801 μL excess MeOH, 2-azidoethyl-2-bromoisobutyrate (3.8 mg, 0.016 mmol, 1 Eq), and L-ascorbic acid (5.6 mg, 0.032 mmol, 2 Eq). Both flasks were subjected to three rounds of freeze-pump-thaw. The reaction was initiated upon injection of 1 mL of the initiator-ascorbic acid solution to the reaction vessel. The reaction was allowed to proceed to 16.7% conversion (by crude ^{1}H NMR). The reaction mixture was dialyzed against 0.1 mM acetic acid for two days with three buffer exchanges and lyophilized to yield 80.2 mg of polymer.

5.5.8 Polymerization of Propargyl-poly(tert-butyl acrylate)

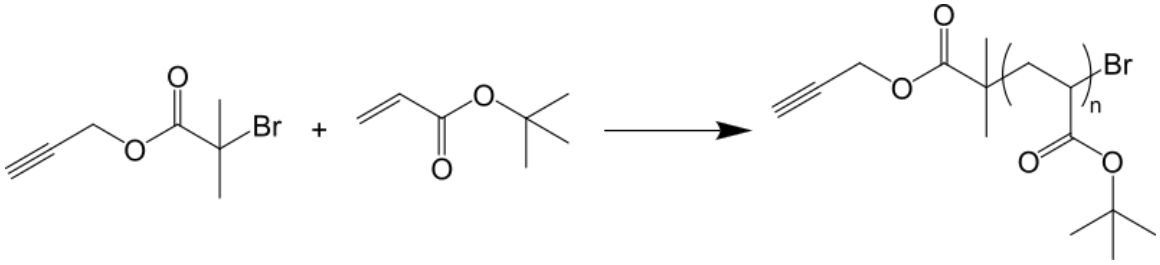

Excess tertbutyl acrylate was passed through a plug of basic alumina to remove inhibitor. To a three-neck 100 mL round bottom flask was added 36 mL of excess MeOH, copper II chloride (26.9 mg, 0.2 mmol, 1 Eq), and N,N,N′,N″,N″-pentamethyldiethylenetriamine (PMDETA, 138.6 mg, 0.8 mmol, 4 Eq). After stirring for 30 minutes, tBA (5.1268 g, 40 mmol, 200 Eq) was added to the flask and sealed. To a separate two-neck 25 mL round bottom flask was added 2.5 mL excess MeOH, alkyne initiator (410 mg, 2 mmol, 10 Eq), and L-ascorbic acid (422.7 mg, 2.4 mmol, 10 Eq) with excess in the same ratio to protect against evaporation and inaccessibility. Both flasks were subjected to three rounds of freeze-pump-thaw. The reaction was initiated upon injection of 10 mL of the initiator-ascorbic acid solution to the reaction vessel. The reaction was allowed to proceed to 54% conversion (by crude ^{1}H NMR, about 3 hours), then quenched by addition of MQ. Upon addition of the MQ, the solution immediately turned milky. The polymer was pelleted by centrifugation at 15000 rcf for 30 minutes. The supernatant was discarded and the clear, viscous pellet was redissolved in MeOH. This process was repeated twice more to purify the polymer. The final product was collected with minimal MeOH, which was dried off in a stream of nitrogen.

5.5.9 Synthesis of Poly((aminoethyl methacrylate-co-hydroxyethyl methacrylate)-b-tertbutyl acrylate) (PtBA-b-PAcH)

Azide-PAcH (36 mg, 1 μmol, 20 mg/ml in DMF, 1 Eq), alkyne-PtBA (26.6 mg, 5 μmol, 10 mg/mL, 5 Eq in MeOH), premixed $CuSO_4 \cdot 5H_2O$ (3.75 mg, 15 μmol, 10 mg/mL in DMF, 15 Eq) and THPTA (8.69 mg, 20 μmol, 30 mg/mL in MeOH, 20 Eq), and L-ascorbic acid (2.64 mg, 15 μmol, 10 mg/mL in MeOH, 15 Eq) were added to a Schlenk tube with 162 μL excess DMF and 308 μL excess MeOH. The reaction was stirred overnight and purified by dialysis in a 10k MWCO dialysis bag.

5.5.10 Diazotransfer

For peptide backbones: ELPK50x8-g-D10 (0.1 mmol free amine, 1 eq), potassium carbonate (1.6 mmol, 16 eq), copper sulfate pentahydrate (0.01 mmol, 0.1 eq), and imidazole-1-sulfonyl azide (1 mmol, 10 eq) were solubilized in 65 ml 1:9 DMSO:water, then stirred overnight at room temperature. The reaction was dialyzed for two days with three buffer exchanges, condensed by rotary evaporation and lyophilized. Conversion was evaluated by IR spectroscopy and NMR.

For synthetic backbones: To PtBA-b-PAcH (7.5 mg in 750 μL in DMSO) was added a pre-mixed solution of potassium carbonate (733.4 μg in DMF), $CuSO_4$ (16.7 μg in DMF), and ISA (906.8 μg in DMF). The solution was stirred overnight and immediately reacted with bristle (see section 5.5.12).

5.5.11 Polymerization of Propargyl-poly((oligoethylene glycol methyl ether methacrylate)-co-(fluoresceine-o-methacrylate)

Excess oligoethyleneglycol methyl ether methacrylate (average Mn = 500Da, EG5) was passed through a plug of basic alumina to remove inhibitor. To a two-neck 250 mL round bottom flask was added 38 mL of excess MeOH which had been sparged with helium for 1 hour, copper II chloride (1.3112g, 9.752 mmol, neat, 5 Eq), and N,N,N′,N″N″-pentamethyldiethylenetriamine (PMDETA, 1.7573g, 10.14 mmol, 175.73 mg/mL, 5.2 Eq). After stirring for 30 minutes, oligoethyleneglycol methyl ether methacrylate (Mn = 300, 4.302g, 14.34 mmol, 43% in MeOH, 7.35 Eq) and fluorescein-o-methacrylate (116.1 mg, 0.29 mmol, 15 mg/mL in MeOH, 0.15 Eq) were added to the flask and sealed. To a separate three-neck flask were added alkyne-initiator(500.2 mg, 2.44 mmol, 51.25 mg/mL, 1.25 Eq) and L-ascorbic acid (516. Mg, 2.93 mmol, 21.13 mg/mL, 1.5 Eq), plus excess in the same ratio to account for evaporation and inaccessibility. Both flasks were subjected to three rounds of freeze-pump-thaw. The reaction was initiated upon injection of 15 mL of the initiator-ascorbic acid solution to the reaction vessel. The reaction was allowed to proceed for three hours, then quenched by addition of 35 mL MQ. 150 mL diethyl ether was added to the reaction vessel, causing the solution to turn milky and to form a black precipitate. The precipitate was removed by vacuum filtration and rinsed with a small volume of MeOH, then more diethyl ether. The solvent was removed under reduced pressure, resolubilized in MeOH, and re-precipitated with diethyl ether. The yellow viscous liquid was dialyzed

against MQ for 5 days in a 10k MWCO dialysis bag with multiple buffer exchanges while covered with aluminum foil to limit photobleaching. The solvent was removed under reduced pressure, yielding 1.4286g orange viscous liquid.

5.5.12 Bristle Attachment

For peptide backbones: Excess water and MeOH were degassed by sparging with nitrogen for one hour. To a 150 mL round bottom flask were added 34.5 mL excess MeOH, 16 mL excess MQ, and 7 mL NEt_3 HOAC (2M, pH 7, 10x). Copper sulfate pentahydrate (60.8 mg, 243.4 μmol, 10 mg/mL, 30 Eq) and THPTA (70.5 mg, 162.2 μmol, 30 mg/mL, 20 Eq) were added and stirred for 30 minutes. Alkyne-POEGMA (6526 Da, 264.8 mg, 40.57 μmol, 5 Eq) was added and the solution was degassed by nitrogen sparging for two hours. Diazo-ELPK50x8-g-D10 (6.0 mg, 8.115 μmol azide, 10 mg/mL, 1 Eq) and sodium ascorbate (24.1 mg, 121.7 μmol, 100 mg/mL, 15 Eq) were added and the vessel was quickly sealed and stirred for 24 hours. The solvent was removed under reduced pressure, mixed with 1 mmol EDTA, and dialyzed against 10 mM EDTA for one day followed by 0.1 mM acetic acid for one day. The product was dried, yielding a slightly green viscous liquid. The product was solubilized in 350 μL MeOH. 10 mL diethyl ether was added to precipitate the mucin analogue. This was repeated three times, yielding 18.3 mg olive green solid.

For synthetic backbones: Premixed $CuSO_4$·THPTA (10 μM, 1 mL), POcF (10 μM, 400 μL), and L-ascorbic acid (1.758 mg, 5 mg/mL, 352 μL) were directly added to the

diazotransfer vessel and allowed to stir overnight. The next day, the reaction mixture was dialyzed for two days in 10k MWCO dialysis tubing against 10 mM EDTA, then 0.1 mM acetic acid. The dilate was dried, yielding 10.2 mg yellow solid.

5.5.13 Hydrolysis of PtBA to COM-Binding PAA

The MA was dissolved to 2 mg/mL in DMSO, then added to 10 mL of 1% methylsulfonic acid in DCM. The solution was stirred for 30 minutes, then washed with water. A white precipitate formed and collected at the interface between the two solvents. The water fraction was dialyzed for two days with three buffer exchanges against 0.1 mM acetic acid and lyophilized.

5.6 Conclusions

In this work, we successfully synthesized two different stone-targeted mucin analogues: one with a peptide backbone (using a biosynthetic approach) and one with a synthetic polymer. Both mucin analogues suffered from solubility issues which hindered their synthesis and limited yield. For example, the biosynthetic approach suffered from excessive aggregation in every reaction of the synthesis. This persisted even in the presence of additional salt to screen charge interactions between the D10 and the lysine of the ELP as well as in the presence of TCEP to break disulfide crosslinks. Very recently, Wensien *et al.* reported a new crosslinking reaction between cystine and lysine under reducing conditions, such as those created by the high pKa of the lysine residue and the additional base added to purify the peptide.[143] This additional reaction

mechanism may be the cause of gelation observed in the reactions involving the peptide backbone.

The synthetic backbone suffered from solubility issues as well, with the hydrophobicity of the PtBA being incompatible with methods our lab has previously used to synthesize mucin analogues. We hypothesize that it is the difference in polarity between the two copolymers, PAcH and PtBA, that caused the low reaction efficiencies observed in this work. We were successful, however, in synthesizing mucin analogues using this method.

The Huisgen cycloaddition used in our work introduces copper to our final product which, if not adequately removed, may be a source of toxicity and binding inhibition for our mucin analogue. Though an essential nutrient for the body, excessive copper can cause cytotoxicity, neurotoxity, and angiogenesis. In the kidney, the primary damage caused by copper is to the nephron as copper is filtered from the blood.[144, 145] Because any residual copper introduced into the kidney by our construct would be down-stream in the urine flow, it is unlikely that copper will cause damage to the nephron. Copper may additionally be chelated by the polyacrylic acid binders of the MA, which may preclude binding of the PAA to the stone surface.[146, 147] However, Haeri *et al*. discovered that copper typically binds PAA as hydrates, which effectively lowers the charge density on the copper and weakens the attraction with the oligoanion. However, calcium was found to bind PAA without the diluted charge density caused by

hydration.[148] We therefore posit that even if copper is chelated by the pAA when administered, the calcium of the stone will out-compete the bound copper and allow the MA to bind. Finally, because the last use of a copper-containing reaction occurs prior to PtBA deprotection, and our use of EDTA to chelate copper in purification by dialysis, we do not anticipate much copper contamination in our final product. By visual observation, we did not observe a high copper concentration in the samples prepared, as indicated by a lack of green coloration. In advancing this product to clinic, we would measure the copper concentration in the final product using copper concentration assays and cytotoxicity using the MTT assay.[149]

6. Interaction of Stone-binding Mucin Analogues with Calcium Oxalate Monohydrate Kidney Stones

6.1 Statement of Effort

The research detailed in this chapter is my own, with experimental assistance from Qihong Qian, then a master's student who I mentored. With my direction and assistance, Qihong synthesized poly(tert-butyl acrylate) and helped to develop the method by which we fabricate stone surfaces in section 6.3.

6.2 Rationale

To characterize the performance of our mucin analogues, we focused on two principle tests, each of which focused on one mechanism of crystal growth. Of course, to mitigate either mechanism the mucin analogue must adsorb to the surface of the stone fragment. Typically, such studies would be performed using native stones and fluorescence. However, this raises two significant problems. Firstly, the kidney is constantly flushed with urine. Therefore, any therapeutically relevant mucin analogue must have quick adsorption kinetics which may not be adequately captured by traditional fluorescence measurements. Secondly, the chemical composition of kidney stones has been shown to be highly variable, especially with respect to the organic matrix which binds the stone. This inherent variability may muddle the interpretation of adsorption results and ultimately complicate optimization of the MA. Because of these limitations, we opted to monitor adsorption using quartz crystal microbalance

with dissipation monitoring, which provides real-time monitoring of adsorption. Additionally, using QCM we can monitor fouling to address growth mechanism 2 of stone formation: adsorption of urinary crystallites. Using QCM necessitates the use of model surfaces, which will reduce the variability of the surface and simplify the analysis of adsorption and fouling comparisons across samples.

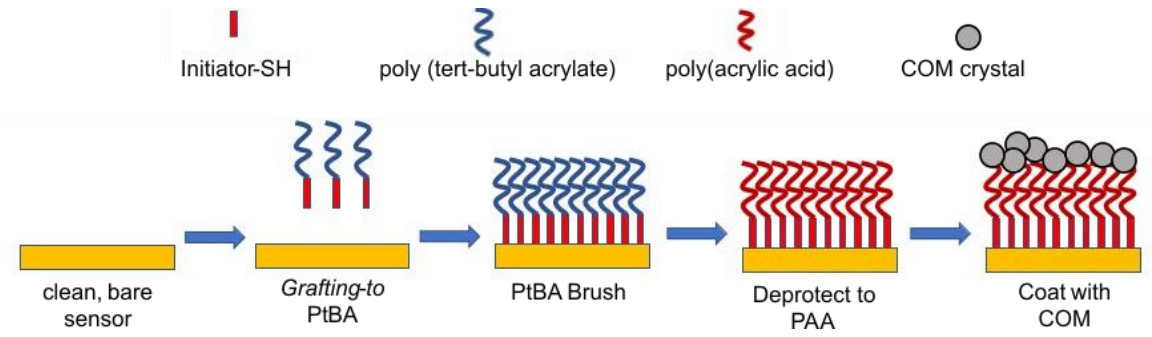

Figure 22: Schematic flow of COM model surface fabrication. We use *grafting-to* to create a PtBA brush. After deprotection, we spincoat the surface with an ethanolic slurry of COM, which is bound to the surface by the PAA brush. Image courtesy of Qihong Qian.

To address growth inhibition, we will use a calcium depletion assay championed from the Rimer research group.[39, 40, 128] In this assay, a supersaturated solution of calcium oxalate in the presence or absence of various potential inhibitors is allowed to crystalize at 37°C. Crystallization is monitored indirectly by measuring the remaining concentration of calcium, with the assumption that any calcium which is removed from solution is forming crystals. In this chapter, I will describe the fabrication of calcium oxalate monohydrate model surfaces on QCM sensors with which to monitor the adsorption and antifouling properties conferred by stone-targeted Mas (growth

mechanism 2). I will then describe the inhibition of crystal growth exhibited by our mucin analogues (growth mechanism 1).

6.3 Fabrication of Calcium Oxalate Model Surfaces

6.3.1 Synthesis of Bis[2-(2'-bromoisobutyryloxy)ethyl]disulfide

We synthesized a thiolated ATRP initiator which can be used for surface-initiated polymerization or for solution polymerization of polymers which can be *grafted to* a surface. The reaction was highly efficient (90.75% yield) and provided a cost-effective substitute for commercially available initiators. Figure 23 depicts the IR spectrogram of the purified initiator, which matches the fingerprint region of published spectra precisely.

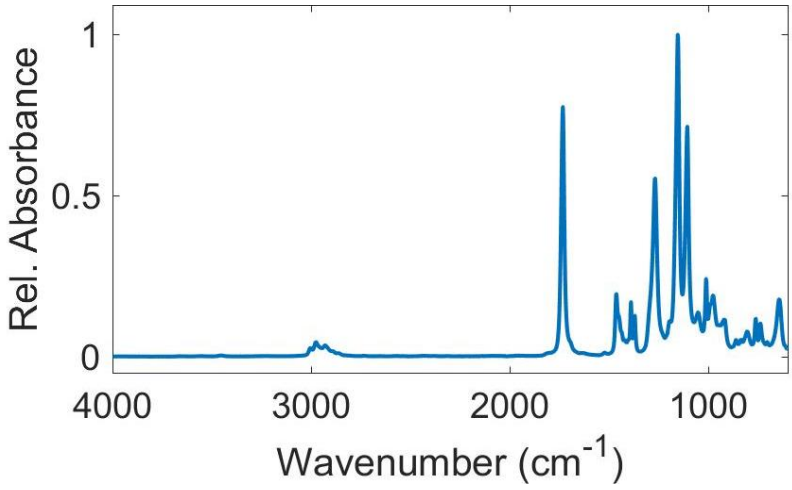

Figure 23: IR spectrum of BIBOEDS initiator.

6.3.2 Synthesis of Poly(tert-butyl acrylate) Disulfide

Poly(tert-butyl acrylate) was synthesized by ARGET ATRP. IR spectroscopy and ^{1}H NMR confirm purity of the PtBA. For the polymer used in this work, a single peak

was identified by gel permeation chromatography, giving an Mn of 40.77 kDa. However, in additional polymerizations (not detailed here) a second peak is present at twice the Mn as the first. We interpret this to indicate the lability of the disulfide bond, the breakage of which would create two polymers of appropriate relative size. However, it is also possible that the observed two-fold molecular weight is the result of termination by combination. This explanation is less likely because ARGET so much favors the dormant state of the polymer that the probability of radicals present on two adjacent polymer chains is quite low.[150]

6.3.3 Fabrication of COM-functionalized QCM Sensors

We use a PAA brush to form an adhesive layer between the relatively inert gold surface and calcium oxalate monohydrate. This is typically done by first creating a brush of PtBA so that the high charge density of PAA does not inhibit the packing density of the brush. The brush is then deprotected to yield PAA. We are prompted to use the *grafting-to* method because this approach reduces batch-to-batch variability and eliminates the need for a glove box during synthesis. Though *grafting-from* typically produces lower grafting density, we observed larger and more consistent thicknesses from *grafting-to* than surface-initiated polymerization.

We have used *grafting-to* to form our initial brush. Briefly, sensors were thoroughly cleaned by alternative sonication and rinsing in sodium dodecyl sulfate, MQ, acetone, and ethanol. The sensors were then ashed in an air plasma and immediately

submerged in a 15 mg/ml methanolic solution of $(PtBAS)_2$ for two days. Sensors were cleaned of non-bound polymer by rinsing and brief sonication in ethanol. We consistently form brushes ranging from 5-8 nm (ellipsometric dry thickness), with water contact angles ranging from 85° to 90°.

Sensors were deprotected in a solution of 1% v/v methanesulfonic acid in dichloromethane and incubated in dilute acetic acid to deprotonate the resulting acid. Film thicknesses were reduced to 2.19 nm and contact angle decreased to 42°. Sensors were spincoated with an ethanolic slurry of calcium oxalate monohydrate and incubated at 90°C overnight.

6.3.4 Stability of Calcium Oxalate Surface Coatings

QCM surfaces were exposed to PBS which had been saturated with calcium oxalate monohydrate, at a flow rate of 100 μL/min. While some desorption of the COM coating was observed, the sensors stabilized in about 4 hours (Figure 24). The film after stabilization was relatively uniform to the level of visual observation. As such, these methods are acceptable for creating model surfaces by which to monitor adsorption and anti-fouling properties of the MA in real time.

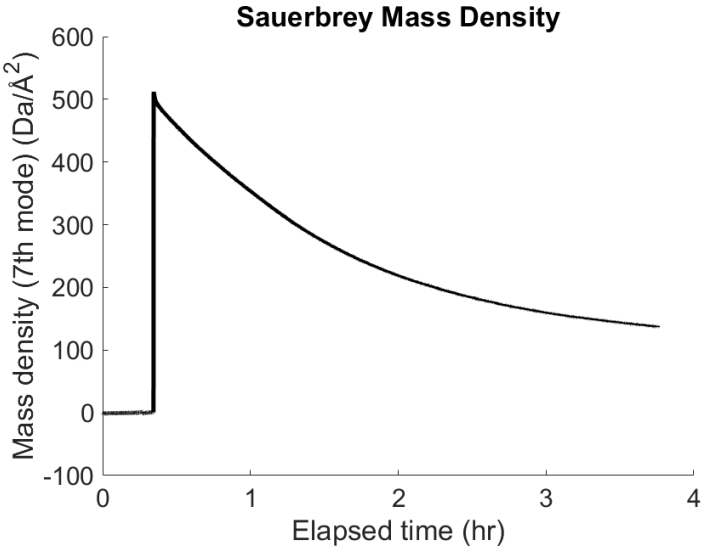

Figure 24: Stability of COM-functionalized QCM sensors under flow conditions. Sensors exhibit a loss of mass density with time, likely the loss of loosely-bound COM. Sensors stabilize in about 4 hours.

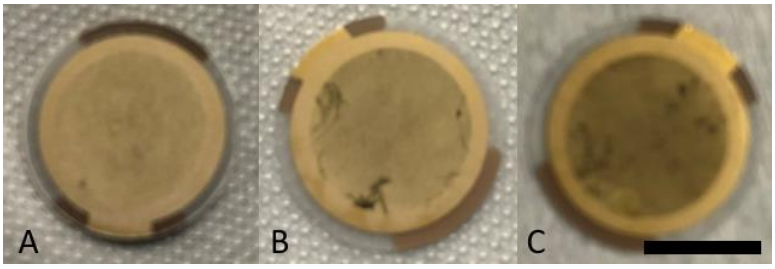

Figure 25: Visual confirmation of sensor stability. COM-Coated sensors immediately after spincoating (A), after 20 minutes of sonication in COM-saturated PBS (B), and after exposure to flow for 4 hours (C). Scale bar: 7 mm.

6.4 Inhibition of Mineralization

We assessed the ability of our Mucin Analogues to inhibit COM crystal growth. Three compounds previously demonstrated to bind COM and inhibit growth of COM crystals (citrate, polyaspartate (D10, aka oAsp), and poly-acrylic acid) serve as positive controls. Citrate is the "gold standard" for stone inhibition and is currently clinically

prescribed to limit the growth of stones.[151, 152] Poly-aspartate, an oligo-peptide, has been demonstrated to both bind stone and inhibit growth.[41] It will serve as the closest comparison to our binding peptides, as well as an alternative binding module should our own peptides perform poorly. Finally, poly-acrylic acid, a polyanionic synthetic polymer, is included to compare between polyanioinic peptides and synthetic polymers.[39] We observed that even coupling D10 to a much longer non-binding polymer did not inhibit its ability to bind COM crystals and inhibit growth. D10-PEG conjugate also inhibits better than citrate, which is currently prescribed to inhibit kidney stone recurrence.

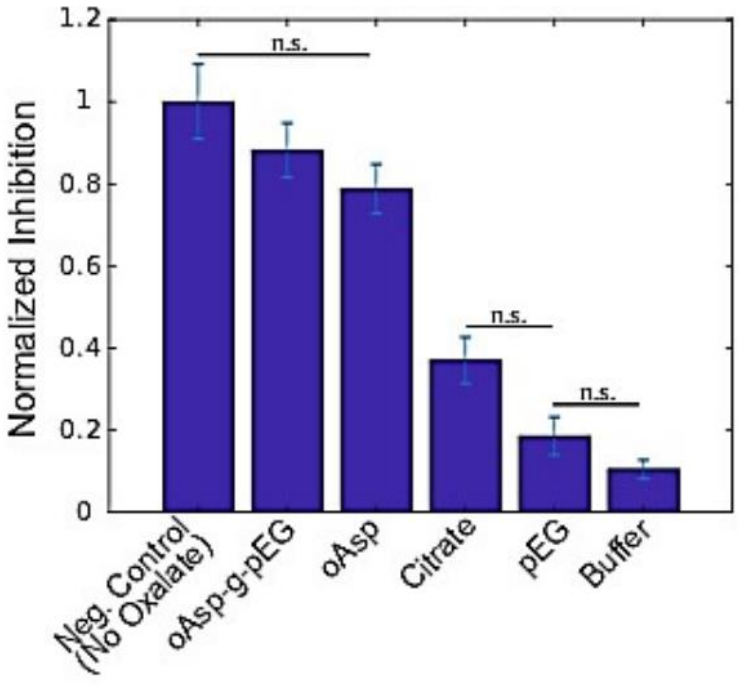

Figure 26: Inhibition of crystal growth by a simplified mucin analogue.

The mucin analogue also inhibited the growth of calcium oxalate monohydrate (Figure 27), which exhibited virtually no crystallization compared to the sample with no inhibitor ("No Sample"). However, unlike with linear PEG, we observed that 9 kDa POEGMA-co-FOM bristles also inhibited growth to a considerable extent with approximately 87% of calcium remaining in solution or a reduction of 72% of the mineralization which occurred in samples with no inhibitor. This result questions whether the polyacrylate block is necessary for binding or inhibiting the adsorption of urinary ionic precursors (GM1). If not, the synthesis of the modified bottlebrush polymer would be considerably simplified. We do note, however, that the mineralization which occurred in the presence of POcF bristle occurred within the 6-hour timeframe of this particular experiment. If allowed to continue to crystalize, it is possible that we would observe more of a stark difference between the full mucin analogue and POcF bristle.

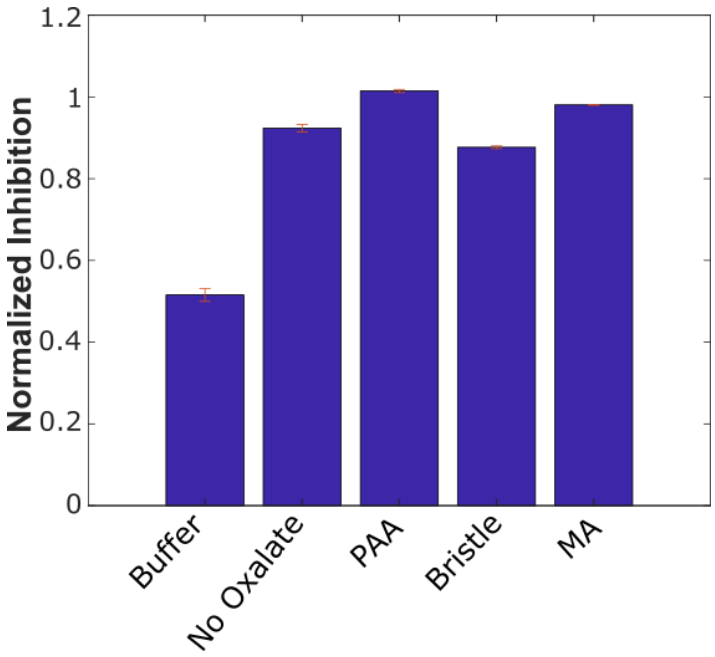

Figure 27: Inhibition of crystal growth by COM-targeted mucin analogues.

6.6 Detailed Methods

6.6.1 Synthesis of Bis[2-(2'-bromoisobutyryloxy)ethyl]disulfide

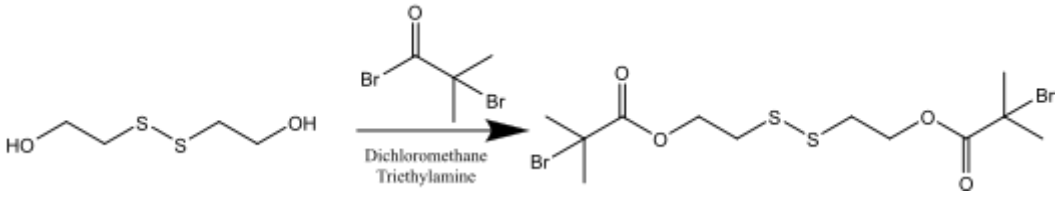

Scheme 5: Synthesis of Bis[2-(2'-bromoisobutyryloxy)ethyl]disulfide.

All glassware was baked at 100°C, quickly assembled, and allowed to cool to room temperature under vacuum. A round bottom flask was equipped with a stirbar, adapter, addition funnel, and vacuum adapter. The apparatus was evacuated and backfilled with dry nitrogen three times. 60 mL dichloromethane (DCM), 9.51 mL 2-

hydroxyethyldisulfide (12.0 g, 77.7 mmol), and 23.85 mL triethylamine (17.32 g, 171.1 mmol) were added to the flask via the sidearm under positive nitrogen pressure. The mixture was cooled in an ice bath. To the addition funnel was added 30 mL DCM and 19.25 mL α-bromoisobutyryl bromide (10.35 g, 155.7 mmol) and the mixture was added dropwise over 30 minutes. The reaction was stirred on ice for 1.5 hours and 18 hours at room temperature, at which point a white precipitate had formed. The solid was removed by filtration and the filtrate was rinsed three times with 30 mL of DCM. The solution was washed once with water, twice with 0.25 M hydrochloric acid, twice with 0.25 M sodium bicarbonate, again with water, and once with brine, each time using 200 mL of solution and keeping the lower organic layer. The organic layer was dried with magnesium sulfate and excess solvent removed by under reduced pressure, yielding 32.7 g amber oil (97.8 % purity by ^{1}H NMR, 90.8 % yield). ^{1}H NMR (400 MHz, $CDCl_3$): δ 7.26 (s,1H, $CDCl_3$), 5.3 (s, 2H, DCM), 4.44 (t,4H, ester-adjacent CH_2 BIBOED), 2.98 (t, 4H, disulfide-adjacent CH_2 BIBOED), 1.94 (s, 12H, CH_3 BIBOED), and 1.59 (s, 2H, water) ppm. ^{13}C NMR (100 MHz, $CDCl_3$): δ 171.60 (ester), 63.66 (ester-adjacent CH_2), 55.64 (quaternary C), 36.89 (disulfide-adjacent CH_2), and 30.86 (CH_3) ppm. FTIR-ATR (neat): 2976 (C-H stretch), 1732 (ester C=O stretch), 1462, 1389, 1369, 1267, 1153, 1105, 1051, 1011, 976, 918, 860, 835, 802, 762, and 737 cm-1. Density: 1.466 g/mL (Theoretical 1.478 g/mL). ESI-MS: 475.0 ($M + Na^+$)(expected 452.22, difference 22.78: likely sodium adduct).

6.6.2 Polymerization of Poly(tert-butyl acrylate) disulfide

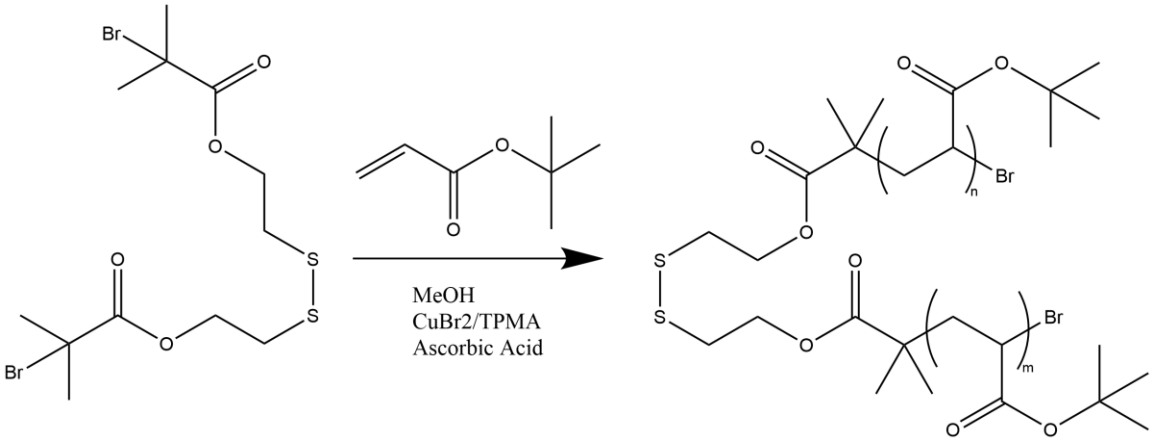

Scheme 6: Polymerization of $(PtBAS)_2$.

Excess tertbutyl acrylate was passed through a plug of basic alumina to remove inhibitor. To a three-neck 100 mL round bottom flask was added 36 mL of excess MeOH, copper II bromide (15.2 mg, 68 μmol, 1 Eq), and N"-pentamethyldiethylenetriamine (PMDETA, 47.3 mg, 272.9 μmol, 4 Eq). After stirring for 30 minutes, tBA (8.759 g, 68 mmol, 1000 Eq) was added to the flask and sealed. To a separate two-neck 25 mL round bottom flask was added excess MeOH, BIBOEDS (30.9 mg, 68 μmol, 1 Eq), and ascorbic acid (192 mg, 1.1 mmol, 16 Eq). Both flasks were subjected to three rounds of freeze-pump-thaw. The reaction was initiated upon injection of 10 mL of the initiator-ascorbic acid solution to the reaction vessel. The reaction was allowed to proceed for three hours, then quenched by addition of MQ. Upon addition of the MQ, the solution immediately turned milky. The polymer was pelleted by centrifugation at 15000 rcf for 30 minutes. The supernatant was discarded and the clear, viscous pellet was redissolved in MeOH.

This process was repeated twice more to purify the polymer. The final pellet was dried for several days in a stream of nitrogen, resulting in a soft solid which was marbled with clear and bright yellow polymer.

6.6.3 *Grafting-to* of Poly(tert-butyl acrylate) Disulfide

Gold-coated sensors for the quartz crystal microbalance were thoroughly cleaned prior to functionalization. Sensors were first cleaned in a 3:1 solution of 96% sulfuric acid and 30% hydrogen peroxide (acidic piranha solution) for five minutes. The sensors were rinsed with DI water, acetone, and isopropanol, then dried in a stream of nitrogen. The sensors were sonicated in 1% SDS solution for five minutes at 50°C. The sensors were rinsed with 1% SDS and MQ, then sonicated in MQ for five minutes at 50°C. The sensors were rinsed with MQ, acetone, and EtOH, then sonicated in EtOH for five minutes at 50°C. The sensors were rinsed with EtOH and blown dry in a stream of nitrogen. The sensors were cleaned in an air plasma for two minutes then immediately submerged in a 15 mg/mL solution of $(PtBAS)_2$. The container was backfilled with nitrogen and sealed with parafilm. After two days of incubation, the sensors were rinsed with EtOH, sonicated for five minutes in EtOH at room temperature, rinsed again with EtOH, and blown dry in a stream of nitrogen. Samples were characterized by ellipsometry and contact angle goniometry.

6.6.4 Deprotection of Poly(tert-butyl acrylate) brushes to poly(acrylic acid)

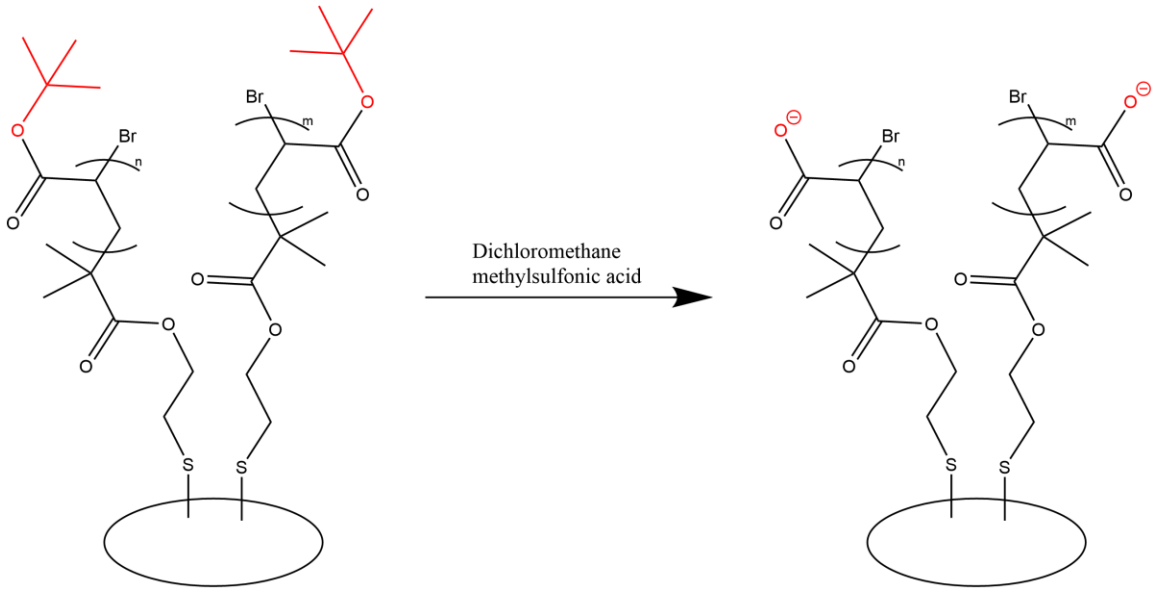

Scheme 7: Deprotection of surface-tethered PtBA to PAA.

100 mL of 1% methanesulfonic acid in dichloromethane was chilled in the refrigerator. To this solution was added PtBA-coated QCM sensors. After 10 minutes reaction at 4°C, the sensors were removed and immediately plunged into ethanol. The sensors were rinsed with acetone and EtOH, sonicated in EtOH for five minutes at room temperature, rinsed again with EtOH, and dried in a stream of nitrogen. The sensors were incubated in 175 mM acetic acid for 30 minutes, then rinsed with MQ and blown dry in a stream of nitrogen. The sensors were characterized by ellipsometry and contact angle goniometry.

6.6.5 Spincoating of Calcium Oxalate Microcrystals

Sensors were mounted on a spin coater. 150 uL of a 5 mg/mL slurry of calcium oxalate monohydrate in EtOH was applied to the surface of the sensor. The sensors were spun in two phases: 5 seconds at 500 rpm and 30 seconds at 1500 rpm. The sensors were incubated at 90°C overnight, then sonicated for a minimum of 5 minutes in COM-saturated PBS.

6.6.7 Inhibition of mineralization

Mineralization was observed using the QuantiChrom™ Calcium Assay Kit according to established protocols.[39, 40, 128] To each well of a 96-well 2 mL conical bottom culture plate was added MQ (20 μL), sodium oxalate (1.34 mg/mL, 60 μL), sodium cacodylate dichloride (600 mM, 20 μL), sample (50 μL) were added in that order. Finally, a solution of calcium chloride in sodium chloride (0.67 mM $CaCl_2$, 200 mM NaCl) was added. The plate was tightly covered with aluminum foil and sealed with parafilm. The plate was shaken 6-9 hours at 37°C. Immediately before a measurement, equal kit components "reactant A" and "reactant B" were mixed and 100 μL were portioned into each cell of a clear, flat bottomed cell culture plate. 10 μL of each sample was added to the mixed reactant. Transmittance at 612 nm was recorded for each cell using a Tecan infinite 200Pro with Tecan i-control v. 1.11.1.0. Sample measurements were normalized against the initial transmittance on a per-cell basis.

6.7 Conclusions

To monitor the binding capability of our peptides, and ultimately our analogue mucins, we have modified QCM sensors with a thin COM coating. Though similar sensors have been created previously using hydroxyapatite,[153] to our knowledge our work represents the first fabrication of COM model surfaces on QCM sensors. These sensors are stable under flow conditions, but can be improved. While we examined one MW polymer, a study examining the thickness of the initial PtBA film as a function of polymer molecular weight may help to optimize the thickness of the brush. Additionally, we heat treat the surfaces at 90°C overnight prior to use. A systematic study of the effect of heat treatment may help to improve the stability of the sensors.

If we can extend these fabrication methods to thicker coatings, we may have broader impact in the kidney stone research community. For example, researchers commonly employ artificial kidney stones made of Begostone, a calcium sulfate-based plaster, to study lithotripsy because it exhibits similar mechanical properties to native kidney stones.[154] However, the chemical mis-match of Begostone fails to capture the thermo-optical properties of calcium oxalate kidney stones, which are critical for the thermoablative mechanism which plays a role in URS.[155] Additionally, layers on glass from 100 um – 1 mm in thickness could be used to study stone damage using photoelastic imaging.[156, 157] However, in our current approach, our polymer binder is only used to tether COM to a supporting surface; there is no polymer binder to stabilize

a COM layer with any thickness. If we are to realize these additional applications of COM model materials, we will have to incorporate a binder throughout the thickness of the material. Candidates for such a binder would logically be charged (bio)polymers, including PAA, poly(ethylene imine), poly(styrene sulfonate) or bovine serum albumin. We have briefly forayed into this space, creating 1 cm cylinders of 15%wt BSA in COM. These stone phantoms had mechanical properties resembling those of native stones (data not shown), but the process needs to be refined to improve batch-to-batch consistency.

While the mucin analogue did inhibit crystal growth, it is important to question whether our lengthy synthesis warrants the complex structure of the mucin analogue. For example, pAA itself is commonly used as an anti-fouling coating, especially for hollow fiber membranes.[158, 159] In these applications, the strong negative charge repels albumin, the protein most abundant in blood and therefore the most likely to foul a surface. Because many common proteins found in the kidney stone matrix, PAA may similarly inhibit fouling by these proteins. However, many cationic proteins also bind stone and the anionic character of the PAA may instead promote fouling by these proteins.

Our results demonstrate that D10-PEG inhibits COM crystallization to the same extent as free D10. Therefore, it may follow that linear co-polymers may serve as potential design targets. This contradicts the findings of Akyol *et al.*, who determined

that coupling PEG to PAA diminishes its ability to inhibit crystal growth.[43] Therefore, it would be beneficial to explore the minimum construct necessary to adequately bind to COM surfaces and inhibit crystallization. I would propose keeping a common binder and examining free-binder, binder-PEG, binder-POEGMA, and full mucin analogue. Critical parameters for future comparison include adsorption kinetics, desorption, mineral inhibition, and anti-fouling character].

In this work, we focused on proof-of-principle experiments which demonstrated preliminary efficacy of the COM-targeted mucin analogue in terms of inhibitory potential. For these constructs to become realized technologies, a crucial parameter to study is desorption rate. The kidney is constantly flushed with urine, so once a molecule desorbs, it likely will be immediately removed from the vicinity of the stone surface and unable to reattach. Therefore, it is critically important to study the rate at which the mucin analogue desorbs from the surface. We can use the sensors developed in this aim for preliminary studies lasting up to one day, which will allow us to quickly screen constructs for those most likely to strongly bind the surface. However, we will eventually need to construct a system in which we can monitor long-term desorption. For these experiments, we target a duration of 3-months as certain materials are applied to the kidney via catheter clinically on this periodicity. Others have created flow systems which may be adapted to this purpose, and typically include a holding-chamber for COM phantoms or stone fragments to monitor desorption or long-term growth.[160]

While clinicians are able to exactly control the fluid conditions (pH, salinity, etc.) during MA adsorption, desorption will occur in urine. We suggest therefore to use model urine for desorption experiments, recipes for which are available in the literature.[161] We anticipate that the high salinity and low pH typical of stone formers will prove an obstacle to coating stability through charge screening and charge reduction, respectively. Clinically, these effects can be lessened through dietary and pharmacological measures, as has been well documented as long as patients are compliant with their regiment. However, because patient compliance can already be a problem for stone-formers, we expect that additional chemical measures to enhance durability as described in Section 5.6.

7. Conclusions

Through my doctoral research, we have identified peptides which bind calcium oxalate kidney stones, I have explored two different synthetic routes to synthesizing stone-targeted mucin analogues, and I have developed COM-functionalized model surfaces for examining adsorption and fouling by QCM.

We performed phage display to identify sequences which may defy the conventional approach of using oligoanions to bind calcium oxalate kidney stones. We performed two complete rounds, in both cases revealing the peptide SKYRADA as a potential binder. In one of the rounds, the peptides LPNKETQ and AMTAAPN were also overrepresented. We coupled these peptides to elastin-like peptides to facilitate expression and purification as well as to mimic the mucin analogue into which effective peptides would be included. However, it was determined by a calcium depletion assay that none of the overexpressed peptides inhibit stone regrowth, at least when coupled to ELP4-30. This is not an unreasonable outcome; others have identified peptide binders which bind native stone, but do not inhibit (or even promote) mineralization. We did observe, however, that the performance of the peptides behaved most like the ELP4-40.

To test whether the lack of inhibition is because the peptides do not inhibit growth or because the behavior of the ELP fusion dominates, we suggest to synthetically produce the binders without the ELP fusion or to create a fusion with D10 and compare performance with the free binder. Additionally, once we determined that the binding

tags would not inhibit growth of calcium oxalate, we did not pursue them any further and did not characterize binding strength. As such, these peptides may yet serve as strong binders for COM, perhaps in combination with oligoanions which will inhibit stone growth. In sum, the inability of these peptides to inhibit COM crystallization prompted us to use oligo anions, specifically oligo-aspartate and poly(acrylic acid), in subsequent aims.

We next pursued two methods of synthesizing mucin analogues targeted to calcium oxalate monohydrate kidney stones. We first designed and synthesized an ELP-based backbone comprised of a lysine-rich block for coupling POEGMA anti-fouling bristles and a cysteine-rich block for orthogonally coupling oligoanionic binders to the mucin analogue. Because of the low grafting density exhibited by collagen-targeted mucin analogues (appendix A), we opted for a head-tail design which will enhance adsorption. Throughout the course of the synthesis, we observed considerable gelation which complicated synthesis and diminished yields. After switching to fully-synthetic mucin analogues, it was reported that lysine can form covalent bonds with cysteine.

We additionally synthesized analogue mucins comprised entirely of synthetic polymers. Using a PtBA-b-PAcH diblock, we were able to avoid the gelation observed with peptide-based mucin analogues due to the lack of charge and eliminating the potential for crosslinking caused by the cysteine-lysine switch. However, the disparate hydrophilicity exhibited by this diblock greatly complicated the solvent systems

necessary to perform each reaction and ultimately limited reaction efficiency and yield. For these complex polymer systems to become viable methods by which to produce treatments, a thorough examination and optimization of these reactions must be performed.

In order to serve as a viable long-duration treatment strategy, mucin analogues must remain bound to the surface of residual stone fragments on month-long timescales. Specifically, we target a 3-month effective duration. As patients with non-invasive bladder cancer often undergo cystoscopy as frequently as every 3 months, we feel that this will be an acceptable timeframe for re-application of the MA coating. If the existing PAA coating is insufficient to tether the MA to the surface over this timeframe, we may adjust the binding moiety to extend duration. We could test additional binders, such as different molecular weight PAA, polycations such as poly(ethyleneimine), or dendritic binders. Additionally, crosslinking moieties will likely extend the durability of the coating by keeping a desorbed molecule in close proximity to the surface, allowing it to re-adsorb. For this strategy, we anticipate that a physical crosslink, such as with ureidopyrimidinone which can be injected and form physical crosslinks after injection.

Finally, we developed methods by which to characterize the adsorption, anti-fouling, and growth inhibition of these mucin analogues. We fabricated COM-modified QCM sensors with which to monitor adsorption kinetics in real time. To do this, we successfully synthesized a thiolated ATRP initiator and used it to polymerize surface-

active poly(tert-butyl acrylate). Using *grafting to*, we adsorbed the PtBA to the sensors, deprotected them to yield a polyanionic surface, and functionalized the sensors with calcium oxalate monohydrate. These sensors were stable under flow with COM-saturated PBS and serve as a useful tool for the field to study adsorption processes in real time. However, we only observed one molecular weight polymer. By examining the effect of polymer molecular weight on brush height, and ultimately sensor stability, we may optimize the sensors to these purposes.

We additionally examined the ability of mimic mucin analogues to inhibit the growth of calcium oxalate monohydrate using a calcium depletion assay. We demonstrated that our synthetic mucin analogue was capable of inhibiting the growth of calcium oxalate monohydrate over the course of 6 hours. It performed similar to free polyacrylic acid, which has been shown to be an effective inhibitor of crystal growth and is indistinguishable from the control in which no oxalate was present with which to crystalize. Notably, we observed considerable inhibition exhibited by the POcF alone, which inhibited 73% of the crystallization which occurred in samples without inhibitor. When comparing to figure 7, we observe that the high concentration of citrate continued to crystalize even past the 6-hour mark, indicating that we may observe further divergence between free bristle and MA with increased duration.

The work I have completed during my doctoral research builds on the general modular mucin platform developed in our lab,[107, 123] moving from fundamental physics

to patient-driven applications. I have customized our mucin analogues toward two disease states, recurrent kidney stone disease and osteoarthritis, demonstrating the customizability of our platform technology. An additional niche market for our therapeutic is veterinary medicine. Dog, cat, and dolphin are susceptible to kidney stones,[162, 163] therefore it follows that veterinary treatment with this device could apply as well. In contrast to humans, animals with stones may undergo urohydropropulsion, application of pressure to an animal's filled bladder, to expel the stone from the anesthetized animal.[164] In this indication, coating the stone with a low-friction coating could be of particular use in helping such stones to pass. In sum, I have demonstrated the ability of our mucin analogue platform technology to two disease state which cause incredible morbidity and are further a burden on the healthcare industry. Further extension of my work may lead to development of these technologies toward the clinic or new exciting areas of research.

Appendix A: Design and Synthesis of Elastin-like Polypeptides for Mucin Analogues Targeting Collagen-I

A1. Statement of Effort

The work detailed in section A3 pertaining to the design and synthesis of elastin-like polypeptide (ELP) backbones is my own. In this section, Luis Navarro synthesized reagents which I used in my work, namely imidazole-1-sulfonyl azide hydrochloride (ISA), tris-hydroxypropyltriazolylmethylamine (THPTA), and azido-poly(ethylene glycol methylether methacrylate) (alkyne-POEGMA). Work detailed in section A4 comprises a portion of the paper "Synthesis of Modular Brush Polymer-Protein Hybrids Using Diazotransfer and Copper Click Chemistry", of which I am a co-author.[107] In this work, I completed the design and synthesis of the oligopeptides (section A4.2). Luis Navarro, Ph.D. completed the coupling chemistry detailed in section A4.3, which has been included to demonstrate the impact of my own contribution.

A2. Rationale

Though my primary research focus is applying bottlebrush coatings to kidney stones, my initial goal was to target bottlebrush coatings to cartilage for treatment of osteoarthritis (OA). Osteoarthritis is characterized by joint deterioration caused by increase friction and wear. Affecting 34% of Americans over 65, this painful condition is made worse by the lack of available treatment options. Viscosupplements, NSAIDS, and other treatments have been used to lessen the pain associated with OA, but to date there is no commercially available treatment which slows the degeneration of arthritic

cartilage.[84] Our system would provide a means to specifically tether a lubricious molecule to the surface of articular cartilage. Moreover, the ability to incorporate cross-linking modules may provide a coating which is lasting-enough to serve as a viable treatment.

Our construct is based on the structure of lubricin, a mucinous lubricant of the joint, tendon, and eye.[53-55] Lubricin has been shown to be down-regulated during osteoarthritis (OA) and loss of this glycoprotein is thought to be one of the major factors contributing to the degeneration of the joint in OA.[74, 77, 78] However, supplementation by native human lubricin, recombinant lubricin, and a lubricin-mimic have been shown to mitigate this degeneration.[56, 75, 83] Additionally, others have demonstrated that synthetic constructs also based on the structure of lubricin are able to lubricate model surfaces to near the levels of the joint.[80, 94] We believe our construct could therefore be applied as a treatment for OA by combining binding modules for articular cartilage with lubricating and non-fouling bristles. In this regard, we have used WYRGRL, a peptide which has previously been employed for drug delivery and lubrication in the joint,[80, 165] in combination with POEGMA bristles, a synthetic polymer which is lubricating and non-fouling. Such a construct could be used as a tribo-supplement, applied similarly to hyaluronan injections, to treat chronic or post-traumatic osteoarthritis.

In cooperation with my colleague Luis Navarro, Ph.D., I synthesized and purified peptides containing the WYRGRL collagen II binding motif described in section

A3. Using this peptide, Luis demonstrated that peptide binders could be coupled to the synthetic backbone of our modular bottlebrush platform technology. This work is significant in that it demonstrates that the full peptide expression isn't the only manner in which to incorporate peptide binders, which are necessary for binding our bottlebrush to biological targets.

A3. Design and Synthesis of Collagen-1 Binding Mucin Analogues with Entirely Elastin-like Polypeptide Backbones

A3.1 Genetic Engineering

Protein synthesis was completed as in section 5.5, with the following differences. Oligonucleotides encoding for a collagen-binding domain (WYRGRL) was annealed into double-stranded DNA inserts. They were ligated into a plasmid and transformed into a NEB10B cloning vector. Using PReRDL, these inserts were assembled with the ELPK and flexible linker from section 4.3 to form a gene encoding for the peptide $(G_3S(G_4S)_2WYRGRLG)_2(VPGKG)_{100}(G_3S(G_4S)_2WYRGRLG)_2$ (hereafter, CKC). Plasmid inserts were verified by a combination of DNA sequencing and gel electrophoresis with a diagnostic digestion by *Bam*HI and *Xba*I.

A3.2 Protein Synthesis

The peptide was expressed as in Section 4.3 and analyzed by SDS-PAGE. Through the expression modifications noted in section 5.3.2, we increased total protein yield from 7 mg/L to 125 mg/L. Figure 28depicts the process of inverse transition cycling of our peptides, which are principally observable in cold spins, denoted "C" and the round number. Molecular weight is confirmed by MALDI-TOF (**Error! Reference source not found.**).

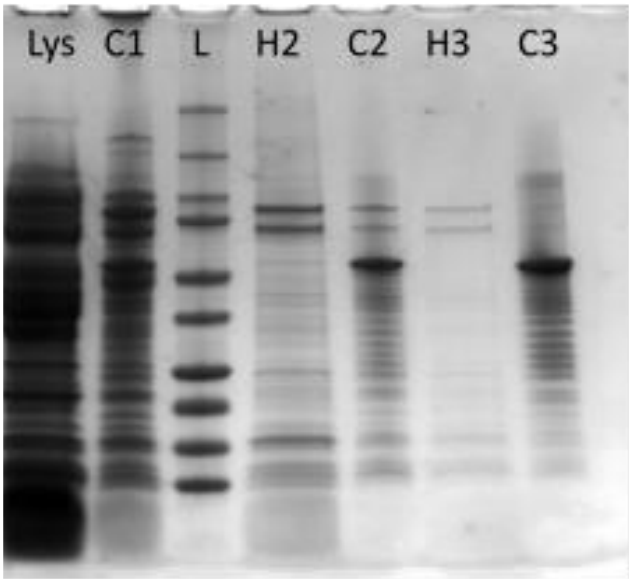

Figure 28: Inverse transition cycling purification of CKC. "Lys" denotes cell lysate. "L" denotes protein ladder. Hot and cold cycles are denoted by "H" or "C", respectively, and the number of the cycle.

Table 4: Theoretical and Measured Molecular Weights of Collagen-Targeted MAs

Label	*Sequence*	*Theoretical MW*	*MALDI MW*
CKC	$(G_3S$**WYRGRL**$(G_4S)_2G)_2(GKGVP)_{100}(G_3S$ **WYRGRL**$(G_4S)_2G)_2GY$	**50734**	**51404**
K100	(GKGVP)100GWP	**44158**	**44784**

A3.3 Brush Synthesis

Bristles were coupled to the peptides using copper-based click chemistry. First, the primary amines of the lysine sidechain were converted to azides by reaction with imidazole-1-sulfonyl azide (ISA) in presence of copper sulfate pentahydrate and purified by dialysis. Presence of the azide was confirmed by IR spectroscopy (Figure 29) and nuclear magnetic resonance.

Poly(ethyleneglycol methylethermethacrylate) (pOEGMA) bristles were coupled to the azido-backbones using copper click chemistry. Alkyne-terminated pOEGMA bristles (Mn = 3782 Da, synthesized by labmate Luis Navarro), azido-backbone, copper sulfate pentahydrate, and THPTA were stirred at room temperature for 24 hours. Full analogue mucins were purified by dialysis and repeated solubilization and precipitation in methanol and diethyl ether, respectively. Purity from unreacted bristle was confirmed by gel permeation chromatography (single peak, chromatogram not shown). IR and NMR were used to further verify the purity of our constructs and calculate conversion. Final bristle grafting density was calculated to be 48-62% for CKC and 47.3-63.1% for K100 by NMR peak integration, as in Chapter 5.

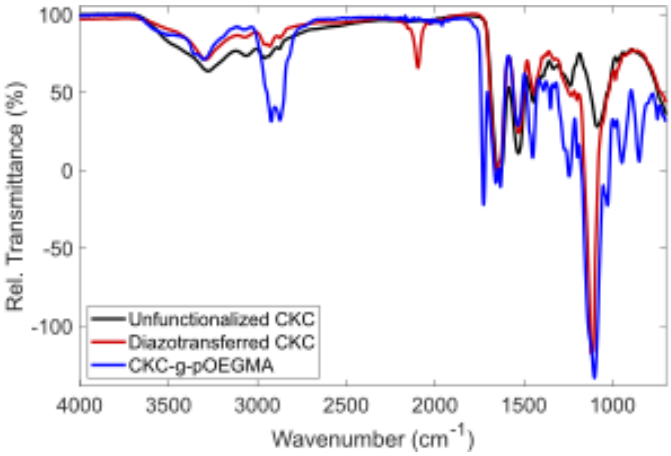

Figure 29: Infrared spectrum detailing synthetic steps of mucin analogue synthesis. As in Chapter 5, the appearance and disappearance of the peak at 2100 can be used to track the formation and subsequent reaction of azide-functionalized backbones.

A3.4 Sensor Fabrication

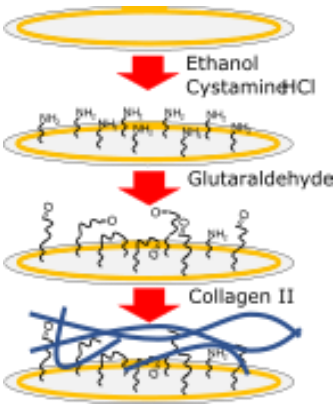

Scheme 8: QCM Sensor Functionalization.

To assess the binding of our cartilage-targeted analogue mucins, we created collagen-coated QCM sensors. Collagen II was grafted to the surface of QCM crystals as previously reported by our group (**Error! Reference source not found.**).[166] Briefly, QCM sensors were cleaned as in section 6.6.3 and incubated in a 2 mM ethanolic solution of cysteamine HCl for 18 hours. The sensors were sonicated in ethanol to remove

physiosorbed thiol. The SAM-covered sensors were then activated in a 12.5% glutaraldehyde solution for 30 minutes, followed by two hours in a 100 ug/mL acidic solution of collagen II. Thickness and contact angle of the coatings were measured by ellipsometry and contact angle goniometry, respectively. Average thicknesses of 3 nm and contact angles of 35° are commensurate with previous published values.

A3.5 Adsorption and Anti-fouling Character of ELP-based Mucin Analogues

In a first proof-of-principal experiment, binding of our analogue mucins to collagen-coated surfaces was monitored in real time by quartz crystal microbalance with dissipation monitoring. A convenient feature of this model is the ability to run four channels in parallel. As such, we measured the adsorption of CKC-g-pOEGMA and K100-g-pOEGMA onto collagen coated sensors. K100-g-pOEGMA was run in duplicate to verify consistency across channels. A final sensor will be exposed to no construct as a negative control. After equilibrating in PBS overnight, the sensors were probed with 0.2 mg/mL solutions of either CKC-g-pOEGMA or K100-g-pOEGMA for 45 minutes, followed by 1 mg/mL for an additional 45 minutes. Following adsorption of our analogue mucins, loosely bound material was rinsed form the surface with PBS for an additional 1.5 hours. After equilibration, these coatings were probed with 4% BSA to analyze the non-fouling character of our AM coatings. Again, loosely-bound material was rinsed from the surface with PBS.

Preliminary results are displayed in Figure 30. The Sauerbrey equation ignores fluid effects and assumes that all measured frequency shifts are the result of added analyte to the surface of the crystal. It therefore overestimates the true adsorbed mass and represents the maximum possible mass adsorbed to the surface. Conversely, the Parlak equation assumes that all dissipation in the system is the result of coupled fluid effects and corrects the measured frequency change (and therefore mass of analyte adsorbed) to account for these effects.[167] However, this is not strictly true. Some dissipation in the system arises from the adsorption of a viscoelastic, rather than rigid, layer on the surface of the crystal. Therefore, the Parlak equation yields an underestimate of the mass adsorbed and represents the lower bound for adsorbed mass. By bounding our measurement in this way, we provide a range of mass which could be coupled to the sensor. These bounds are represented by a thin trace for the upper bound of each channel and a bold trace for each lower bound. The range of possible adsorbed masses is shaded for convenience.

In this first preliminary study, we observed adsorption of our analogue mucin conjugates above PBS baseline, indicating that our constructs do, in fact, adsorb to the collagen-coated sensor. Moreover, though some non-specific adsorption is observed for K100-g-pOEGMA, we note that the minimum observed adsorption for CKC-g-pOEGMA is greater than the maximum for the negative control. This suggests that the presence of

binding domains may provide additional energetic incentive to adsorb to the surface, and therefore form a more stable surface coating.

We also observe non-fouling behavior conferred by our adsorbed layers. Figure 30 displays the adsorption of BSA onto our brush coatings. For convenience, only the Parlak model (the minimum adsorbed mass) is plotted and the frequency shift immediately before the adsorption of BSA is set to zero to more visually represent only the additional frequency shift from adsorbed BSA. As can be seen in Figure 30, the inverse trend from adsorption is observed for non-fouling character. That is, unprotected collagen (green trace) adsorbs the most, followed by K100-g-pOEGMA, and CKC-g-pOEGMA is the most non-fouling. Peaks on either edge of the adsorption plateau and the high dissipation observed during exposure to BSA are the result of the increased viscosity of the BSA solution.

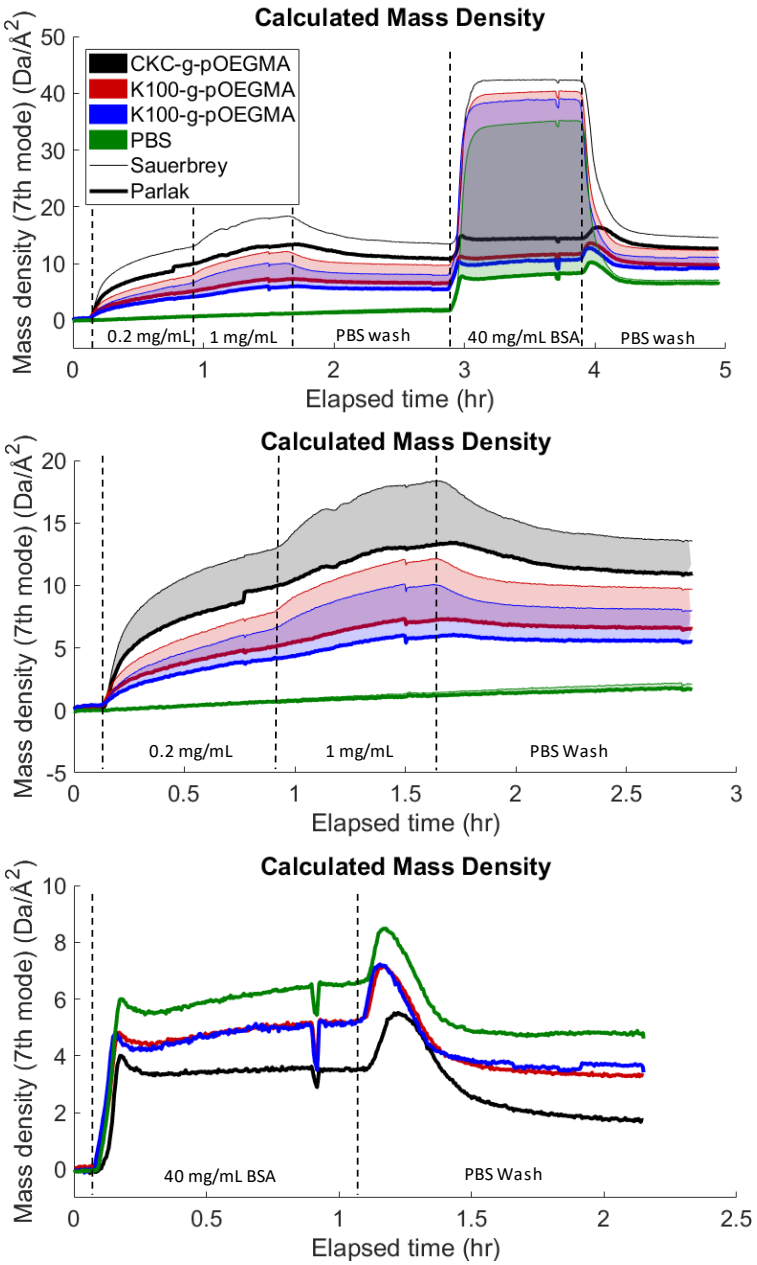

Figure 30: Adsorption of collagen-targeted mucin analogues to collagen-II model surfaces by QCM.

A3.6 Protease Inhibition of ELP-based Mucin Analogues

The osteoarthritic knee is highly proteolytic because of the inflammation caused by the disease.[168] This is especially problematic for lysine-rich peptides such as our

proteinaceous backbones, which are labile to numerous proteolytic enzymes. Thus, we probed whether the modification of our lysine residues with synthetic polymers makes them less susceptible to proteolytic degradation. We incubated unmodified CKC and the POEGMA-modified bottlebrush in a tryptic solution for up to three days at 37°C and analyzed by SDS-PAGE. Figure 31 depicts the degradation of unmodified CKC and the full mucin analogue at 3 days incubation. While unmodified backbone was completely degraded in three hours (data not shown), the mucin analogue survived proteolysis for three days.

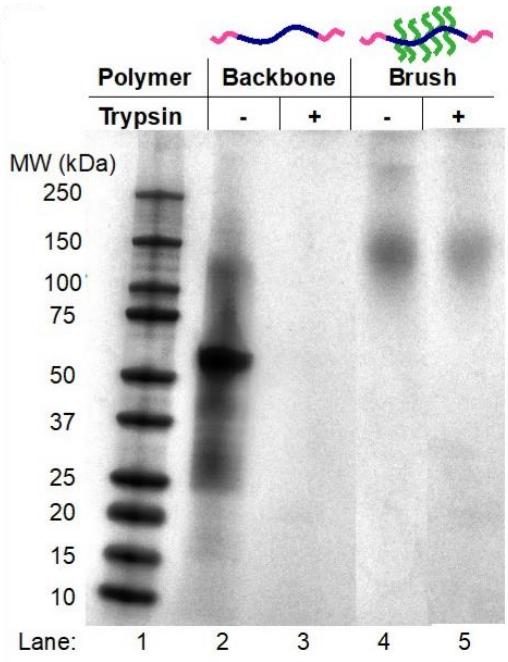

Figure 31: Protease inhibition conferred by synthetic polymer bristles in mucin analogues with peptide backbones.

A4. Design and Synthesis of Collagen-I Binding Elastin-like Polypeptides for Coupling with Synthetic Mucin Analogues

A4.1 Genetic Engineering

To test the ability of our reaction synthesis pathway to accommodate peptide binders, we synthesized C-tag coupled to a charge-neutral elastin-like polypeptide ($(VPGVG)_{30}(G_3SWYRGRL(G_4S)_2G)_2GY$, hereafter "VC"). DNA sequencing data of the colony from which expression media was inoculated confirms the peptide sequence and a diagnostic digest of the DNA confirms purity (data not shown).

A4.2 Peptide Expression and Purification

The peptide was expressed using TBII media without the addition of n-acetyl cysteine, as the modified expression media described in section 5.5 was not required due to the lack of lysine-rich sequences in this construct. However, upon analyzing the purified ELP product by SDS-PAGE, it was revealed that there was an impurity of ELP4-30 (Figure 32). The identity of this impurity was confirmed by MALDI-TOF mass spectrometry (Figure 54).

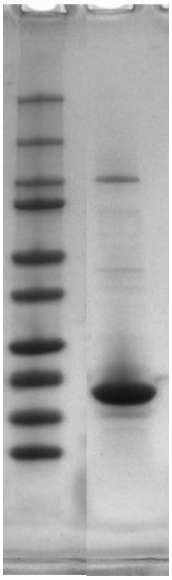

Figure 32: SDS-PAGE gel of ELPVC with ELP4 contaminant.

We used cation exchange chromatography to further purify our construct (net charge +4) from the ELP4 contaminant (net neutral). Each run had three collection periods (Figure 33). Collection 1 contained a mixture of ELPVC and ELP4 as a result of overloading the column. Collection 2, which eluted with a low concentration of salt to screen charge, contained mostly ELPVC, as did collection 3, which eluted in high salinity. This product was dialyzed and used to couple collagen binding tags to synthetic mucin analogues.

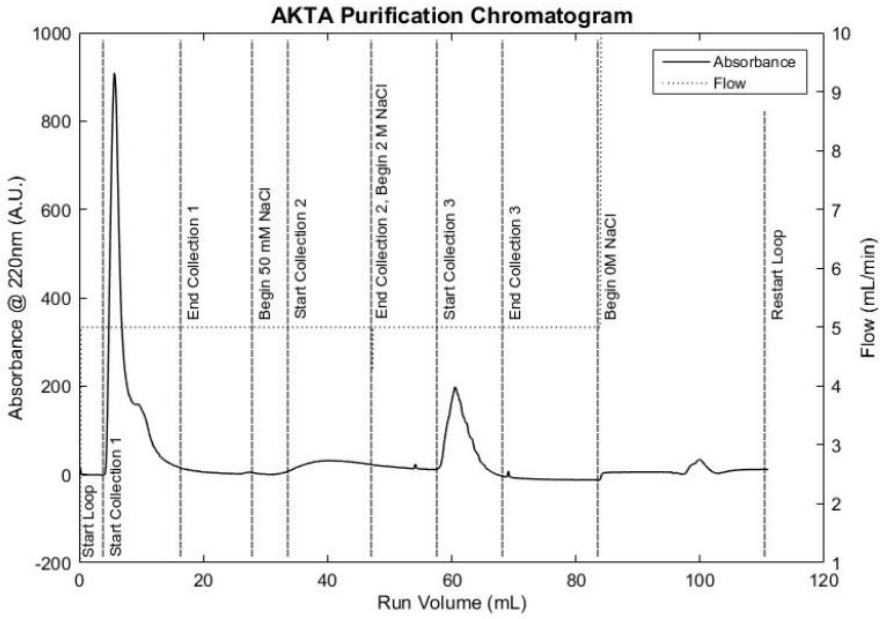

Figure 33: Purification of ELP4 contaminant from ELPVC.

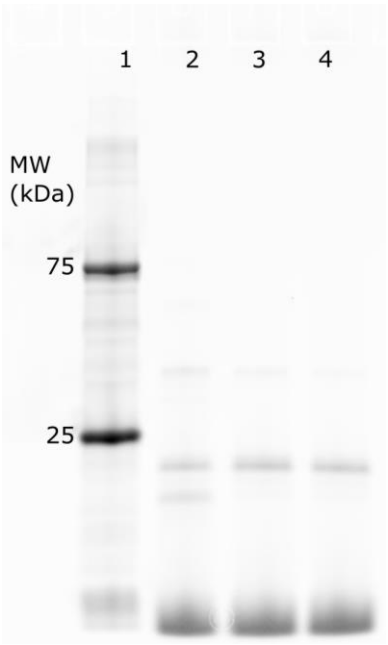

Figure 34. SDS-PAGE depicting purification of ELP4-30 from ELPVC by affinity chromatography. Lanes: 1) ladder, 2) collection 1, 3) collection 2, 4) collection 3.

A4.3 Incorporation into Synthetic Mucin Analogues

Luis Navarro successfully coupled ELPVC to synthetic PAcH backbones using copper-based click chemistry Figure 35). Specifically, the presence of bands in excess of 75kDa in lanes 7,10, and 11 of gel B demonstrate successful coupling. An excerpt of his work is included here to demonstrate the ability to couple ELP binders I've synthesized to synthetic mucin analogues. The ability of our platform technology to independently pair backbone length/spacing with binders of interest is critical for potential rapid development of mucin analogues for different surfaces as well as optimizing the design of a mucin analogue for a specific application.

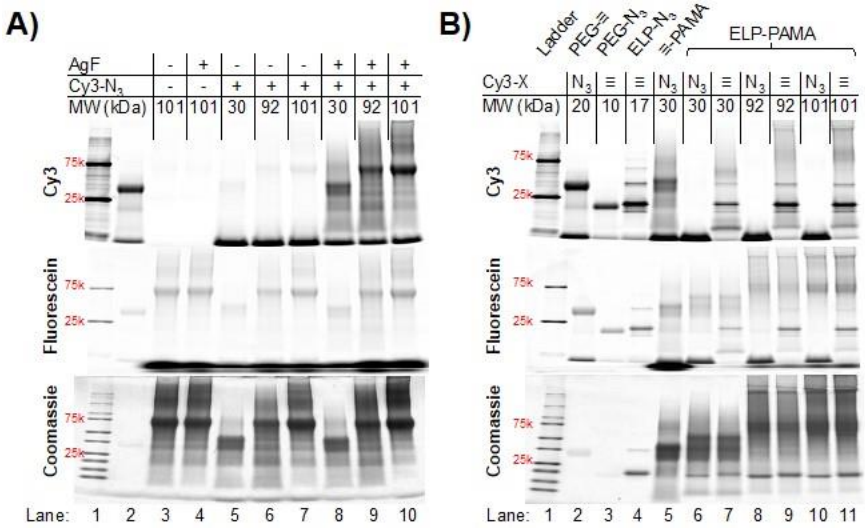

Figure 35: Coupling of ELPVC to PAcH backbones. Reproduced from Navarro *et al.*[107]

A5 Detailed Methods

A5.1 Materials

Materials used in this section are the same as those detailed in previous chapters except for the following. Collagen type II from chicken sternal cartilage (BioReagent, Sigma-Aldrich), cysteamine hydrochloride (98%, Sigma-Aldrich), and glutaraldehyde (25% aqueous solution, Alfa Aesar), Terrific Broth II (TBII, MO Bio), Trypsin-Ultra (mass spectrometry grade, NEB) Trypsin-Ultra Buffer (2x: 100 mM Tris-HCl, 40 mM $CaCl_2$, pH 8, NEB) were used as received.

Forward and reverse oligonucleotides encoding for a collagen-binding domain (WYRGRL) with a flexible linker $(GGGGS)_3$ (hereafter, C-tag) were dissolved to a concentration of 100 μM in MQ (4 nmol "ultramer", Integrated DNA Technologies).

A5.2 Protein Synthesis

Protein synthesis and characterization was performed as in Section 5.5. PReRDL was performed as described previously to create $(G_3S(G_4S)_2WYRGRLG)_2(VPGKG)_{100}(G_3S(G_4S)_2WYRGRLG)_2$ (hereafter, CKC) $(VPGVG)_{30}(G_3S(G_4S)_2WYRGRLG)_2$ (hereafter, VC). The constructs were expressed and purified as described in Section 5.5.4. For VC, the following changes were implemented: 1) TBII-Kan was used rather than 2x YT-KAN. 2) N-acetyl cysteine was not added to the culture medium. 3) Cation-exchange chromatography was used to further purify the VC peptide from ELP4-30 impurity.

Protein purification was carried out with an AKTApurifier system (GE Healthcare) equipped with modules P-960, PV-908, PV-907, NV-907, and M-925. Samples were separated by cation exchange columns (three HI-Trap SPFF columns in series) with 300−600 μL injections of roughly 40 mg/mL protein. Separation was monitored using an inline UV-detector (UPC-900) and analyzed by Unicorn (v5.1).

A5.3 Diazotransfer and Bristle Click

Diazotransfer and bristle attachment for CKC were performed as in sections 5.5.10 and 5.5.12 with the difference of the molecular weight of the POEGMA bristles. In this construct, 3280 Da alkyne-POEGMA bristles were used.

A5.4 Collagen Sensor Fabrication

Fresh gold-coated qcm chips were cleaned as in section 6.6.3. Following plasma cleaning, the surfaces were submerged in a 1 mM ethanolic solution of cysteamine hydrochloride overnight. The chips were rinsed, sonicated in ethanol for five minutes, rinsed again, and blown dry in a stream of nitrogen. The samples were transferred to a 12.5% solution of glutaraldehyde. After 30 minutes, the samples were transferred to a 100 ug/mL aqueous solution of collagen type II collagen which had been allowed to self-assembled in PBS at room temperature for 2 hours. After 2 hours, the sensors were rinsed with water and blown dry in a stream of nitrogen. The sensors were characterized by contact angle goniometry, and ellipsometry.

A5.7 Protease Inhibition

To a 1.5 mL microcentrifuge tube were added Trypsin-Ultra Buffer (2x, 100 mM Tris-HCl, 40 mM $CaCl_2$, pH 8, 10 μL), MQ (7 μL), Trypsin (50 ng, 0.5μL), and sample (1 mg/mL, 2.5 μL). The solution was mixed briefly by pipetting and incubated at 37°C for up to three days. The resulting digest was analyzed by SDS-PAGE.

A5.8 Coupling of elastin-like Polypeptides to Poly(2-aminoethyl methacrylate-co-hydroxyethyl methacrylate) Mucin Analogue Backbones

The following is an excerpt from our journal article "Synthesis of Modular Brush Polymer-Protein Hybrids using Diazotransfer and Copper Click Chemistry."[107] "To a 1.5 mL centrifuge tube was added alkyne-P(AMA-co-HEMA) (16.0 mg, 0.219 umol, 1 Eq), azido-ELP (35.8 mg, 2.19 umol, 10 Eq), water (463 uL), 2 M Net3 HOAc buffer (109 uL, pH 7.1, 10x conentrated), and premixed CuSO4-THPTA solution (10 mM in H2O, 328 uL, 3.28 umol, 15 Eq). The contents of the vial were mixed by inversion into a homogenous, deep highlighter-yellow solution, followed by addition of L-ascorbic acid solution (578 ug, 3 mg/mL in water, 192.5 uL, 3.279 umol, 15 Eq), leading to a total solution volume of 1093 uL. Argon was blown into the vial before sealing with parafilm and shaking briefly. The unchanged, homogeneous solution was covered in foil and allowed to mix by inversion for 23 hours. To the homogeneous yellow solution was added (NH4)2SO4 solution (400 mg/mL in water) to a final concentration of 66.6 mg/mL (NH4)2SO4 solution, instantly forming a large amount of white precipitate. The tube

was then spun at 10,000 rcf for 10 min, and the lime supernatant was collected. The pellet was redissolved into 833 uL of water, precipitated with 166 uL of (NH4)2SO4 solution, and spun down, and the lime supernatant was collected twice more for a total of three precipitations. The combined lime supernatants were dialyzed against 0.1 mM acetic acid in 25k MWCO Spectra/POR regenerated cellulose dialysis tubing for a day with two buffer exchanges. The dialyte was transferred with water and lyophilized to yield 19.5 mg of deep yellow fluffy solid. Due to material constraints, the pellet, consisting mostly of protein, was also purified by dialysis against 0.1 mM acetic acid in 3.5k MWCO Snakeskin RC dialysis tubing for a day with three buffer exchanges, recollected with water, and lyophilized to yield 28.0 mg of pale beige fluffy solid as the final product. The pellet's purity was verified quickly by FTIR (neat) to show it predominantly consisted of protein. The pellet was then reused for a second batch of protein-polymer conjugate while taking precautions to never potentially cross-contaminate different molecular weight backbones by keeping those sample pellets separate. FTIR (neat) of supernatant samples matched a combination of ELP and polymer precursors. FTIR (neat) of pellets matched that of ELP precursors. Functionalization was confirmed by diagnostic SDS-PAGE."

A6. Conclusions and Future Directions

In this appendix, I have demonstrated our ability to create mucin analogues for diverse applications. As demonstrated in Chapter 5, we can synthesize MAs using both

biological and synthetic backbones. Coupling efficiency was slightly lower than reported literature values,[107] principally because of the lower solubility of ELP backbones, especially after diazotransfer of the primary amines of the lysine residues. Our collagen-targeted mucin analogues successfully bound collagen model surfaces and rendered them non-fouling compared to analogues without binder. Finally, decoration of the peptide-based MA with synthetic polymer bristles considerably diminished the susceptibility of the peptide backbone to proteolytic degradation. Therefore, we are confident that peptide-based MAs could be deployed to inflammatory tissues without concern for degradation.

Moreover, we can express peptide binders and couple them to synthetic backbones using copper-based click chemistry. This allows us to take advantage of the higher-order structure of proteins to enhance the strength and specificity of binding of our MA to biological targets.

While we did observe enhanced binding through the addition of binding motifs to our peptide backbone, the overall adsorption was very low, only twice as much as non-specific adsorption. We attribute this primarily to the high grafting density and telechelic design, causing the MA to likely adsorb flat on the surface rather than to extend into solution. To enhance binding, we may incorporate more peptide binders, substitute our telechelic design for head-tail, or adjust the spacing of grafting points in our peptide backbone.

Additionally, we should characterize the adsorption and anti-fouling properties of our construct on cartilage explants. While we believe our collagen-II model surfaces were appropriate for initial characterization, the collagen is only one component of cartilage (20-30% w/w, 90% collagen type II).[68] The addition of aggrecan (10% w/w), and chondrocytes (5% v/v) may influence the adsorption process, as they are net charge-negative. Others have taken advantage of this to use oligo-cations which penetrate the cartilage surface for drug delivery[169] or surface attachment.[94]

Appendix B: Instrumentation and Analysis

B1: DNA Sequencing

Plasmid DNA (800 - 1000 ng) was supplied to Eton Bioscience, who sequenced the DNA using the Sanger method of chain termination using proprietary primers. Chromatogram was analyzed for data quality using FinchTV (Geospiza, Inc.). The sequence was read using the DNAStar Lasergene structural biology suite.

B2: Agarose Gel Electrophoresis

Samples mixed with 5x loading dye (BioRad) and were run in a 1% agarose gel impregnated with 0.01% SybrSafe dye (120 mV, 45 minutes) in TAE Buffer. Gels were imaged using a Universal Hood II gel imager (BioRad).

B3: SDS-PAGE

Peptides and polymers were visualized by sodium dodecyl sulfate polyacrylamide gel electrophoresis (SDS-PAGE). Samples were diluted 4x in 4:1 Laemlli loading buffer (BioRad) and glycerol. 10 μL were loaded into each well of a 10- to 15-well 4-20% MiniPROTEAN TGX polyacrylamide gel. Gels were run at 130 mV for 55 minutes. Gels containing fluorescent samples (Cy3 or fluoresceine) were imaged on a Typhoon 9410 gel imager (GE). Gels were stained for 20 minutes in 0.05% Coomassie Brilliant Blue R-250 (BioRad) dissolved in staining solvent (10% acetic acid, 40% water, 50% methanol). Gels were destained for 30 minutes in staining solvent without dye, and one day in water with multiple exchanges.

B4: MALDI-TOF

Matrix Assisted Laser Desorption/Ionization Mass Spectroscopy with Time-of-Flight Detection (MALDI-TOF MS) was performed using a Bruker AutoflexSpeed MALDI Mass Spectrometer (Billerica, MA). 10 μM samples were prepared in Milli-Q grade water. 5 μL of each sample was mixed 2:1 with a saturated solution of sinapinic acid and spotted onto the provided MALDI sample plate. Spectra were calibrated against insulin (5,733.49 Da) and aldolase (39,211.38 Da) molecular weight standards.

B6: NMR Spectroscopy

Nuclear Magnetic Resonance spectroscopy (NMR) was performed using a Bruker 500 MHz Spectrometer. Data were processed using MestReNova.

B7: IR Spectroscopy

Fourier transform infrared-attenuated total reflection (FTIR-ATR) was performed using an ABB FTLA2000 spectrometer. Data were processed using GRAMS/AI (Thermo Galactic).

B8: GPC

Gel Permeation Chromatography (GPC) for uncharged samples was performed using an Agilent 1260 Infinity GPC system equipped with 2 Agilent PL gel 105 Å 7.5x300 mm columns with THF eluent. Samples were filtered through a 0.2 μm PTFE syringe filter prior to injection. Molecular weights were calculated using a Wyatt Optilab T-rEX refractive index detector and Wyatt miniDAWN TREOS multi-angle light scattering

detector using *dn*/*dc* values measured in the course of the run. Data were analyzed using Astra (Wyatt Technologies).

GPC for PAcH was performed by the Genzer laboratory at North Carolina State University using Styragel HR4, Styragel HR 4E, and Styragel HR3 columns with dimethylformamide eluent doped with $LiBr_2$. Samples were filtered through a 0.2 μm polypropylene syringe filter prior to injection. Molecular weights were calculated using a Wyatt Optilab Rex refractive index detector and Wyatt miniDAWN multi-angle light scattering detector using *dn*/*dc* values measured in the course of the run. Data were analyzed using Astra (Wyatt Technologies).

B9: Ellipsometry

Dry ellipsometric thicknesses were measured using an M-88 J. A. Woollam Co. ellipsometer with a Xe arc lamp calibrated against a silicon oxide standard. Spectra were recorded at 65°, 70°, and 75°. Thicknesses were obtained by modeling the spectral data using a two-layer model consisting of a thick base layer of gold and a Cauchy layer which is fit using the spectral data. Optical properties of the thick base layer were fit using a bare surface of the same thickness of gold as the samples. Data were collected and processed using WVase32 (J. A. Woollam Co.).

B10: Contact Angle Goniometry

Water contact angles were measured using a 290-F4 contact angle goniometer (Rame-Hart) with DROPImage software.

B11: Quartz Crystal Microbalance with Dissipation Monitoring

Surface adsorption was monitored using an E4 quartz crystal microbalance with dissipation monitoring (Biolin Scientific). Sensor fundamental frequencies and real-time frequency and dissipation shifts were recorded using QSoft (Biolin Scientific). Briefly, functionalized sensors were loaded into the flow cells and tubing assembled per manufacturers instructions. Resonant frequencies and dissipation (including overtones 3-13) of the dry sensors were recorded and the surfaces were hydrated with 1X PBS flowing over the chips at 150 μL/min, controlled by a peristaltic pump. Wet frequencies were recorded prior to the beginning of the experiment. The baseline was set to the fundamental frequency of the hydrated sensor at the beginning of each experiment. Each experiment is begun in buffer to establish baseline, then switched to various solutions to monitor adsorption of mucin analogues or fouling challenges (4% bovine serum albumin). Solutions were changed by stopping flow, transferring the inlet tubing to the new solution, reversing flow briefly to eliminate air bubbles resulting from transfer, then resuming flow in the positive direction. Data were analyzed using custom MATLab code written by Luis Navarro, which calculates the Sauerbray and Parlak mass densities. The 7^{th} overtone data is presented.

Appendix C: Additional Data

C1. Chapter 4

```
  5′  C GGA AGC GGG GGT GGT TCG GGC GGT
  3′CCG CCT TCG CCC CCA CCA AGC CCG CCA …
GGC TCT AGT AAA TAT CGC GCG GAT GCC GGC GG 3′
CCG AGA TCA TTT ATA GCG CGC CTA CGG CCG    5′

G(VGVPG)30GSGGGSGGGSSKYRADAGGY
```

Figure 36: DNA and amino acid sequence of SKYRADA.

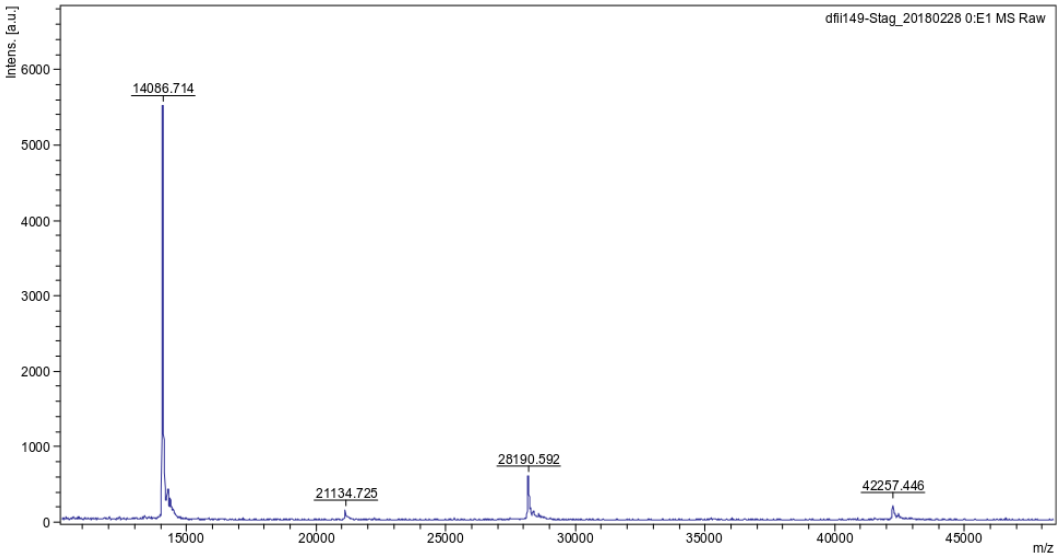

Figure 37: MALDI-TOF spectrum of STag.

```
 5′   C GGA TCA GGT GGT GGA TCA GGC GGC
 3′ CCG CCT AGT CCA CCA CCT AGT CCG CCG …
GGG TCC GCA ATG ACT GCT GCG CCA AAC GGC GG 3′
CCC AGG CGT TAC TGA CGA CGC GGT TTT CCG    5′

G(VGVPG)30GSGGGSGGGSAMTAAPNGGY
```

Figure 38: DNA and amino acid sequence of AMTAAPN.

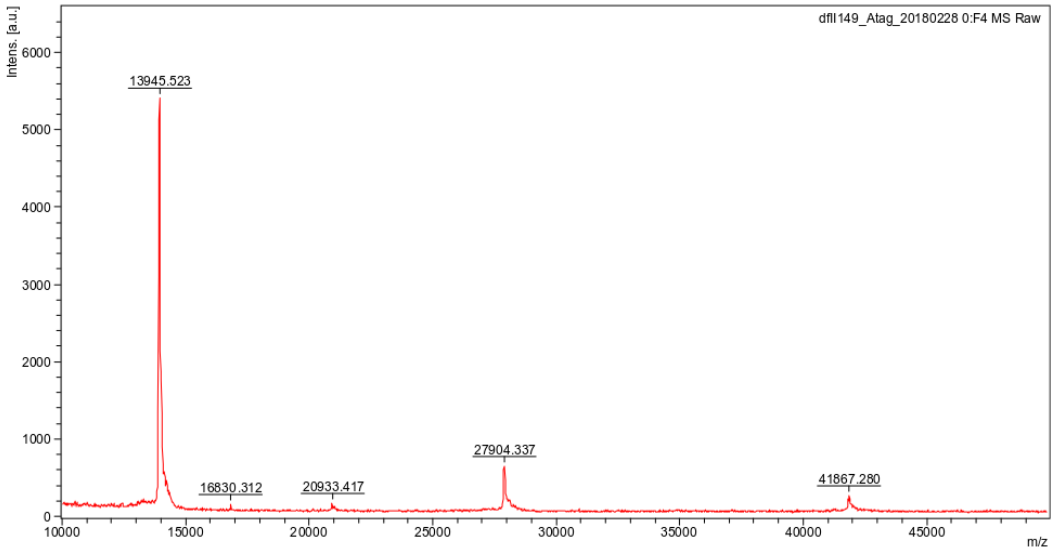

Figure 39: MALDI-TOF spectrum of ATag.

```
5′   C GGG AGC GGT GGG GGA TCT GGG GGA
3′ CCG CCC TCG CCA CCC CCT AGA CCC CCT …

GGT TCG TTA CCT AAC AAA GAA ACG CAG GGC GG 3′
CCA AGC AAT GGA TTG TTT CTT TGC GTC CCG    5′
```

G(VGVPG)$_{30}$**GSGGGSGGGSLPNKETQG**GY

Figure 40: DNA and amino acid sequence of LPNKETQ.

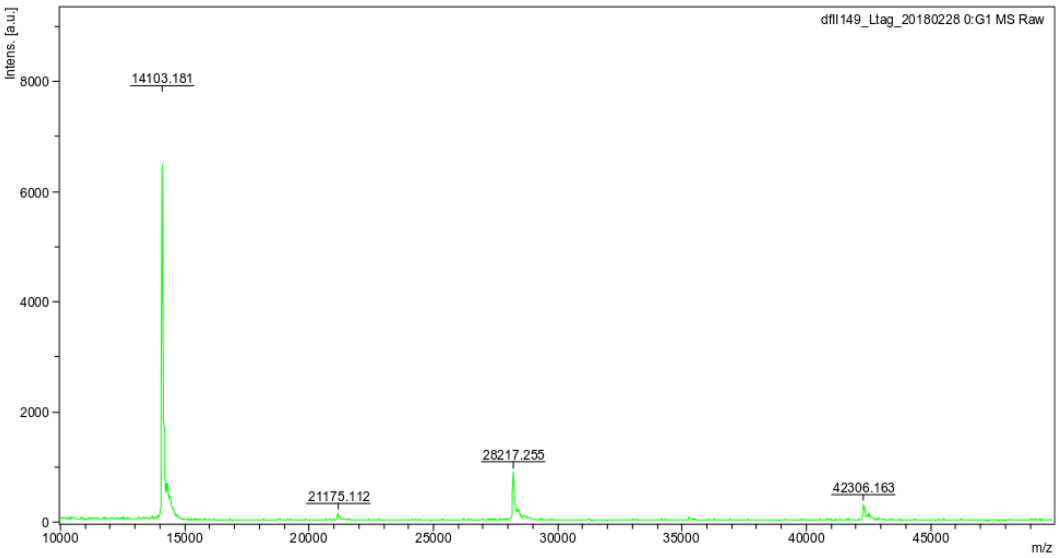

Figure 41: MALDI-TOF spectrum of LTag.

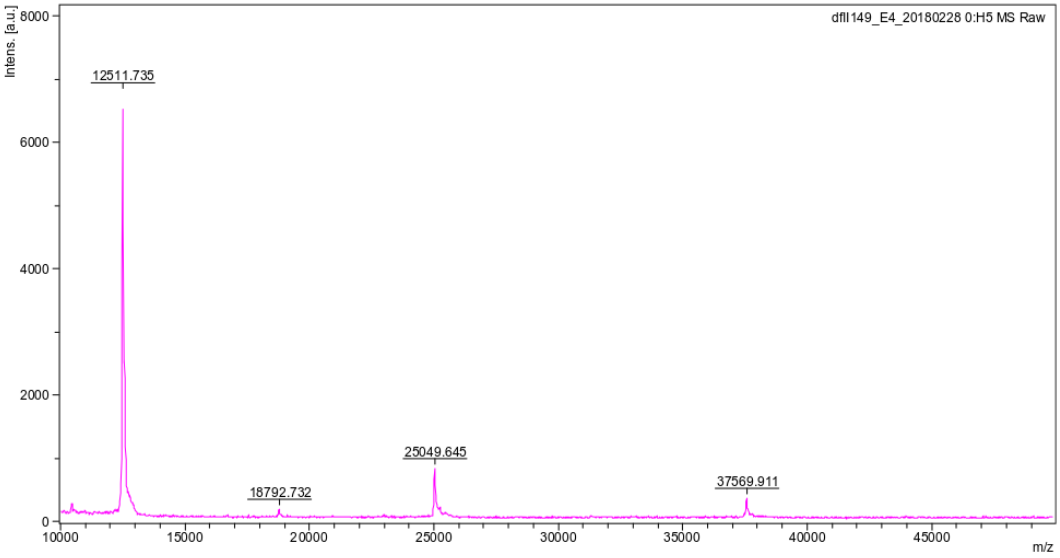

Figure 42: MALDI-TOF of ELP4-30.

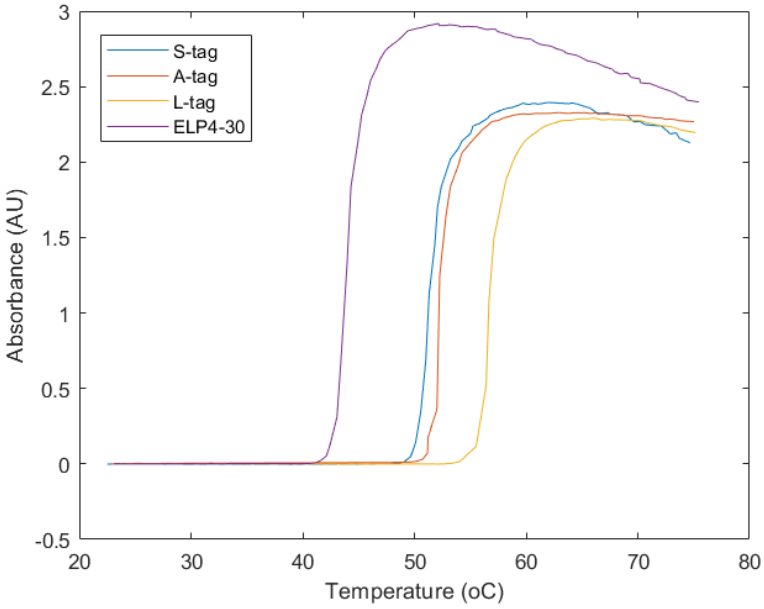

Figure 43: Transition temperatures of ELP-tagged COM binders discovered by phage display.

C2. Chapter 5

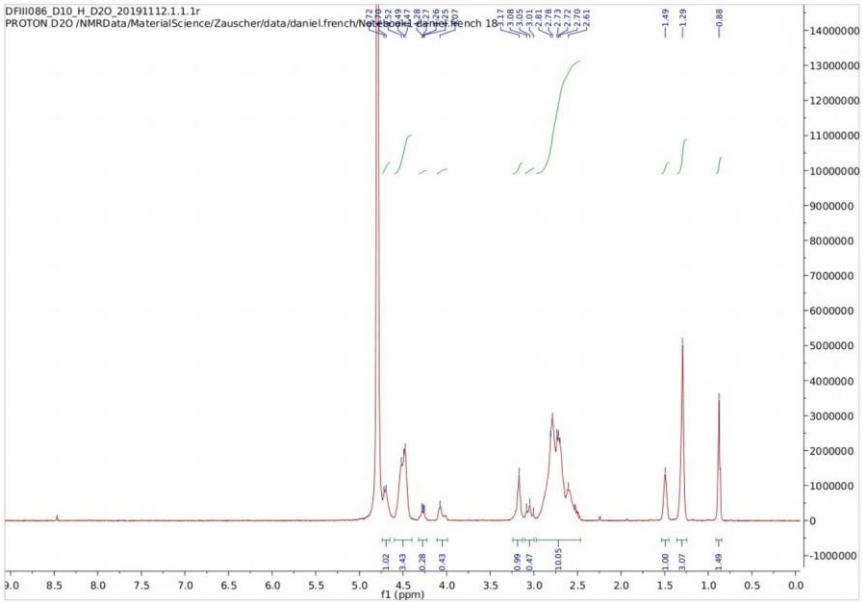

Figure 44: ^{1}H NMR of D10.

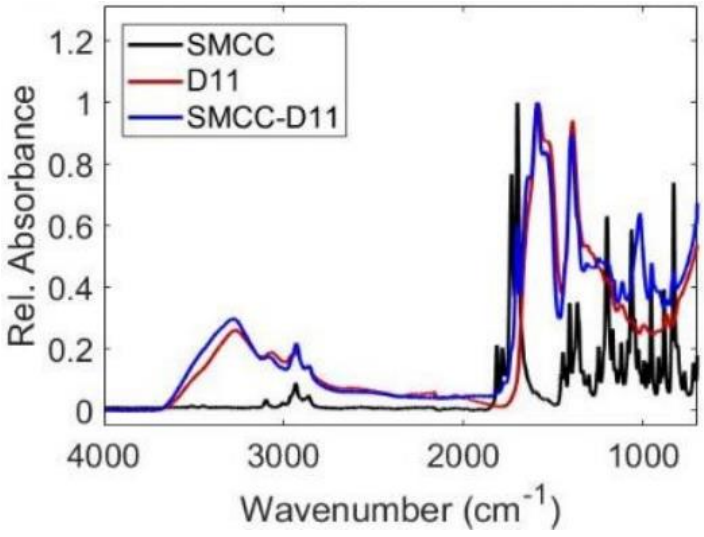

Figure 45: IR spectrum of SMCC-D10 coupling.

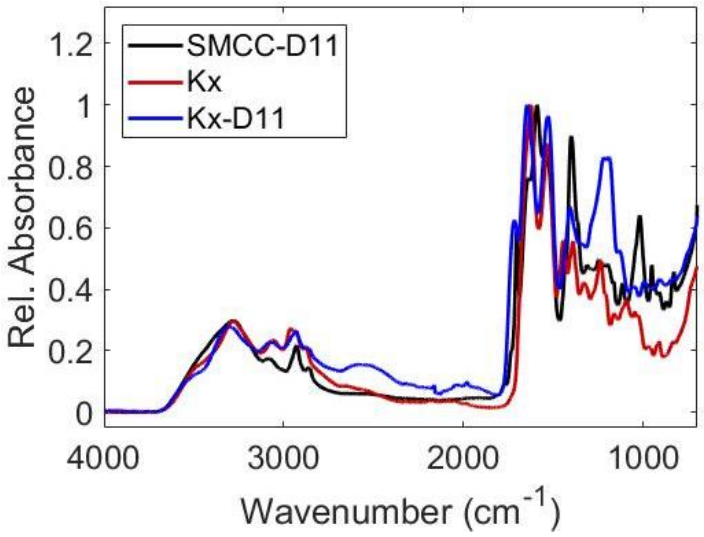

Figure 46: IR spectrum of oligo-aspartate binder attachment.

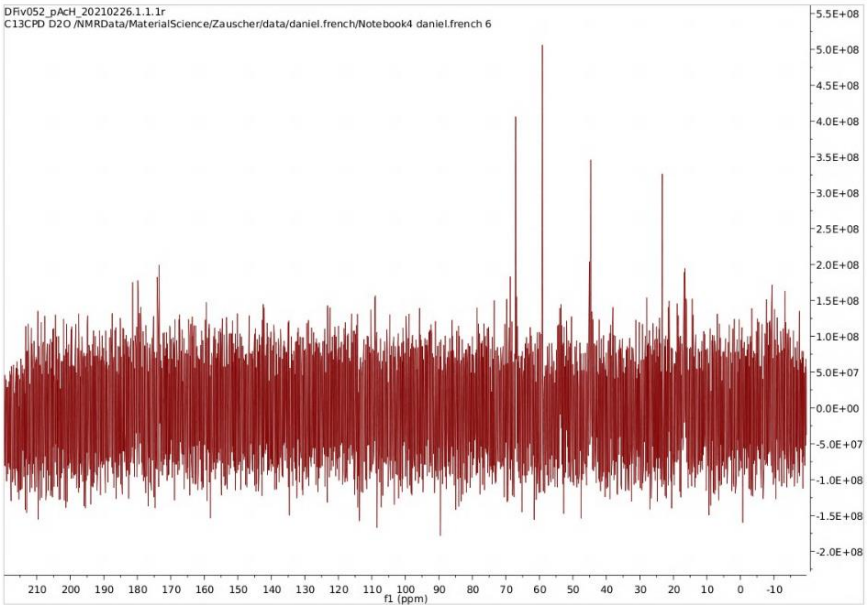

Figure 47: ^{13}C NMR of PAcH.

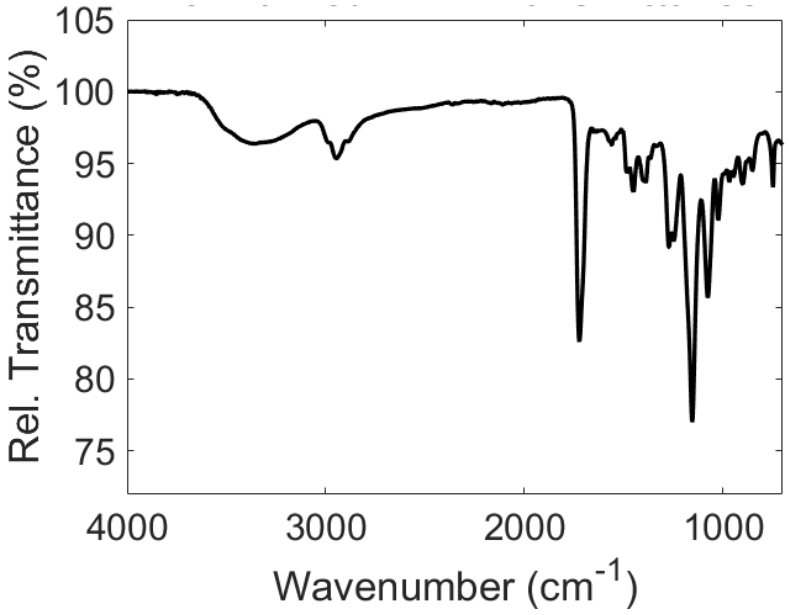

Figure 48: IR spectrum of PAcH.

C3. Chapter 6

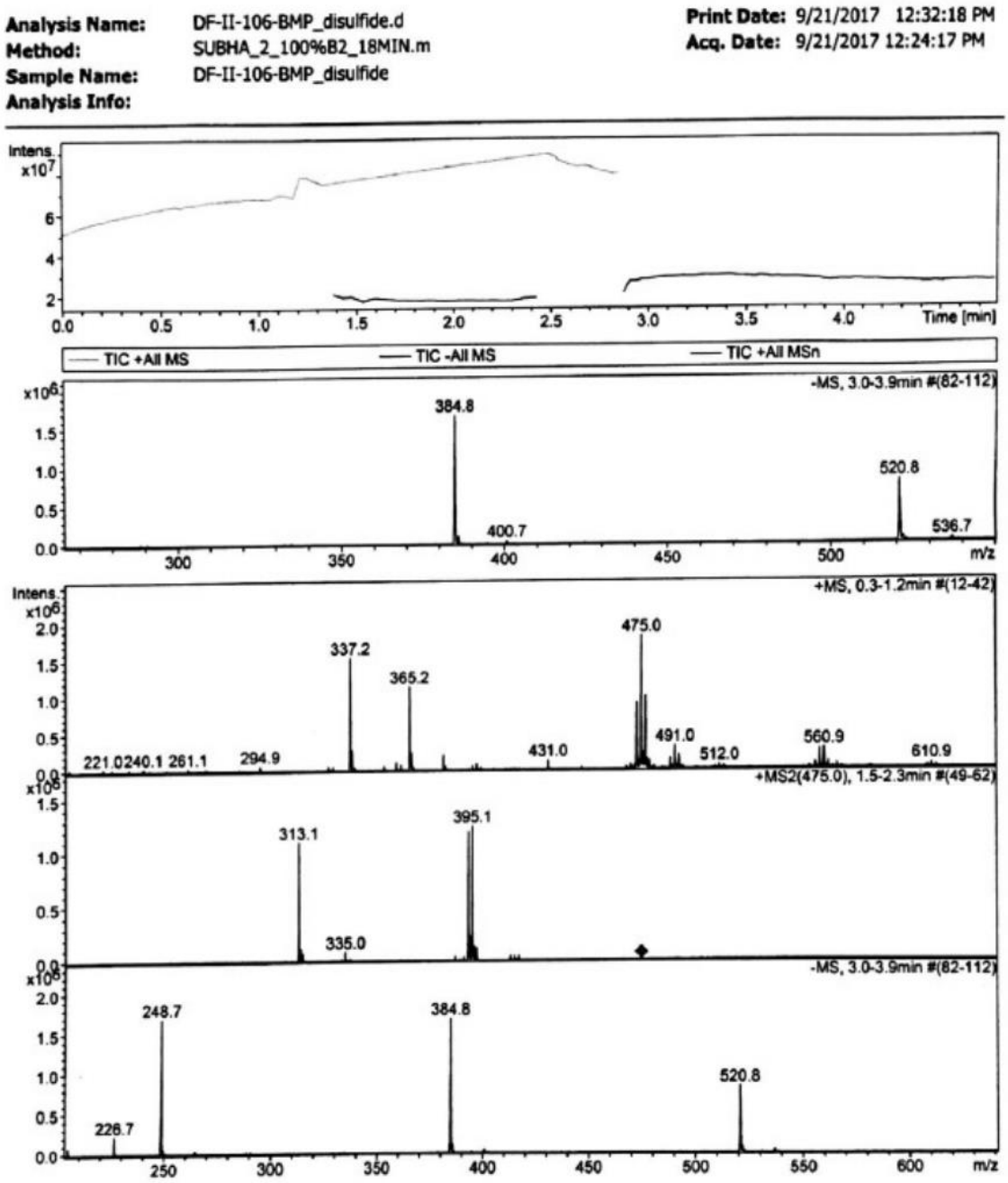

Figure 49: ESI-MS of BIBOEDS.

C4. Appendix A

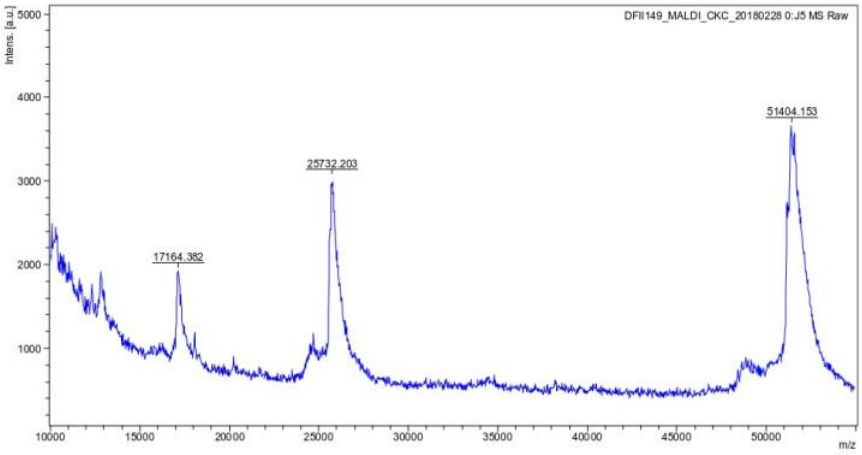

Figure 50: MALDI-TOF of CKC.

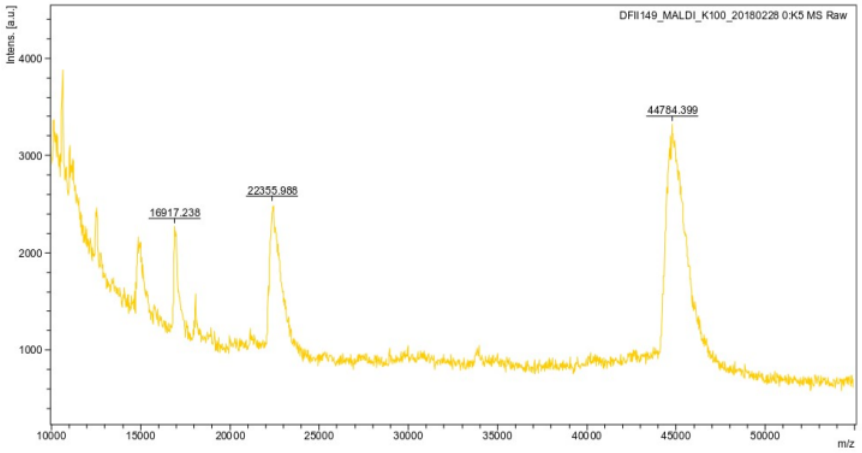

Figure 51: MALDI-TOF of ELPK100.

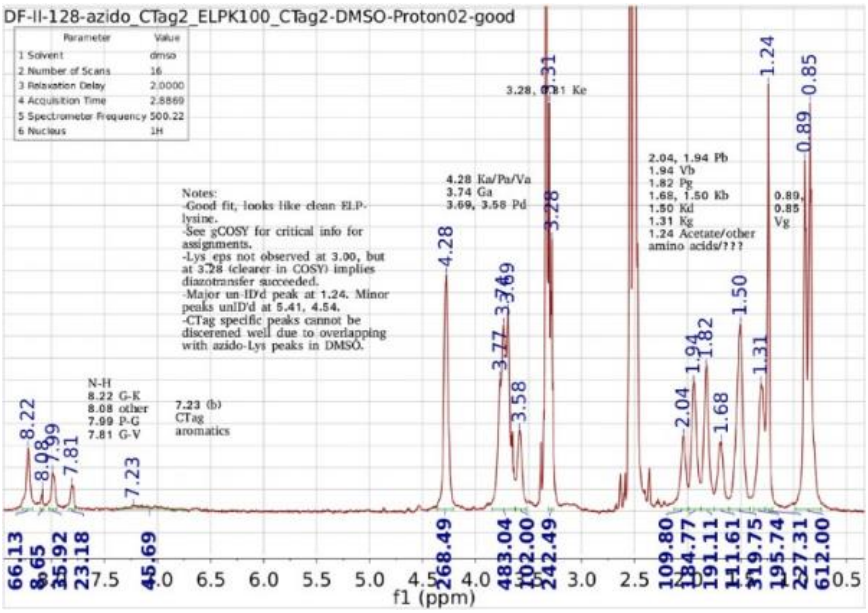

Figure 52: ^{1}H NMR Spectrum of diazo-CKC.

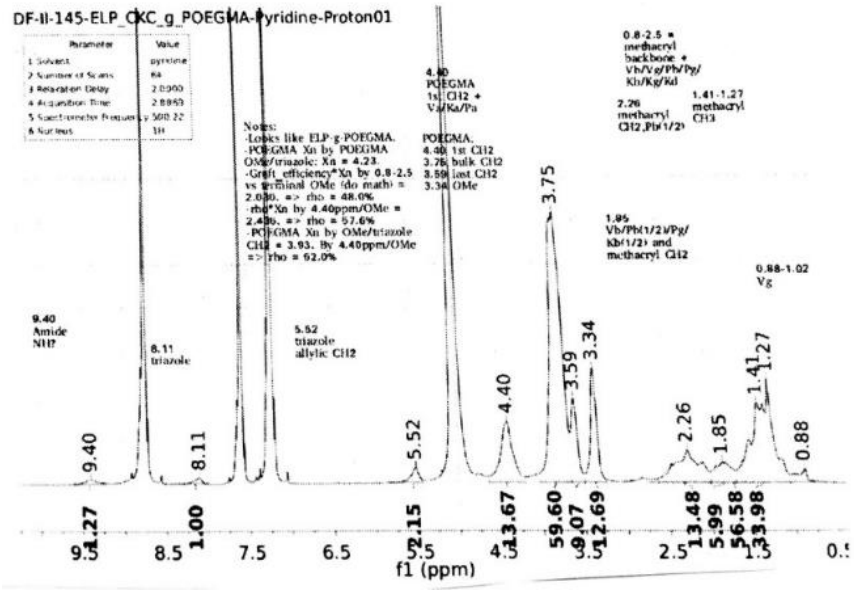

Figure 53: ^{1}H NMR spectrum of CKC-g-POEGMA.

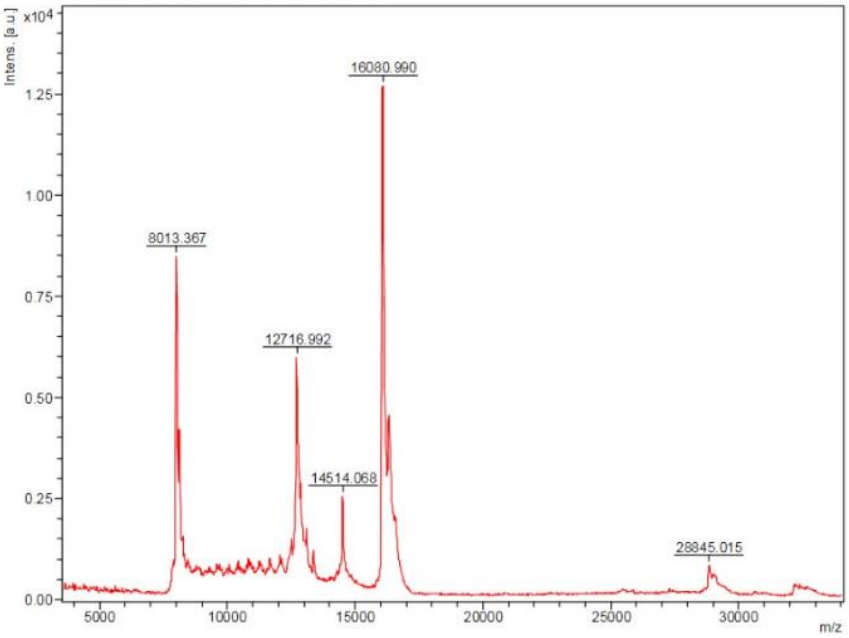

Figure 54: MALDI-TOF of ELPVC and contaminants.

References

1. Scales, C. D., Jr.; Smith, A. C.; Hanley, J. M.; Saigal, C. S.; Urologic Diseases in America, P., Prevalence of kidney stones in the United States. *Eur Urol* **2012,** *62* (1), 160-5.

2. Hein, S.; Schoenthaler, M.; Wilhelm, K.; Schlager, D.; Thiel, K.; Brandmann, M.; Richter, K.; Grunwald, I.; Wetterauer, U.; Miernik, A., Novel Biocompatible Adhesive for Intrarenal Embedding and Endoscopic Removal of Small Residual Fragments after Minimally Invasive Stone Treatment in an Ex Vivo Porcine Kidney Model: Initial Evaluation of a Prototype. *J Urol* **2016,** *196* (6).

3. Tracy, C. R.; McLeroy, S. L.; Best, S. L.; Gnade, B. E.; Pearle, M. S.; Cadeddu, J. A., Rendering stone fragments paramagnetic with iron-oxide microparticles improves the efficiency and effectiveness of endoscopic stone fragment retrieval. *Urology* **2010,** *76* (5), 1266 e10-4.

4. Tokas, T.; Habicher, M.; Junker, D.; Herrmann, T.; Jessen, J. P.; Knoll, T.; Nagele, U., Uncovering the real outcomes of active renal stone treatment by utilizing non-contrast computer tomography: a systematic review of the current literature. *World Journal of Urology* **2016**, 1-9.

5. Macejko, A.; Okotie, O. T.; Zhao, L. C.; Liu, J.; Perry, K.; Nadler, R. B., Computed tomography-determined stone-free rates for ureteroscopy of upper-tract stones. *J Endourol* **2009,** *23* (3), 379-82.

6. Rippel, C. A.; Nikkel, L.; Lin, Y. K.; Danawala, Z.; Olorunnisomo, V.; Youssef, R. F.; Pearle, M. S.; Lotan, Y.; Raman, J. D., Residual fragments following ureteroscopic lithotripsy: incidence and predictors on postoperative computerized tomography. *J Urol* **2012,** *188* (6), 2246-51.

7. Chew, B. H.; Brotherhood, H. L.; Sur, R. L.; Wang, A. Q.; Knudsen, B. E.; Yong, C.; Marien, T.; Miller, N. L.; Krambeck, A. E.; Charchenko, C.; Humphreys, M. R., Natural History, Complications, and Re-Intervention Rates of Asymptomatic Residual Stone Fragments Post-Ureteroscopy: a Report from the EDGE Research Consortium. *J Urol* **2015**.

8. Pearle, M. S.; Goldfarb, D. S.; Assimos, D. G.; Curhan, G.; Denu-Ciocca, C. J.; Matlaga, B. R.; Monga, M.; Penniston, K. L.; Preminger, G. M.; Turk, T. M.; White, J. R., Medical management of kidney stones: AUA guideline. *J Urol* **2014,** *192* (2), 316-24.

9. Eisner, B. H.; Goldfarb, D. S.; Pareek, G., Pharmacologic treatment of kidney stone disease. *Urol Clin North Am* **2013,** *40* (1), 21-30.

10. Litwin, M. S.; Saigal, C. S., Urologic Diseases in America. . USDHHS, Ed. Washington, D.C., 2012; p 486.

11. Scales, C. D., Jr.; Tasian, G. E.; Schwaderer, A. L.; Goldfarb, D. S.; Star, R. A.; Kirkali, Z., Urinary Stone Disease: Advancing Knowledge, Patient Care, and Population Health. *Clin J Am Soc Nephrol* **2016,** *11* (7), 1305-12.

12. Ratkalkar, V. N.; Kleinman, J. G., Mechanisms of Stone Formation. *Clin Rev Bone Miner Metab* **2011,** *9* (3-4), 187-97.

13. Moses, R. A.; Vollstedt, A. J.; Pais, V. M., Jr., "Allergic-like" reaction risk in patients undergoing non-intravenous contrast urography. *Can J Urol* **2018,** *25* (6), 9601-9605.

14. Kenigsberg, A. P.; Gold, S.; Grant, L.; Lotan, Y., The Economics of Cystoscopy: A Microcost Analysis. *Urology* **2021,** *00* (00), 1-6.

15. Paloian, N. J.; Leaf, E. M.; Giachelli, C., Osteopontin protects against high phosphate-induced nephrocalcinosis and vascular calcification. *Kidney International* **2016,** *89*, 1027-36.

16. Wesson, J. A.; Johnson, R. J.; Mazzali, M.; Beshensky, A. M.; Stietz, S.; Giachelli, C.; Liaw, L.; Alpers, C. E.; Couser, W. G.; Kleinman, J. G.; Hughes, J., Osteopontin is a critical inhibitor of calcium oxalate crystal formation and retention in renal tubules. *J Am Soc Nephrol* **2003,** *14*, 139-147.

17. Bader, M. J.; Eisner, B. H.; Porpiglia, F.; Preminger, G. M.; Tiselius, H. G., Contemporary management of ureteral stones. *Eur Urol* **2012,** *61* (4), 764-72.

18. Jr., C. D. S.; Smith, A. C.; Hanley, J. M.; Saigal, C. S., Prevalence of Kidney Stones in the United States. *European Urology* **2012,** *62*, 160-165.

19. Sammon, J. D.; Ghani, K. R.; Karakiewicz, P. I.; Bhojani, N.; Ravi, P.; Sun, M.; Sukumar, S.; Trinh, V. Q.; Kowalczyk, K. J.; Kim, S. P.; Peabody, J. O.; Menon, M.;

Trinh, Q., Temporal Trends, Practice Patterns, and Treatment Outcomes for Infected Upper Urinary Tract Stones in the United States. *European Urology* **2013,** *64* (1), 85-92.

20. Selby, M. G.; Vrtiska, T. J.; Krambeck, A. E.; McCollough, C. H.; Elsherbiny, H.; Bergstralh, E. J.; Liesky, J. C.; Rule, A. D., Quantification of asymptomatic kidney stone burden by computed tomography for predicting future symptomatic stone events. *Urology* **2015,** *85* (1), 45-50.

21. Burgher, A.; Beman, M.; Holtzman, J. L.; Monga, M., Progression of nephrolithiasis: long-term outcomes with observation of asymptomatic calculi. *J Endourol* **2004,** *18* (6), 534-9.

22. Scales, C. D.; Lai, J. C.; Dick, A. W.; Hanley, J. M.; van Meijgaard, J.; Stetodji, C. M.; Saigal, C. S., Comparative Effectiveness of Shock Wave Lithotripsy and Ureteroscopy for Treating Patients with Kidney Stones. *JAMA Surg* **2014,** *149* (7), 648-653.

23. Candau, C.; Saussine, C.; Lang, H.; Roy, C.; Faure, F.; Jacqmin, D., Natural history of residual renal stone fragments after ESWL. *Eur Urol* **2000,** *37* (1), 18-22.

24. Kohri, K.; Nomura, S.; Kitamura, Y.; Nagata, T.; Yoshioka, K.; Iguchi, M.; Tamate, T.; Umekawa, T.; Suzuki, Y.; Sinohara, H.; Kurita, T., Structure and Expression of the mRNA Encoding Urinary Stone Protein (Osteopontin). *Journal of Biological Chemistry* **1993,** *268* (20), 15180-15184.

25. Xie, Y.; Sakatsume, M.; Nishi, S.; Narita, I.; Arakawa, M.; Gejyo, F., Expression, roles, receptors, and regulation of osteopontin in the kidney. *Kidney International* **2001,** *60* (5), 1645-1657.

26. Mo, L.; Huang, H. Y.; Zhu, X. H.; Shapiro, E.; Hasty, D. L.; Wu, X. R., Tamm-Horsfall protein is a critical renal defense factor protecting against calcium oxalate crystal formation. *Kidney International* **2004,** *66* (3), 1159-1166.

27. Klaning, E.; Christensen, B.; Sorensen, E. S.; Vorup-Jensen, T.; Jensen, J. K., Osteopontin binds multiple calcium ions with high affinity and independently of phosphorylation status. *Bone* **2014,** *66*, 90-5.

28. Rampoldi, L.; Scolari, F.; Amoroso, A.; Ghiggeri, G.; Devuyst, O., The rediscovery of uromodulin (Tamm-Horsfall protein): from tubulointerstitial nephropathy to chronic kidney disease. *Kidney Int* **2011,** *80* (4), 338-47.

29. Cloutier, J.; Cordeiro, E. R.; Kamphuis, G. M.; Villa, L.; Letendre, J.; de la Rosette, J. J.; Traxer, O., The glue-clot technique: a new technique description for small calyceal stone fragments removal. *Urolithiasis* **2014**.

30. Mir, S. A.; Best, S. L.; McLeroy, S.; Donnally, C. J., 3rd; Gnade, B.; Hsieh, J. T.; Pearle, M. S.; Cadeddu, J. A., Novel stone-magnetizing microparticles: in vitro toxicity and biologic functionality analysis. *J Endourol* **2011,** *25* (7), 1203-7.

31. McDougal, W. S.; Sacco, D. E.; Schwarz, A.; Vogel, J. Non-Lithotripsic Kidney-Stone Therapy. 2013.

32. Evan, A. P.; Worcester, E. M.; Coe, F. L.; Williams Jr., J.; Lingeman, J. E., Mechanisms of human kidney stone formation. *Urolithiasis* **2015,** *43*, 19-32.

33. Lotan, Y.; Jimenez-Barbero, J.; Lenoir-Wijnkoop, I.; Daudon, M.; Molinier, L.; Tack, I.; Nuijten, M. J. C., Increased water intake as a prevention strategy for recurrent urolithiasis: Major impact of compliance on cost-effectiveness. *J Urol* **2013,** *189* (3), 935-939.

34. Borghi, L.; Meschi, T.; Amato, F.; Briganti, A.; Novarini, A.; Giannini, A., Urinary volume, water, and recurrences in idiopathic calcium nephrolithiasis: a 5-year randomized perspective study. *J. Urol.* **1996,** *155* (3), 839-843.

35. Nuss, G. R.; Rackley, J. D.; Assimos, D. G., Adjunctive Therapy to Promote Stone Passage. *Rev Urol* **2005,** *7* (2), 67-74.

36. Miyatake, R.; Tomiyama, Y.; Murakami, M.; Park, Y. C.; Kurita, T., Effects of isoproterenol and butyloscopolamine on the friction between an artificial stone and the intraureteral wall in anesthetized rabbits. *J urol* **2001,** *166* (3), 1083-7.

37. Kolbach-Mandel, A. M.; Kleinman, J. G.; Wesson, J. A., Exploring calcium oxalate crystallization: a constant composition approach. *Urolithiasis* **2015,** *43*, 397-409.

38. Milose, J. C.; Kaufman, S. R.; Hollenbeck, B. K.; Wolf, J. S., Jr.; Hollingsworth, J. M., Prevalence of 24-hour urine collection in high risk stone formers. *J Urol* **2014,** *191* (2), 376-80.

39. Ramamoorthy, S.; Kwak, J. H.; Karande, P.; Farmanesh, S.; Rimer, J. D., A High-throughput assay for screening modifiers of calcium oxalate crystallization. *American Institute of Chemical Engineers* **2016,** *62* (10), 3538-3546.

40. Farmanesh, S.; Chung, J.; Chandra, D.; Sosa, R. D.; Karande, P.; Rimer, J. D., High-Throughput platform for design and screening of peptides as inhibitors of calcium oxalate monohydrate crystallization. *Journal of Crystal Growth* **2013,** *373*, 13-19.

41. Kleinman, J. G.; Alatalo, L. J.; Beshensky, A. M.; Wesson, J. A., Acidic polyanion poly(acrylic acid) prevents calcium oxalate crystal deposition. *Kidney International* **2008,** *74*, 919-924.

42. Kirboga, S.; Oner, M., The role of vinyl sulfonic acid homopolymer in calcium oxalate crystallization. *Colloids and Surfaces B: Biointerfaces* **2010,** *78*, 357-62.

43. Akyol, E.; Oner, M., Inhibition of calcium oxalate monohydrate crystal growth using polyelectrolytes. *Journal of Crystal Growth* **2007,** *307* (1), 137-44.

44. Selvam, R.; Kalaiselvi, P., A novel basic protein from human kidney which inhibits calcium oxalate crystal growth. *BJU International* **2000,** *86*, 7-13.

45. Aggarwal, K. P.; Tandon, S.; Naik, P. K.; Singh, S. K.; Tandon, C., Novel antilithiatic cationic proteins from human calcium oxalate renal stone matrix identified by MALDI-TOF-MS endowed with cytoprotective potential: an insight into the molecular mechanism of urolithiasis. *Clin Chim Acta* **2013,** *415*, 181-90.

46. Govindaraj, A.; Selvam, R., An oxalate-binding protein with crystal growth promotor activity from human kidney stone matrix. *BJU International* **2002,** *90*, 336-344.

47. Sheng, X.; Jung, T.; Wesson, J. A.; Ward, M. D., Adhesionat calcium oxalate crystal surfaces and the effect of urinary constituents. *PNAS* **2004,** *102* (2), 267-272.

48. Navarro, L. A.; French, D. L.; Zauscher, S., Advances in mucin mimic synthesis and applications in surface science. *Current Opinion in Colloid & Interface Science* **2018,** *38*, 122-134.

49. Corfield, A. P., Mucins: A biologocially relevent glycan barrier in mucosal protection. *Biochimica et Biophysica Acta* **2015,** *1850*, 236-52.

50. Round, A. N.; Berry, M.; McMaster, T. J.; Corfield, A. P.; Miles, M. J., Glycopolymer charge density determines conformation in human ocular mucin gene products: an atomic force microscope study. *Journal of Structural Biology* **2004,** *145*, 246-53.

51. Ostedgaard, L. S.; Moninger, T. O.; McMenimen, J. D.; Sawin, N. M.; Parker, C. P.; Thornell, I. M.; Powers, L. S.; Ganswmer, N. D.; Bouzek, k. D.; Cook, D. P.;

Meyerholz, D. K.; Abou Alaiwa, M. H.; Stoltz, D.; Welsh, m. d., Gel-forming mucins form distinct morphologic structures in airways. *PNAS* **2017,** *114* (26), 6842-6847.

52. Arike, L.; Hansson, G. C., The Densely O-Glycosyjlated Mucin Protects the Intestine and Provides food for the Commensal Bacteria. *Journal of Molecular Biology* **2016,** *428*, 3221-29.

53. Swann, D. A.; Radin, E. L., The molecular basis of articular lubrication. I. Purification and properties of a lubricating fraction from bovine synovial fluid. *J Biol Chem* **1972,** *247* (24), 8069-73.

54. Swann, D. A.; Silver, F. H.; Slayter, H. S.; Stafford, W.; Shore, E., The molecular structure and lubricating activity of lubricin isolated from bovine and human synovial fluids. *Biochem J* **1985,** *225* (1), 195-201.

55. Swann, D. A.; Slayter, H. S.; Silver, F. H., The molecular structure of lubricating glycoprotein-I, the boundary lubricant for articular cartilage. *J Biol Chem* **1981,** *256* (11), 5921-5.

56. Rhee, D. K.; Marcelino, J.; Baker, M.; Gong, Y.; Smits, P.; Lefebvre, V.; Jay, G. D.; Stewart, M.; Wang, H.; Warman, M. L.; Carpten, J. D., The secreted glycoprotein lubricin protects cartilage surfaces and inhibits synovial cell overgrowth. *Journal of Clinical Investigation* **2005,** *115* (3), 622-631.

57. Bansil, R.; Stanley, E.; LaMont, J. T., Mucin Biophysics. *Annu. Rev. Physiol* **1995,** *57*, 635-57.

58. Bansil, R.; Turner, B. S., Mucin Structure, aggregation, physiological functions and biomedical applications. *Current Opinion in Colloid and Interface Science* **2006,** *11*, 164-170.

59. Cornick, S.; Tawiah, A.; Chadee, K., Roles and regulation of the mucus barrier in the gut. *Tissue Barriers* **2015,** *3* (1-2).

60. Estrella, R. P.; Whitelock, J. M.; Packer, N. H.; Karlsson, N. G., The glycosylation of human synovial lubricin: implications for its role in inflammation. *Biochem J* **2010,** *429* (2), 359-67.

61. Coles, J. M.; Chang, D. P.; Zauscher, S., Molecular mechanisms of aqueous boundary lubrication by mucinous glycoproteins. *Current Opinion in Colloid & Interface Science* **2010,** *15* (6), 406-416.

62. Sheehan, J. K.; Oates, K.; Carlstedt, I., Electron microscopy of cervical, gastric and bronchial mucus glycoproteins. *Biochem J* **1986,** *239* (1), 147-153.

63. Frenkel, E. S.; Ribbeck, K., Salivary Mucins Protect Surfaces from Colonization by Cariogenic Bacteria. *Applied and Environmental Microbiology* **2015,** *81* (1), 332-338.

64. Tabak, L. A., Structure and Function of Human Salivary Mucins. *Oral Biology and Medicine* **1990,** *1* (4), 229-234.

65. Hannig, C.; Hannig, M.; Kensche, A.; Carpenter, G., The mucosal pellicle - An underestimated factor in oral physiology. *Arch Oral Biol* **2017,** *80*, 144-152.

66. Chang, D. P.; Abu-Lail, N. I.; Guilak, F.; Jay, G. D.; Zauscher, S., Conformational mechanics, adsorption, and normal force interactions of lubricin and hyaluronic acid on model surfaces. *Langmuir* **2008,** *24* (4), 1183-93.

67. Kopesky, P. W.; Lee, H. Y.; Vanderploeg, E. J.; Kisiday, J. D.; Frisbie, D. D.; Plaas, A. H.; Ortiz, C.; Grodzinsky, A. J., Adult equine bone marrow stromal cells produce a cartilage-like ECM mechanically superior to animal-matched adult chondrocytes. *Matrix Biol* **2010,** *29* (5), 427-438.

68. Han, L.; Grodzinsky, A. J.; Ortiz, C., Nanomechanics of the Cartilage Extracellular Matrix. *Annu Rev Mater Res* **2011,** *41*, 133-168.

69. Jay, G. D., Lubricin and surfacing of articular joints. *Current Opinion in Orthopaedics* **2004,** *15*, 355-359.

70. Jones, A. R.; Gleghorn, J. P.; Hughes, C. E.; Fitz, L. J.; Zollner, R.; Wainwright, S. D.; Caterson, B.; Morris, E. A.; Bonassar, L. J.; Flannery, C. R., Binding and localization of recombinant lubricin to articular cartilage surfaces. *J Orthop Res* **2007,** *25* (3), 283-292.

71. Tam, E. M.; Wu, Y. I.; Butler, G. S.; Stack, M. S.; Overall, C. M., Collagen binding properties of the membrane type-1 matrix metalloproteinase (MT1-MMP) hemopexin C domain. The ectodomain of the 44-kDa autocatalytic product of MT1-MMP inhibits cell invasion by disrupting native type I collagen cleavage. *J Biol Chem* **2002,** *277* (41), 39005-39014.

72. Z. Hrkal, K. K., U. Muller-Eberhard, R. Stern, Hyaluronan-binding properties of human serum hemopexin. *FEBS Letters* **1996,** *383*, 72-74.

73. Jay, G. D.; Harris, D. A.; Cha, C. J., Boundary lubrication by lubricin is mediated by O-linked beta(1-3)Gal-GalNAc oligosaccharides. *Glycoconj J* **2001,** *18* (10), 807-815.

74. Coles, J. M. Cartilage Lubrication and Joint Protections by the Glycoprotein PRG4 Studied on the Microscale. Duke University, Durham, NC, 2010.

75. Cui, Z.; Xu, C.; Li, X.; Song, J.; Yu, B., Treatment with recombinant lubricin attenuates osteoarthritis by positive feedback loop between articular cartilage and subchondral bone in ovariectomized rats. *Bone* **2015,** *74*, 37-47.

76. Aninwene, G. E., 2nd; Abadian, P. N.; Ravi, V.; Taylor, E. N.; Hall, D. M.; Mei, A.; Jay, G. D.; Goluch, E. D.; Webster, T. J., Lubricin: a novel means to decrease bacterial adhesion and proliferation. *J Biomed Mater Res A* **2015,** *103* (2), 451-62.

77. Elsaid, K. A.; Fleming, B. C.; Oksendahl, H. L.; Machan, J. T.; Fadale, P. D.; Hulstyn, M. J.; Shalvoy, R.; Jay, G. D., Decreased lubricin concentrations and markers of joint inflammation in the synovial fluid of patients with anterior cruciate ligament injury. *Arthritis Rheum* **2008,** *58* (6), 1707-15.

78. Elsaid, K. A.; Jay, G. D.; Chichester, C. O., Reduced expression and proteolytic susceptibility of lubricin/superficial zone protein may explain early elevation in the coefficient of friction in the joints of rats with antigen-induced arthritis. *Arthritis Rheum* **2007,** *56* (1), 108-16.

79. Wen, D. Y., Intra-articular hyaluronic acid injections for knee osteoarthritis. *Am Fam Physician* **2000,** *62* (3), 565-572.

80. Lawrence, A.; Xu, X.; Bible, M. D.; Calve, S.; Neu, C. P.; Panitch, A., Synthesis and characterization of a lubricin mimic (mLub) to reduce friction and adhesion on the articular cartilage surface. *Biomaterials* **2015,** *73*, 42-50.

81. Teeple, E.; Elsaid, K. A.; Jay, G. D.; Zhang, L.; Badger, G. J.; Akelman, M.; Bliss, T. F.; Fleming, B. C., Effects of supplemental intra-articular lubricin and hyaluronic acid on the progression of posttraumatic arthritis in the anterior cruciate ligament-deficient rat knee. *Am J Sports Med* **2011,** *39* (1), 164-172.

82. Flannery, C. R.; Zollner, R.; Corcoran, C.; Jones, A. R.; Root, A.; Rivera-Bermudez, M. A.; Blanchet, T.; Gleghorn, J. P.; Bonassar, L. J.; Bendele, A. M.; Morris, E. A.; Glasson, S. S., Prevention of cartilage degeneration in a rat model of osteoarthritis by intraarticular treatment with recombinant lubricin. *Arthritis Rheum* **2009,** *60* (3), 840-847.

83. Gleghorn, J. P.; Jones, A. R.; Flannery, C. R.; Bonassar, L. J., Boundary mode lubrication of articular cartilage by recombinant human lubricin. *J Orthop Res* **2009,** *27* (6), 771-7.

84. Rutjes, A. W.; Juni, P.; da Costa, B. R.; Trelle, S.; Nuesch, E.; Reichenbach, S., Viscosupplementation for osteoarthritis of the knee: a systematic review and meta-analysis. *Ann Intern Med* **2012,** *157* (3), 180-91.

85. Bannuru, R. R.; Natov, N. S.; Dasi, U. R.; Schmid, C. H.; McAlindon, T. E., Therapeutic trajectory following intra-articular hyaluronic acid injection in knee osteoarthritis--meta-analysis. *Osteoarthritis Cartilage* **2011,** *19* (6), 611-619.

86. Jay, G. D.; Fleming, B. C.; Watkins, B. A.; McHugh, K. A.; Anderson, S. C.; Zhang, L. X.; Teeple, E.; Waller, K. A.; Elsaid, K. A., Prevention of cartilage degeneration and restoration of chondroprotection by lubricin tribosupplementation in the rat following anterior cruciate ligament transection. *Arthritis Rheum* **2010,** *62* (8), 2382-2391.

87. Martinez-Saez, N.; Peregrina, J. M.; Corzana, F., Principles of mucin structure: implications for the rational design of cancer vaccines derived from MUC1-glycopeptides. *Chem Soc Rev* **2017,** *46* (23), 7154-7175.

88. Haas, M. J., Mimicking Mucins. *Science–Business eXchange* **2008**.

89. Ron, T.; Patil, N. J.; Ajalloueian, F.; Rishikesan, S.; Zappone, B.; Chronakis, I. S.; Lee, S., Gastric mucus and mucuslike hydrogels: Thin film lubricating properties at soft interfaces. *Biointerphases* **2017,** *12* (5), 051001.

90. Zappone, B.; Ruths, M.; Greene, G. W.; Jay, G. D.; Israelachvili, J. N., Adsorption, lubrication, and wear of lubricin on model surfaces: polymer brush-like behavior of a glycoprotein. *Biophys J* **2007,** *92* (5), 1693-708.

91. Schuman, J.; Campbell, A. P.; Koganty, R. R.; Longenecker, B. M., Probing the conformational and dynamical effects of O-glycosylation within the immunodominant region of a MUC1 peptide tumor antigen. *J Pept Res* **2003,** *61* (3), 91-108.

92. Corzana, F.; Busto, J. H.; Jimenez-Oses, G.; Garcia de Luis, M.; Asensio, J. L.; Jimenez-Barbero, J.; Peregrina, J. M.; Avenoza, A., Serine versus threonine glycosylation: the methyl group causes a drastic alteration on the carbohydrate orientation and on the surrounding water shell. *J Am Chem Soc* **2007,** *129* (30), 9458-9467.

93. Sterner, O.; Karageoraki, C.; Zurcher, M.; Zurcher, S.; Scales, C. W.; Fadli, Z.; Spencer, N. D.; Tosatti, S. G. P., Reducing Friction in the Eye: A Comparative Study of Lubrication by Surface-Anchored Synthetic and Natural Ocular Mucin Analogues. *Applied Materials and Interfaces* **2017,** *2017* (9), 20150-60.

94. Banquy, X.; Burdynska, J.; Lee, D. W.; Matyjaszewski, K.; Israelachvili, J., Bioinspired bottle-brush polymer exhibits low friction and Amontons-like behavior. *J Am Chem Soc* **2014,** *136* (17), 6199-202.

95. Sharma, S.; Panitch, A.; Neu, C. P., Incorporation of an aggrecan mimic prevents proteolytic degradation of anisotropic cartilage analogs. *Acta Biomater* **2013,** *9* (1), 4618-4625.

96. Prudnikova, K.; Yucha, R. W.; Patel, P.; Kriete, A. S.; Han, L.; Penn, L. S.; Marcolongo, M. S., Biomimetic Proteoglycans Mimic Macromolecular Architecture and Water Uptake of Natural Proteoglycans. *Biomacromolecules* **2017,** *18* (6), 1713-1723.

97. Tachibana, Y.; NMatsubara, N.; Nakajima, F.; Tsuda, T.; Tsuda, S.; Monde, K.; Nishimura, S., Efficient and versatile synthesis of mucin-like glycoprotein mimics. *Tetrahedron* **2002,** *58* (10213-24).

98. Kramer, J. R.; Onoa, B.; Bustamante, C.; Bertozzi, C. R., Chemically tunable mucin chimeras assembled on living cells. *PNAS* **2015,** *112* (41), 12574-79.

99. Kasdorf, B. T.; Weber, F.; Petrou, G.; Srivastava, V.; Crouzier, T.; Lieleg, O., Mucin-Inspired Lubrication on Hydrophobic Surfaces. *Biomacromolecules* **2017,** *18*, 2454-62.

100. Artigas, G.; Hinou, H.; Garcia-Martin, F.; Gabius, H. J.; Nishimura, S. I., Synthetic Mucin-Like Glycopeptides as Versatile Tools to Measure Effects of Glycan Structure/Density/Position on the Interaction with Adhesion/Growth-Regulatory Galectins in Arrays. *Chem-Asian J* **2017,** *12* (1), 159-167.

101. Kang, S.; Lee, M.; Kang, M.; Noh, M.; Jeon, J.; Lee, Y.; Seo, J.-H., Development of anti-biofouling interface on hydroxyapatite surface by coating zwitterionic MPC polymer containing calcium-binding moieties to prevent oral bacterial adhesion. *Acta Biomaterialia* **2016,** *40*, 70-77.

102. Lee, M.; Kim, H.; Seo, J.; Kang, M.; Kang, S.; Jang, J.; Lee, Y.; Seo, J.-H., Surface zwitterionization: Effective method for preventing oral bacterial biofilm formation on hydroxyapatite surfaces. *Applied Surface Science* **2018,** *427*, 517-524.

103. Samaroo, K. J.; Tan, M.; Andresen Eguiluz, R. C.; Gourdon, D.; Putnam, D.; Bonassar, L. J., Tunable Lubricin-mimetics for Boundary Lubrication of Cartilage. *Biotribology* **2017,** *9*, 18-23.

104. Samaroo, K. J.; Tan, M.; Putnam, D.; Bonassar, L. J., Binding and lubrication of biomimetic boundary lubricants on articular cartilage. *J Orthop Res* **2017,** *35* (3), 548-557.

105. Chen, X.; Lee, G. S.; Zettl, A.; Bertozzi, C. R., Biomimetic engineering of carbon nanotubes by using cell surface mucin mimics. *Angew Chem Int Ed Engl* **2004,** *43* (45), 6111-6116.

106. Parthasarathy, R.; Rabuka, D.; Bertozzi, C. R.; Groves, J. T., Molecular orientation of membrane-anchored mucin glycoprotein mimics. *J Phys Chem B* **2007,** *111* (42), 12133-12135.

107. Navarro, L. A.; French, D. L.; Zauscher, S., Synthesis of Modular Brush Polymer–Protein Hybrids Using Diazotransfer and Copper Click Chemistry. *Bioconjugate Chemistry* **2018,** *29* (8), 2594-2605.

108. Andresen Eguiluz, R. C.; Cook, S. G.; Tan, M.; Brown, C. N.; Pacifici, N. J.; Samak, M. S.; Bonassar, L. J.; Putnam, D.; Gourdon, D., Synergistic Interactions of a Synthetic Lubricin-Mimetic with Fibronectin for Enhanced Wear Protection. *Front Bioeng Biotechnol* **2017,** *5*, 36.

109. Liu, X.; Dedinaite, A.; Rutland, M.; Thormann, E.; Visnevskij, C.; Makuska, R.; Claesson, P. M., Electrostatically anchored branched brush layers. *Langmuir* **2012,** *28* (44), 15537-15547.

110. Liu, X.; Thormann, E.; Dedinaite, A.; Rutland, M.; Visnevskij, C.; Makuska, R.; Claesson, P. M., Low friction and high load bearing capacity layers formed by cationic-block-non-ionic bottle-brush copolymers in aqueous media. *Soft Matter* **2013,** *9* (22), 5361-5371.

111. Kenausis, G. L.; Voros, J.; Elbert, D. L.; Huang, N. P.; Hofer, R.; Ruiz-Taylor, L., Poly(L-lysine)-g-poly(ethylene glycol) layers on metal oxide surfaces: surface-analytical characterization and resistance to serum and fibrinogen adsorption. *J Phys Chem B* **2000,** *104*, 3298-3309.

112. Huang, N. P.; Michel, R.; Voros, J.; Textor, M.; Hofer, R.; Rossi, A.; Elbert, D. L.; Hubbell, J. A.; Spencer, N. D., Poly(L-lysine)-g-poly(ethylene glycol) layers on metal oxide surfaces: Surface-analytical characterization and resistance to serum and fibrinogen adsorption. *Langmuir* **2001,** *17* (2), 489-498.

113. Muller, M. T.; Yan, X. P.; Lee, S. W.; Perry, S. S.; Spencer, N. D., Preferential solvation and its effect on the lubrication properties of a surface-bound, brushlike copolymer. *Macromolecules* **2005,** *38* (9), 3861-3866.

114. Lee, S.; Spencer, N. D., Adsorption properties of poly(L-lysine)-graft-poly(ethylene glycol) (PLL-g-PEG) at a hydrophobic interface: Influence of tribological stress, pH, salt concentration, and polymer molecular weight. *Langmuir* **2008,** *24* (17), 9479-9488.

115. Authimoolam, S. P.; Vasilakes, A. L.; Shah, N. M.; Puleo, D. A.; Dziubla, T. D., Synthetic oral mucin mimic from polymer micelle networks. *Biomacromolecules* **2014,** *15* (8), 3099-30111.

116. Bernhard, J. C.; Panitch, A., Synthesis and characterization of an aggrecan mimic. *Acta Biomater* **2012,** *8* (4), 1543-50.

117. Charulatha, V.; Rajaram, A., Influence of different crosslinking treatments on the physical properties of collagen membranes. *Biomaterials* **2003,** *24* (5), 759-67.

118. Zhulina, E. B.; Rubinstein, M., Lubrication by Polyelectrolyte Brushes. *Macromolecules* **2014,** *47* (16), 5825-5838.

119. Jahn, S.; Seror, J.; Klein, J., Lubrication of Articular Cartilage. *Annu Rev Biomed Eng* **2016,** *18*, 235-258.

120. Kolb, H. C.; Finn, M. G.; Sharpless, K. B., Click Chemistry: Diverse Chemical Function from a Few Good Reactions. *Angew Chem Int Ed Engl* **2001,** *40* (11), 2004-2021.

121. Conibear, A. C.; Farbiarz, K.; Mayer, R. L.; Matveenko, M.; Kahlig, H.; Becker, C. F., Arginine side-chain modification that occurs during copper-catalysed azide-alkyne click reactions resembles an advanced glycation end product. *Org Biomol Chem* **2016,** *14* (26), 6205-6211.

122. Li, S.; Cai, H.; He, J.; Chen, H.; Lam, S.; Cai, T.; Zhu, Z.; Bark, S. J.; Cai, C., Extent of the Oxidative Side Reactions to Peptides and Proteins During the CuAAC Reaction. *Bioconjug Chem* **2016,** *27* (10), 2315-2322.

123. Navarro, L. A.; Shah, T. P.; Zauscher, S., Grafting To of Bottlebrush Polymers: Conformation and Kinetics. *Langmuir* **2020,** *36* (17), 4745-4756.

124. Sumerlin, B. S.; Vogt, A. P., Macromolecular Engineering through Click Chemistry and Other Efficient Transformations. *Macromolecules* **2010,** *43* (1), 1-13.

125. Parmley, S. F.; Smith, G. P., Antibody-selectable filamentous fd phage vectors: affinity purification of target genes. *Gene* **1988,** *73* (2), 305-18.

126. Scott, J. K.; Smith, G. P., Searching for peptide ligands with an epitope library. *Science* **1990,** *249* (4967), 386-90.

127. Smith, G. P., Filamentous fusion phage: novel expression vectors that display cloned antigens on the virion surface. *Science* **1985,** *228* (4705), 1315-1317.

128. Farmanesh, S.; Chung, J.; Sosa, R. D.; Kwak, J. H.; Karande, P.; Rimer, J. D., Natural Promotors of Calcium Oxalate Monohydrate Crystallization. *Journal of the American Chemical Society* **2014,** *136*, 12648-12657.

129. Clark, R. H.; Campbell, A. A.; Klumb, L. A.; Long, C. J.; Stayton, P. S., Protein Electrostatic Surface Distribution Can Determine Whether Calcium Oxalate Crystal Growth is Promoted or Inhibited. *Calcified Tissue International* **1999,** *64* (6), 516-521.

130. Kyte, J.; Doolittle, R. F., A simple method for displaying the hydropathic character of a protein. *Journal of Molecular Biology* **1982,** *157* (1), 105-132.

131. McLeroy, S. L.; Gnade, B. E.; Cadeddu, J. A.; Pearle, M. Functionalization of micro- and nano particles for selective attachment to calcium biomineral surfaces. 2009.

132. Jin, H. E.; Chung, W. J.; Lee, S. W., Phage display for the discovery of hydroxyapatite-associated peptides. *Methods Enzymol* **2013,** *532*, 305-23.

133. Roy, M. D.; Stanley, S. K.; Amis, E. J.; Becker, M. L., Identification of a Highly Specific Hydroxyapatite-binding Peptide using Phage Display. *Advanced Materials* **2008,** *20*, 1830-1836.

134. Pensa, N. W.; Curry, A. S.; Reddy, M. S.; Bellis, S. L., The addition of a polyglutamate domain to the angiogenic QK peptide improves peptide coupling to bone graft materials leading to enhanced endothelial cell activation. *PLoS One* **2019,** *14* (3), e0213592.

135. Boda, S. K.; Almoshari, Y.; Wang, H.; Wang, X.; Reinhardt, R. A.; Duan, B.; Wang, D.; Xie, J., Mineralized nanofiber segments coupled with calcium-binding BMP-2 peptides for alveolar bone regeneration. *Acta Biomater* **2019,** *85*, 282-293.

136. Sun, X.-Y.; Ouyang, J.-M.; Liu, A.-J.; Ding, Y.-M.; Gan, Q.-Z., Preparation, characterization, and in vitro cytotoxicity of COM and COD crystals with various sizes. *Materials Science and Engineering C* **2015,** *57*, 147-56.

137. Willmott, G. R.; Vogel, R.; Yu, S. S. C.; Groenewegen, L. G.; Roberts, G. S.; Kozak, D.; Anderson, W.; Trau, M., Use of tunable nanopore blockade rates to investigate colloidal dispersions. *J. Phys. Condens. Matter* **2010,** *22* (45).

138. McDaniel, J. R.; Mackay, J. A.; Quiroz, F. G.; Chilkoti, A., Recursive directional ligation by plasmid reconstruction allows rapid and seamless cloning of oligomeric genes. *Biomacromolecules* **2010,** *11* (4), 944-52.

139. Perez-Vilar, J.; Hill, R. L., The Structure and Assembly of Secreted Mucins. *Journal of Biological Chemistry* **1999,** *274* (45), 31761-65.

140. Chen, X.; Zaro, J.; Shen, W., Fusion Protein Linkers: Property, Design and Functionality. *Adv Drug Deliv Rev* **2014,** *65* (10), 1357-1369.

141. Cho, Y.; Zhang, Y.; Christensen, T.; Sagle, L. B.; Chilkoti, A.; Cremer, P. S., Effects of Hofmeister anions on the phase transition temperature of elastin-like polypeptides. *J Phys Chem B* **2008,** *112* (44), 13765-71.

142. Meyer, D. E.; Chilkoti, A., Purification of recombinant proteins by fusion with thermally-responsive polypeptides. *Nat Biotechnol* **1999,** *17* (11), 1112-15.

143. Wensien, M.; von Pappenheim, F. R.; Funk, L. M.; Kloskowski, P.; Curth, U.; Diederichsen, U.; Uranga, J.; Ye, J.; Fang, P.; Pan, K. T.; Urlaub, H.; Mata, R. A.; Sautner, V.; Tittmann, K., A lysine-cysteine redox switch with an NOS bridge regulates enzyme function. *Nature* **2021,** *593* (7859), 460-464.

144. Haywood, S., The effect of excess dietary copper on the liver and kidney of the male rat. *J Comp Pathol* **1980,** *90* (2), 217-32.

145. Haywood, S., Copper toxicosis and tolerance in the rat. *J. Path.* **1985,** *145*, 149-158.

146. Kotliar, A. M.; Morawetz, H., Chelation of Copper (II) with Polyacrylic and Polymethacrylic Acid. *J. Am. Chem. Soc.* **1955,** *77* (14), 3692-3695

147. Lv, Q.; Hu, X.; Zhang, X.; Huang, L.; Liu, Z.; Sun, G., Highly efficient removal of trace metal ions by using poly(acrylic acid) hydrogel adsorbent. *Materials and Design* **2019,** *181*, 107934.

148. Haeri, H. H.; Jerschabek, V.; Sadeghi, A.; Hinderberger, D., Copper-Calcium Poly(Acrylic Acid) Composite Hydrogels as Studied by Electron Paramagnetic

Resonance (EPR) Spectroscopy. *Macromolecular Chemistry and Physics* **2020,** *221*, 202000262.

149. Mosmann, T., Rapid colorimetric assay for cellular growth and survival: application to proliferation and cytotoxic assays. *J. Immun. Methods* **1983,** *65*, 55-63.

150. Pintauer, T.; Matyjaszewski, K., Atom transfer radical addition and polymerization reactions catalyzed by ppm amounts of copper complexes. *Chem Soc Rev* **2008,** *37* (6), 1087-97.

151. Chow, K.; Dixon, J.; Gilpin, S.; Kavanagh, J. P.; Rao, P. N., Citrate inhibits growth of residual fragments in an in vitro model of calcium oxalate renal stones. *Kidney International* **2004,** *65*, 1724-1730.

152. Philips, R.; Hanchanale, V. S.; Myatt, A.; Somani, B.; Nabi, G.; Biyani, C. S., Citrate salts for preventing and treating calcium containing kidney stones in adults. *Cochrane Database of Systematic Reviews* **2015,** (10).

153. Tagaya, M.; Ikoma, T.; Hanagata, N.; Chakarov, D.; Kasemo, B.; Tanaka, J., Reusable hydroxyapatite nanocrystal sensors for protein adsorption. *Sci Technol Adv Mater* **2010,** *11* (4).

154. Liu, Y.; Zhong, P., BegoStone-a new stone phantom for shock wave lithotripsy research. *Journal of the Acoustical Society of America* **2002,** *112* (4).

155. Fried, N. M., Recent advances in infrared laser lithotripsy [Invited]. *Biomed Opt Express* **2018,** *9* (9), 4552-4568.

156. Xi, X.; Zhong, P., Dynamic photoelastic study of the transient stress field in solids during shock wave lithotripsy. *J. Accoust. Soc. Am* **2000,** *109* (3), 1226-1239.

157. Zhang, y.; Yang, C.; Qiang, H.; Zhong, P., Nanosecond shock wave-induced surface acoustic waves and dynamic fracture at fluid-solid boundaries. *Physical review research* **2019,** *1* (3), 033068.

158. Saito, K., Charged polymer brush grafted onto porous hollow-fiber membrane improves separation and reaction in biotechnology. *Separation Science and Tecnhology* **2002,** *37* (3), 535-554.

159. Borzecka, N. H.; Kozlowska, I.; Gac, J. M.; Bojarska, M., Anti-fouling properties of poly(acrylic acid) grafted ultrafiltration membranes-experimental and theoretical study. *Applied Surface Science* **2020,** *506*, 144658.

160. Grases, F.; Isern, B.; Perello, J.; Costa-Bauza, A., The role of glycoproteins in calcium oxalate crystal development. *BJU International* **2004,** *94*, 177-81.

161. Sarigul, N.; Korkmaz, F.; Kurultak, I., A New Artificial Urine Protocol to Better Imitate Human Urine. *Sci Rep* **2019,** *9* (1), 20159.

162. Lulich, J. P.; Berent, A. C.; Adams, L. G.; Westropp, J. L.; Bartges, J. W.; Osborne, C. A., ACVIM Small Animal Concensus Recommendations on the Treatment and Prevention of Uroliths in Dogs and Cats. *J Vet Intern Med* **2016,** *30* (5), 1564-74.

163. Venn-Watson, S.; Smith, C. R.; Johnson, S.; Daniels, R.; Townsend, F., Clinical relevance of urate nephrolithiasis in bottlenose dolphins Tursiops truncatus. *Dis Aquat Organ* **2010,** *89* (2), 167-77.

164. Osborne, C. A.; Polzin, D. J., Nonsurgical Mangement of Canine Obstructive Urolithopathy. *Veterinary Clinics of North America: Small Animal Practice* **1986,** *16* (2), 333-47.

165. Rothenfluh, D. A.; Bermudez, H.; O'Neil, C. P.; Hubbell, J. A., Biofunctional polymer nanoparticles for intra-articular targeting and retention in cartilage. *Nat Mater* **2008,** *7* (3), 248-54.

166. Chang, D. P.; Guilak, F.; Jay, G. D.; Zauscher, S., Interaction of lubricin with type II collagen surfaces: adsorption, friction, and normal forces. *J Biomech* **2014,** *47* (3), 659-66.

167. Parlak, Z.; Biet, C.; Zauscher, S., Decoupling mass adsorption from fluid viscosity and density in quartz crystal microbalance measurements using normalized conductance modeling. *Measurement Science and Technology* **2013,** *24* (8), 085301.

168. Troeberg, L.; Nagase, H., Proteases involved in cartilage matrix degradation in osteoarthritis. *Biochimica et Biophysica Acta* **2013,** *1824* (1), 133-145.

169. Geiger, B. C.; Wang, S.; Padera, R. F.; Gradzinsky, A. J.; Hammond, P. T., Cartilage-penetrating nanocarriers improve delivery and efficacy of growth factor treatment of osetoarthritis. *Science translational medicine* **2018,** *10* (469).